EVALUATION OF THE DURHAM TRIASSIC BASIN OF NORTH CAROLINA AND TECHNIQUE USED TO CHARACTERIZE ITS WASTE-STORAGE POTENTIAL

By George L. Bain and Charles E. Brown

U.S. GEOLOGICAL SURVEY
Open-File Report 80—1295

1981

UNITED STATES DEPARTMENT OF THE INTERIOR

JAMES G. WATT, Secretary

GEOLOGICAL SURVEY

Dallas L. Peck, Director

For additional information write to:

Chief Hydrologist
U.S. Geological Survey, WRD
421 National Center
Reston, Virginia 22092

1981

CONTENTS

ILLUSTRATIONS

TABLES

PLATE

EVALUATION OF THE DURHAM TRIASSIC BASIN OF NORTH CAROLINA AND TECHNIQUES USED TO CHARACTERIZE ITS WASTE-STORAGE POTENTIAL

BY GEORGE L. BAIN AND CHARLES E. BROWN

ABSTRACT

The fault system that produced the Durham Triassic basin is expressed at the surface as a series of en echelon positive and downdropped blocks. The resulting basin contains a facies distribution that reflects changing tectonic-climatic elements and sychronous deposition in separate parts of the basin. The Cumnock, Sanford, and Pekin Formations as previously mapped by Reinemund (1965) are in part facies of one another. The geological characteristics of this basin are believed analogous to that of the Basin and Range Province and the Salton Trough of California. Paleocurrent data suggest an extra-basin source of sediment for much of the basin. Longitudinal streams were active in the distribution of basin-margin fan sediments. The eastern border is stepfaulted into a series of southeasterly rotated, post-depositional slices that trend approximate N. 45° E. subparallel to the eastern border of the Deep River and Wadesboro subbasins. Unfractured diamond- and triangular-shaped blocks are terminated on the northeast and sometimes southwest by north-trending faults. The rocks exhibit low porosity and permeability as a result of extensive lithification and cementation. Lineament mapping from SLAR imagery combined with magnetic and Bouguer gravity maps provided much information on basin architecture, whereas residual gravity, magnetic, seismic, borehole geophysics, and resistivity profiles described basin-fill geometry and basement topography. Resistivity profiling is the only method other than seismic that is suited for detailing spatial facies relationships which must be known to completely assess the waste storage potential of the Triassic rocks.

The Durham Triassic basin does not appear to be suitable for injection of liquid wastes without further hydrologic testing.

INTRODUCTION

Purpose and Objectives

This report contains some of the results of a continuing U.S. Geological Survey investigation of the feasibility of storing liquid wastes in Triassic rocks of the Eastern United States. For the most part, this study has concentrated on the use of geophysical and remote sensing techniques for determination of the structural geometry contained in the Durham Triassic basin. The East Coast Triassic study[1/] is part of a larger effort by the U.S Geological Survey to ascertain factors relevant to waste storage in different geologic environments in several places in the United States. There is no intent by the U.S. Geological Survey to emplace waste fluid in the Earth's crust--only to determine where such storage is possible at the smallest risk to our environment.

An earlier report (Bain, 1973) entitled "Feasibility Study of East Coast Triassic Basins for Waste Storage - Data Availability" contains the results of a search of the literature and public and private files for the data necessary to evaluate subsurface waste disposal and offers some tentative conclusions. The principal conclusion, however, was that the subsurface data in the literature were too few, contradictory, and sporadic to evaluate the waste potential of the East Coast Triassic basins. Subsequently, the Durham Triassic basin was selected for a detailed investigation of the structural geometry of one "graben" and the character and spatial distribution of its sedimentary fill. The data, geophysical techniques, and conceptual models developed may be used for a rapid, comprehensive, and accurate evaluation of subsurface conditions in other East Coast Triassic basins.

Location and Distribution

Triassic basins are distributed along the Atlantic seaboard from Nova Scotia to Florida where they exist in the subsurface. They extend eastward beneath the Cenozoic cover onto the Continental Shelf where they are being discovered by exploratory drilling and geophysical work. Figure 1 illustrates the known East Coast distribution of basins subparallel to the Appalachian trend. The Durham Triassic basin in North Carolina is the southernmost exposed basin formed in tectonically negative areas.

1/ Some of the East Coast Triassic basins are now considered Triassic and Jurassic in age, but for the purposes of this report they are called Triassic basins.

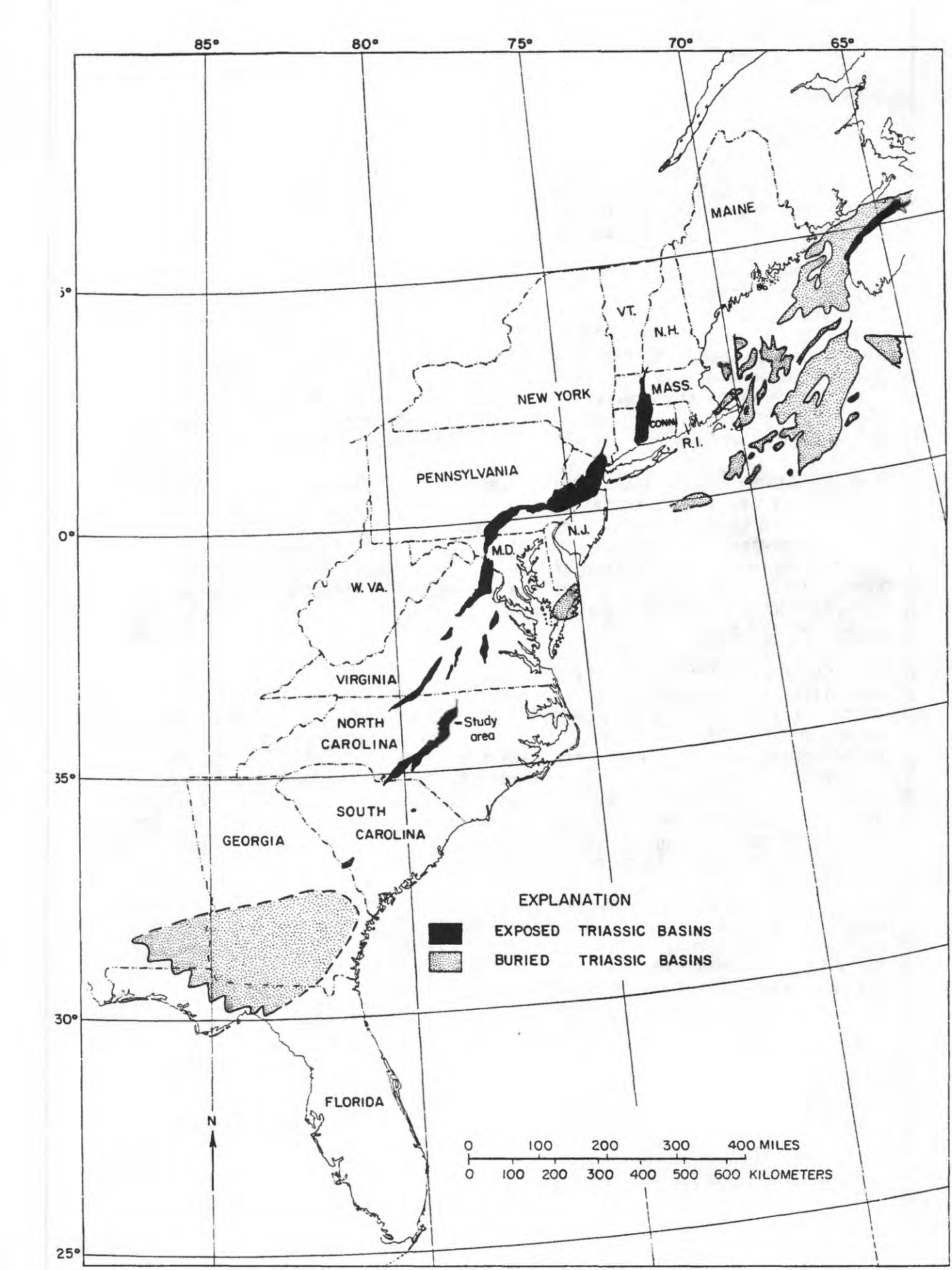

Figure 1. Distribution of East Coast Triassic basins.

Previous Work

The existence of rocks of Triassic age in the Durham Triassic basin has been known since at least 1820 when Olmsted reported the association of sandstone and coal in the Sanford area. Later, Olmsted (1825) outlined the limits of the Deep River coal basin.

Emmons (1852, 1856) in his reports on the geology of North Carolina recognized a stratigraphic sequence from extensive fossil collections in the Durham Triassic basin and proposed a Triassic age for the younger beds and a Permian age for the older beds. Subsequent examination of Emmons' fossil collection by Redfield (1856) and Fontaine (1883) established the age equivalence of the rocks of the Durham Triassic basin to the Upper Triassic rocks of the Newark and Connecticut basins. Russell (1892), who began his studies in New Jersey, is largely responsible for first bringing together the early knowledge of the Triassic basins on the East Coast.

Woodworth (1902) discussed the geologic relationships and chemical analyses of the Triassic coal and gave production statistics for the Virginia and North Carolina mines. Campbell and Kimball (1923) did the first comprehensive study of the Deep River coal field near Sanford, North Carolina. They defined and named the Cumnock, Sanford, and Pekin Formations. They also described the geologic and structural aspects of the coal deposit and described the quality, thickness, and geographic extent of the coal.

Reinemund (1955) made the most comprehensive study to date of the Deep River coal basin. Reinemund found the Deep River coal field of North Carolina to be part of a southeast tilted and downfaulted trough-shaped block of Triassic rocks similar to the Connecticut basin. According to Reinemund, the source of the basal conglomerate in the Sanford area was a short distance to the northwest, but most of the overlying sediments were derived from the southeast, beyond the eastern boundary fault. After deposition ceased, these sediments were broken by tensional cross fractures, were later cut by longitudinal faults, and were then intruded by basic magma along bedding planes and open cross fractures.

Conley (1962) in his report on the geology of Moore County recognized a western border as well as an eastern border fault in the Wadesboro and Deep River subbasins. He found Triassic (?) grey conglomerate overlying the eroded Sanford Formation and proposed that parts of the Cumnock, Sanford, and Pekin Formations were contemporaneous.

Journal articles and theses by many individuals have been used in the preparation of this report. The following reports were especially valuable. Harrington (1951) described the tectonic structure of the western border of the Durham subbasin; Randazzo and others (1970) described the geology and tectonic aspects of the Wadesboro subbasin; Hooks and Ingram (1955) described clay types found in the Durham subbasin; Dennison and Wheeler (1975) described the uranium potential of the Durham Triassic basin. Ebasco Services (1975) presented a detailed geologic examination of the site of a proposed nuclear power plant in the Durham subbasin; and Bell and others (1974) described the geology of the Crowburg basin beyond the southwestern extremity of the Durham Triassic basin in South Carolina. The most recent and detailed work in the Durham Triassic basin is contained in a report by Parker (1978).

General geology

The East Coast Triassic basins are mostly half grabens or tilted grabens containing continental fluvial sedimentary fill. The Durham Triassic basin is bounded on the east and southeast by a high angle normal fault zone traditionally known as the Jonesboro fault. The basin trends southwestward (fig. 2) from near the North Carolina-Virginia line to a point a short distance across the North Carolina-South Carolina line. It is about 226 km long and averages about 16 km in width. The Durham Triassic basin is traditionally divided into four substructures which from north to south are the: Durham subbasin, Colon cross structure, Sanford (or Deep River) subbasin, and Wadesboro subbasin. The term "Durham Triassic basin" is used in this report to refer collectively to the above four substructures. Most of the present study has concentrated on the Durham substructure. The Durham Triassic basin is surrounded and presumed underlain by the crystalline Piedmont complex composed of acid igneous instrusives, metavolcanics, metasediments, and high-grade metamorphic rocks.

Continental sediments preserved in the Durham Triassic basin include maroon to grey fanglomerate, conglomerate, feldspathic sandstone, graywacke, argillite, siltstone, mudstone, black shale, and minor amounts of chert and coal (fig. 3). The exposed sediments can be assigned to sedimentary environments of alluvial fan, interfan, lake, and swamp.

Fanglomerate composed of scree from nearby Piedmont rocks is found adjacent to the Jonesboro fault on the east and is found in some places on the west. Conglomerate and poorly sorted coarse sandstone make up most of the alluvial fans that extend into the basin normal to the basin's edge in large thick tongues.

The finer grained rocks composed of muddy, silty, argillaceous sediments are confined to the distal extremities of the fans and to interfan areas. They are typically deep maroon in color. Facies change rapidly both vertically and laterally. Coarse "cut and fill" channel sandstones record where distributary channels cut through fine deltaic muds.

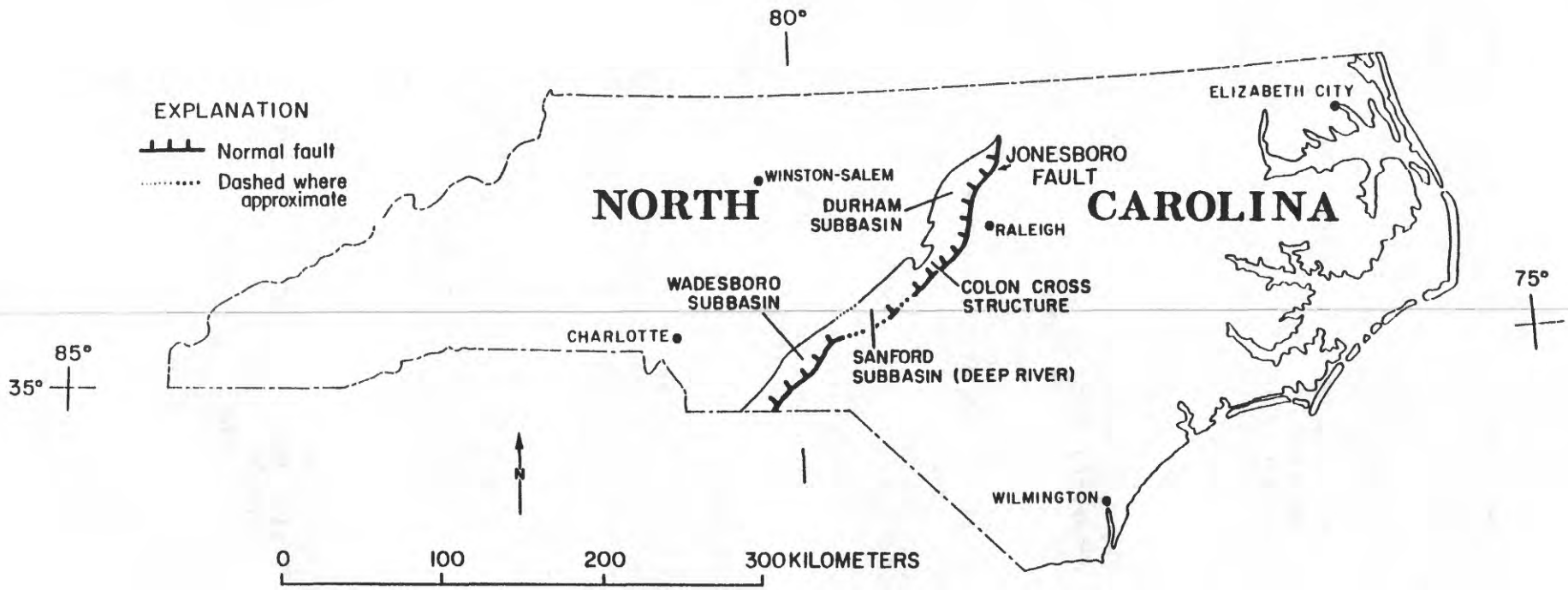

Figure 2. Durham Triassic basin and tectonic features within the Durham Triassic basin.

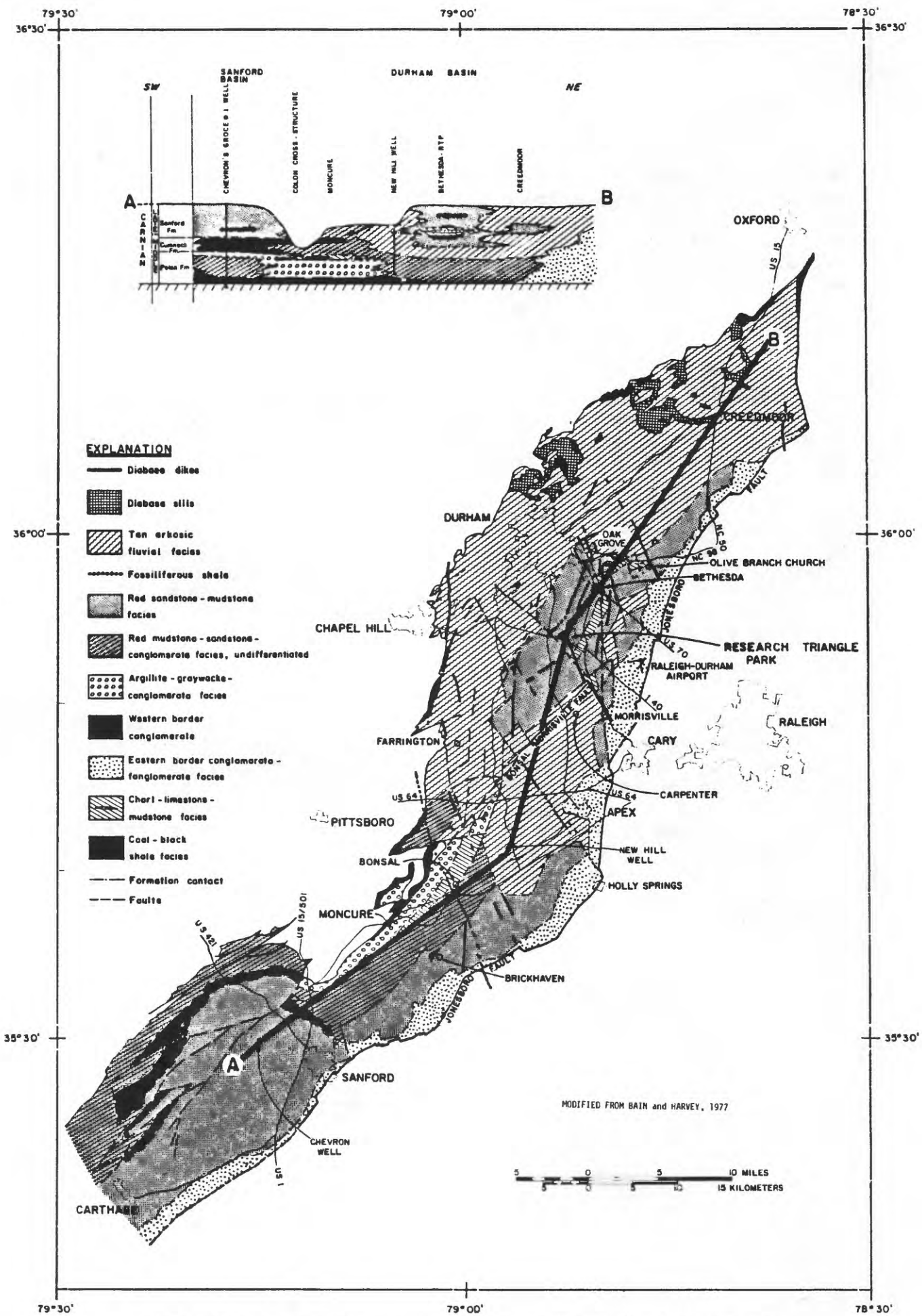

Figure 3. Reconnaissance geologic map for part of the Durham Triassic basin.

The past existence of Triassic lakes in the Durham Triassic basin is indicated by limy red mudstones, flaggy sandstones, varved argillities, graywacke, and chert. Limy mudstones, nodular and thin limestones, and chert are generally confined to the interfan areas. Argillite, graywacke, and also some chert are found along the western edge of the basin.

Coal and black shale are found between the alluvial fan areas where sedimentation was restricted at times when the basin was obviously tectonically stable. All of these lithologies, as did their respective environments, grade laterally and vertically into one another. Only the thin chert and coal beds are useful temporal marker horizons.

The Upper Triassic sedimentary rock mass was intruded by diabase dikes and sills in Late Triassic and Early Jurassic time. Individual dikes are spaced about 1 km apart and range in width from 0.3 to 20 m and as much as 16 km in length. Dikes trend north, northwest, northeast, and east, but the trend is predominately north and northwest.

The basin is faulted longitudinally and transversally creating individual horsts and grabens that are as small as 1 km by 3 km. Most are rotated to the east and southeast. A few horst and graben structures are tilted to the north. Vertical displacement along the largest known intrabasin fault is at least 300 m and perhaps as much as 600 m. All known faults are high angle and normal. Extensive strike slip movement is suspected but has not been demonstrated.

Acknowledgments

This project and the resulting report have benefitted from the contributions and cooperation of many individuals whose assistance is acknowledged. Individuals and corporations who have helped in the interpretation and processing of data include: Officials of Chevron, U.S.A., Inc., Mobil, and Amoco Oil Companies; Drs. D. M. Stewart, R. Ingram, and P. Raggland of the University of North Carolina at Chapel Hill; Officials of the North Carolina Division of Earth Resources; Dr. J. M. Parker, University of North Carolina at Raleigh; Norman Tilford and John Ferguson of Ebasco Corp.; and Bruce Harvey, Campbell College, Buies Creek, North Carolina.

CRITERIA FOR WASTE DISPOSAL EVALUATION

There are many sociological, political, and engineering considerations related to the emplacement and storage of waste in subsurface rocks. The geological considerations that are a concern of this report are the adequacy of the Triassic rocks of the Durham Triassic basin to accept liquid waste, the competency of the host and overlying rock to contain and isolate the waste for a length of time sufficient for acceptable degradation to occur, and the identification and evaluation of those natural resources from which the waste must be contained.

The task of identification, location, and evaluation of those subsurface natural resources that need protection from waste contamination is essentially one of determining the local spatial distribution of those resources that are of economic importance today or have a reasonable chance of being so over the life of the waste reservoir.

The ability of rocks to accept waste in the subsurface depends primarily on porosity, permeability, and the nature of chemical compatibility of the native fluid with the injected wastes. A subsurface geological horizon having high permeability and porosity values is therefore desirable. Injection into formations having reduced porosity and permeability not only reduces the amount and rate of injection, but raises the risk of fracturing the reservoir rock because of the increased head use to maintain injection rates. However, where waste toxicity is high and volumes are low, the "tight" formation may be worthy of consideration.

The chemical composition of the waste fluid to the native fluid can drastically affect injection rates. Chemical reaction at the native-wastewater interface can completely plug the available rock pores and reduce injection rates. Likewise, the chemistry of the rock may be very important if, for instance, swelling clays such as montmorillite are present.

The saturation and pore pressure of the reservoir rock is no less important. A completely saturated reservoir accepts other fluids only by compression of the native fluid, compression of the aquifer skeleton, displacement of native fluid across adjacent rock boundaries or to a surface outcrop, or by rupture of subjacent and superjacent confining layers.

The conditions that control the ability of a waste reservoir to contain and isolate the injected wastes until pollution levels have been reduced to some acceptable level include but are not limited to:

1. the competency or strength of the reservoir rock, that is, the degree to which the rock will react plastically or rigidly to seismic and man-made stress.

2. the nature and extent of the confining layers surrounding the waste reservoir; their permeability should be low enough that waste fluid will not escape and their strength great enough that they will not normally be breached by seismic or hydraulic stress.

3. the internal hydraulic gradient; that is, the hydraulic properties and spatial limits of the reservoir need to be sufficiently known so that the rate, direction, and ultimate discharge of the waste are predictable.

4. the extent to which internal chemical reactions between injected wastes and native fluids and rock minerals cause clay swelling, abnormally high reservoir pressures, or degradation of the confining layers.

The above criteria have guided the data-gathering activities of this project and are used in this report to evaluate the suitability of the Durham Triassic basin for liquid waste storage.

DISTRIBUTION OF NATURAL RESOURCES

The feasibility of waste storage in rocks in the Durham Triassic basin depends in part on the identity, location, and value of any natural resources which are presently economic or have a fair chance of becoming an economic resource during the life of the stored waste.

The Durham Triassic basin contains coal, oil shale, oil, gas, calcium phosphate, ammonium sulfate, ground water, uranium, and thorium. Figure 4 shows the general distribution of the basin's resources. Only coal and water are of proven economic importance and the coal only marginally so.

Coal

The Cumnock Formation of the Sanford subbasin contains bituminous coal in two beds about 8.5 to 12 m apart (Reinemund, 1955). The uppermost coal bed is known as the Cumnock coal. It is the thicker and has produced all but a few hundred tons of the total production from the basin. The Gulf coal below is thinner and has a mineable thickness over a much smaller area than does the Cumnock. The Cumnock coal occurs in three benches over an area of 194 km^2 (fig. 4). It is thickest in the northern part of the Deep River area where it reaches 1.2 m. It thins laterally by an increase in shaliness, finally being replaced by shale, siltstone, and sandstone.

The Gulf coal underlies an area of only about 67 km^2, being thickest and of best quality in the northern part. Generally, it is confined to one bench which is up to 0.8 m thick.

Other coal seams are found elsewhere in the Durham Triassic basin. Reinemund reports a shaley coal between Brickhaven and Moncure that is 13 cm thick (fig. 5) and one north of Merry Oaks which is 28 cm thick. Both were tentatively correlated with the Cumnock Formation by Reinemund (1955). Cornet (personal communication, 1977) reports that coal collected by Emmons (1856) near the Copper Creek Coal prospect west of Moncure has a Pekin age; however, the coal prospect north of Merry Oaks is in a basal position and may also be Pekin in age.

Fossiliferous black shale containing conchostracons, ostracoda, and plant fragments is found in the central part of the Durham Triassic basin (fig. 3) in what appears to be a lacustrine environment. These fragments are tentatively assigned to the Cumnock Formation. Gray shale containing plant fragments is occasionally found in a basal position in the Durham Triassic basin and is probably a Pekin equivalent. It is possible that coal occurs elsewhere in the Durham Triassic basin in the deepest parts. If so, such deposits are most likely of small areal extent for there is no surface evidence of a large paludal environment outside the Deep River coal area.

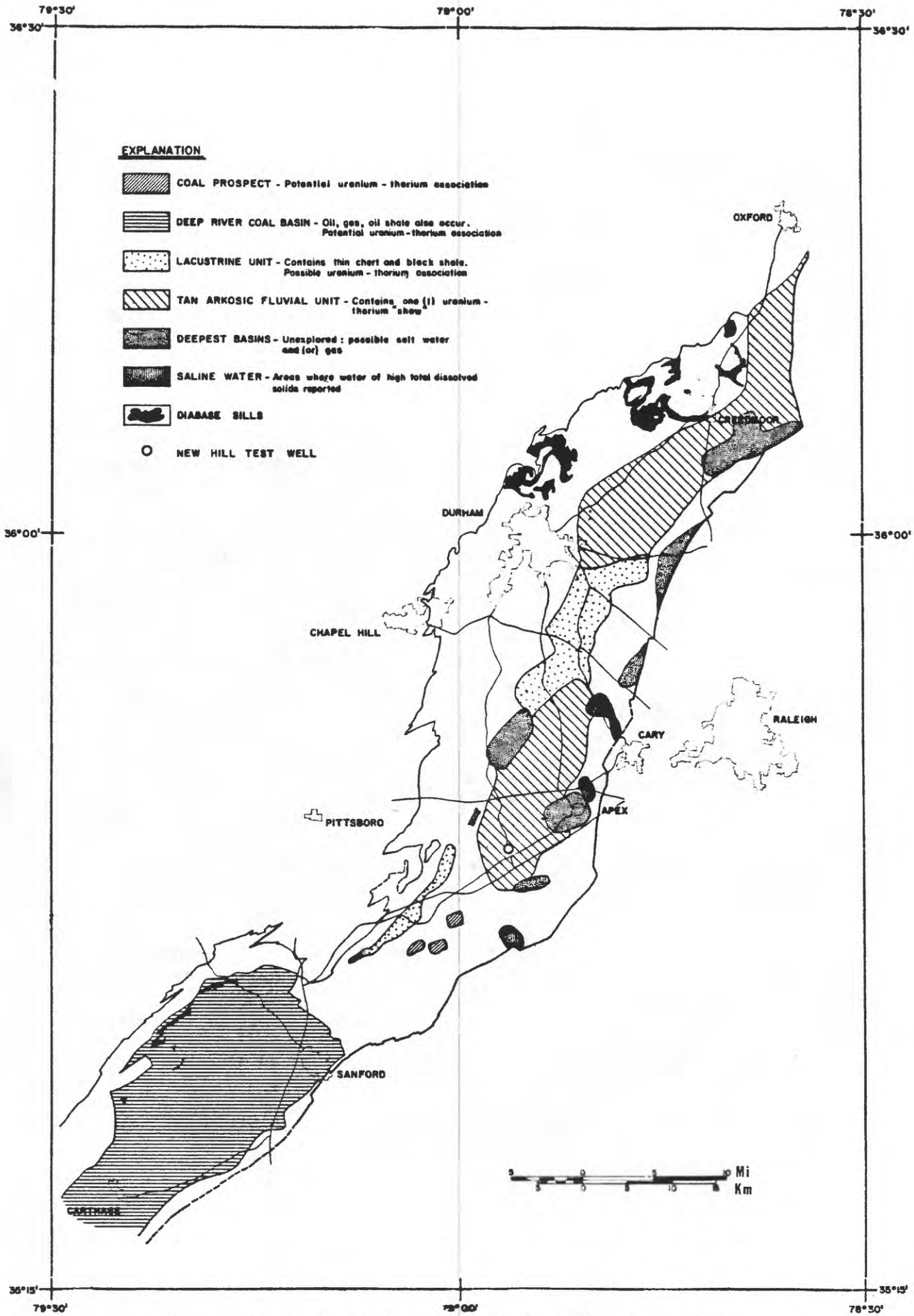

Figure 4. Potential natural resources of the Durham Triassic basin

The coal in the Deep River area is offset by faults and intruded by diabase dikes and sills. The faulting causes local thinning and thickening near the faults that increases the mining difficulty and cost. The diabase dikes have coked the coal for several meters on either side of the dikes (Reinemund, 1955). The sills have coked the adjacent coal for several meters beyond which the coal grades from anthracite to unaltered bituminous coal.

The main bench of the Cumnock coal has a fixed carbon content of 53 to 60 percent, a sulfur content of 1 to 4 percent, and a heat rating of 27,900 to 32,600 kJ/kg (kilojoule per kilogram). Total recoverable (assuming 50 percent recovery) reserves were calculated by Reinemund to be 60.5×10^6 Mg (megagrams).

Oil Shale

Black shale containing kerogen is associated with the coal in the Deep River basin and shows of oil and gas were encountered in core holes drilled by Reinemund and in Chevron's Groce No. 1 test well. Tests made by Vilbrant (1927) and the U.S. Geological Survey (Reinemund, 1955) indicate that the oil yield ranges from a trace to 66.8 L/Mg from beds that range from 0.3 to 15 m thick. Reinemund calculated shale oil reserves of 1.026×10^9 L between depths of 0 to 915 m, assuming an average yield of 121 L/Mg.

Blackband and Fertilizer

The black shale of the Deep River area also contains calcium phosphate and ammonium sulfate which have been used for fertilizer. Analyses of the blackband and shale beds by the U.S. Geological Survey and U.S. Department of Agriculture show that beds near the coal contain as much as 35.5 kg of $(NH_4)_2SO_4$ and 15.5 kg of $Ca_3(PO_4)_2$ per megagram. Reinemund estimated reserves of 732,000 Mg of $(NH_4)_2SO_4$ and 976,000 Mg of $Ca_3(PO_4)$--above a depth of 915 m.

Iron Ore

The blackband beds also contain limonite and siderite having a metallic content averaging about 15 percent. Limited use was made of the ore locally following the Civil War.

Ground Water

Potable ground water in the Durham Triassic basin in amounts suitable for domestic supplies is generally confined to the upper 90 m of Triassic rock. Below that depth yields are so low that the small amount of additional water obtained does not justify the increased cost of drilling. Ground water, however, near the surface in the Triassic rocks occurs in the primary and secondary interstices which have been enhanced by weathering and leaching of cement. The apparent resistivity of the formation water in the Sears No. 1 test well indicates that water having dissolved solids concentrations less than about 5000 mg/L occurs to at least 1009 m in parts of the basin. The yield of rocks at those depths is extremely low, and the water, therefore, is probably of no economic value. There are no data that suggest that major supplies of potable ground water exist at depths greater than 300 m in the Durham Triassic basin; however, only two wells have been drilled deeper than 300 m.

Uranium - Thorium

Reinemund reports that tests made on 140 m of core of the Cumnock Formation show that the uranium content ranges from 0.001 to 0.003 percent.

Analyses of inhole gamma spectrometry logs for the Sears No. 1 well showed that uranium and thorium are present in small quantitities in rocks penetrated by the well (Keys, written communication, 1976). The high gamma-ray anomalies with which the uranium-thorium "shows" have been identified are apparently confined to a medium- to coarse-grained, fluvial, arkosic sandstone. The individual anomalies appear associated with both thin bedded sandstone and shale of possible lacustrine origin. Until the diagenetic history of the uranium-thorium "shows" are known and their association with a particular depositional facies determined, the spatial distribution as well as the economic value of uranium-thorium prospects must be speculative. The geographic extent of the arkosic sandstone unit with which the uranium-thorium shows are probably associated is shown in figure 4.

The areal distribution of the natural resources that needs to be considered in evaluation of the feasibility of waste disposal in Triassic rocks is shown in figure 5.

GEOPHYSICAL INVESTIGATION (STRUCTURAL GEOMETRY)

The external and internal geometry of the Durham Triassic basin must be known before its waste-disposal potential can be considered. Normally, the character and geometry of individual lithofacies and the subsurface architecture of the depositional basin is determined from existing well logs and samples. However, well data, for wells penetrating to underlying crystalline rocks, are practically nonexistent for the East Coast Triassic basins. The determination of the structural geometry of the Durham Triassic basin by the usual surface geologic mapping techniques is complicated by a combination of rapid facies changes, faulting, low relief, extensive vegetation, deep weathering, and a veneer of post-Triassic alluvium in places. The scarcity of outcrops and subsurface data has been alleviated by use of remote sensing and geophysical techniques. These techniques, described below, include: aeromagnetic mapping, side-looking airborne radar (SLAR), Landsat lineament interpretation, seismic profiling, electrical sounding, and gravity mapping.

The geophysical data discussed below describe a fault graben more complex than previously thought. The fault that produced the Durham Triassic basin probably was a deep crustal one expressed at the surface as a series of en echelon positive fault blocks which supplied sediment and negative fault blocks which received sediment. The irregular linear basin which resulted from faulting contains a spatial facies distribution controlled by the then existing combination of tectonic-climatic elements.

The Durham Triassic basin is not a simple half graben formed by a single master fault and the Triassic rocks of the basin do not dip monoclinally toward the Jonesboro fault. Instead, the eastern border is step faulted, and the basin is sliced by faults trending N. 45° E. parallel to the eastern border of the Sanford and Wadesboro subbasins. The subbasins have been rotated toward the east-southeast by postdepositional faulting. The slices are terminated to the northeast and in some places to the southwest by faults or fracture zones that trend nearly due north to northwest subdividing the basin into diamond- and triangular-shaped horsts and grabens. Most of the horsts and grabens tilt to the east and southeast. A few tilt north. The presence of a step-faulted eastern border implies that some of the conglomerate-fanglomerate along the eastern border formerly thought to be a late deposition product is actually an earlier one.

The position of paludal and lacustrine deposits on the eastern side of the Durham subbasin and on the western side of the Sanford subbasin and the presence of fanglomerate on the eastern side of the Durham subbasin and on the western side of the Wadesboro subbasin suggest that, during most of Triassic sedimentation, subsidence occurred on the east side of the Durham subbasin and on the west side of the Wadesboro and Sanford subbasins. Rotation to the east by faulting occurred before the intrusion of diabase.

An exhaustive review of the literature concerning the origin and structural development of the Durham Triassic basin is beyond the scope of this report. For greater insight, the interested reader is referred to Bain (1973), Bain and Harvey (1977), deBoer (1960), Glaeser (1966), Krynine (1950), McKee (1959), and Saunders (1963).

Seismic Reflection and Refraction Studies

The feasibility of subsurface waste storage in Triassic rocks is somewhat dependent upon their thickness and stratigraphic characteristics. Seismic reflection and refraction were used in the Durham Triassic basin to help determine the sedimentary and structural geometry of the Triassic rocks. Three traverses were shot in 1973-75 in cooperation with the Geology Department of the University of North Carolina at Chapel Hill. These seismic traverses, totaling 16 km in length, are located in the basin on either side of U.S. 64 between Cary and Pittsboro, North Carolina (fig. 5). The longest is a 10-km reflection section that crosses the Jonesboro fault at the basin's eastern edge. The second and third are refraction profiles that were located near the basin's western edge.

Seismic Line 1 - Cary to Green Level

Instrumentation used for each traverse consisted of a 24-trace Electrodynamic Instrument Corp., Protable Reflection Seismic System, Model PSS-1A.[1]/. Total line length for any single shot was 2,300 m. The shooting technique was a split spread with each successive shot overlapping to obtain multiple coverage for purposes of common-depth-point stacking.

Figure 6 is a generalized geologic depth section based upon interpretation of the seismic profile and a careful inspection and analysis of the records. Although the records were noisy and difficult to interpret, the following deductions can be salvaged from the data with some confidence.

1. The deepest portion of the basin as indicated on the traverse is about 1,400 m west of, but not immediately adjacent to, the Jonesboro fault. In fact, figure 6 indicates this deepest part of the basin to be located 5.7 to 7.3 km to the west of the Jonesboro fault.

2. Immediately adjacent to the Jonesboro fault the crystalline-rock basement "steps up" eastward toward the fault.

3. The basement is broken into many horsts and grabens, the maximum structural relief indicated to be about 1000 m in this traverse.

---

[1]/ The use of the brand name in this report is for identification purposes only and does not imply endorsement by the U.S. Geological Survey.

Figure 5. Index map of seismic traverses.

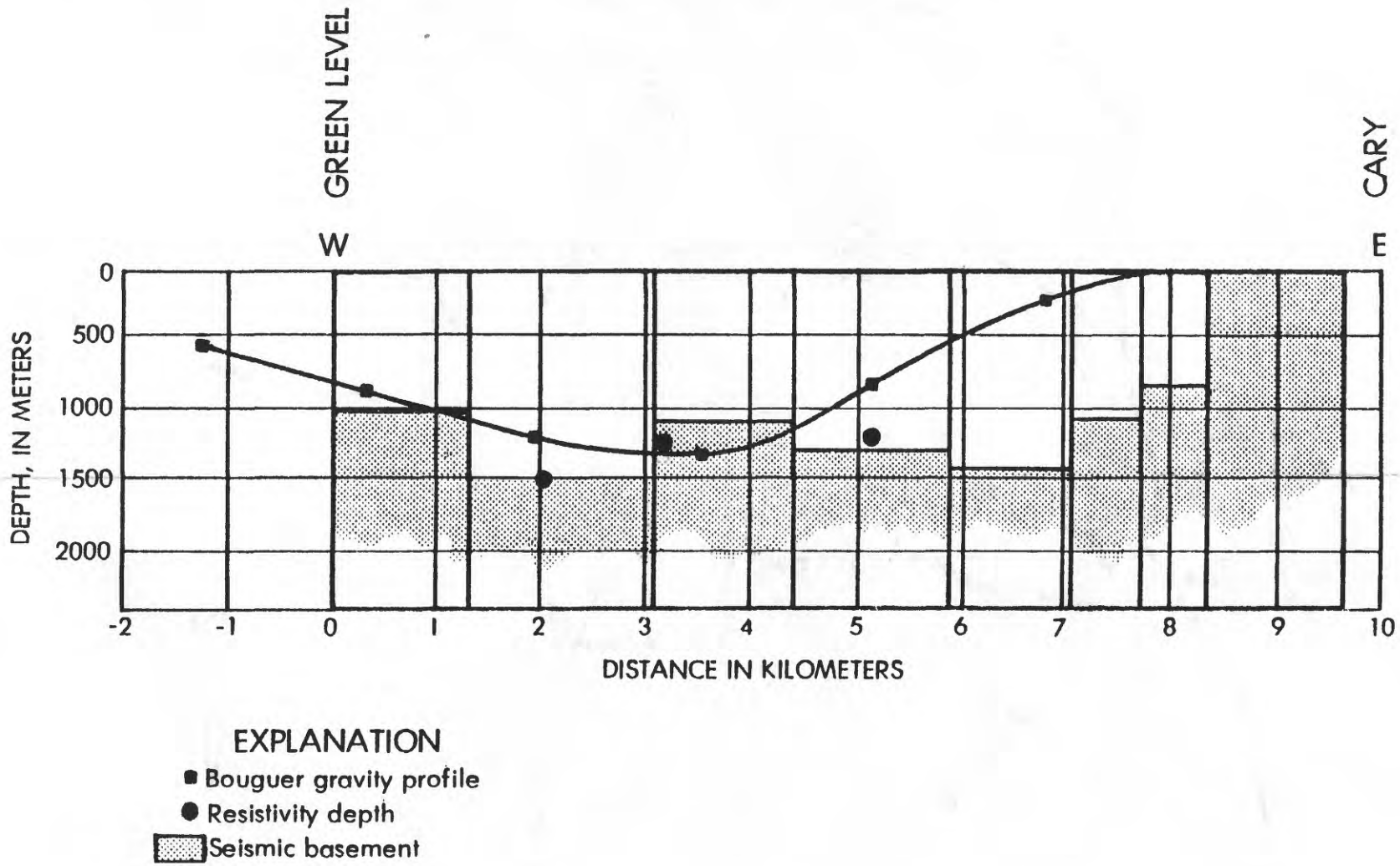

Figure 6. Resistivity depth points and gravity profile along seismic line 1.

4. Basement is shallowest (about 490 m) near the west end of the traverse about 8 km west of the Jonesboro fault.

5. Most of the faulting appears to be vertical, including the Jonesboro fault. Deviation from the vertical is probably not more than $\pm$ 5 degrees.

6. Immediately beneath the base of the Triassic sediments (within 600 m) are some diffractions in the data that could be caused by faulting.

Figure 7 is a map showing seismic traverse No. 1 relative to SLAR (side-looking radar imagery) lineaments, mapped faults, and roadcut geology. The lineaments on this map were transferred from the SLAR imagery using a zoom transfer scope. The black circles along the seismic traverse are the points where the vertical faults drawn in figure 6 intersect the traverse. The transfer of the SLAR lineaments and interpretation of the seismic profile in figure 6 were done indepedently by different people. The correlation is good. However, there are lineaments on figure 6 shown to cross the line of traverse which are not matched by SLAR lineaments on figure 7. The most noticeable example of the latter situation are the two faults just west of the Jonesboro fault. However, these two points are exactly in line along strike from two northeast-trending SLAR lineaments. Thus some, if not most, of the SLAR lineaments appear to be the surface expression of normal, near vertical faults. Correlation of the lineaments with lithologic contacts is less obvious. The most easterly of the northwest trending lineaments marks the contact between fanglomerate-conglomerate and red sandstone-mudstone, but the contact of the red sandstone-mudstone with the coarse tan to pink sand is not marked by an obvious SLAR lineament. Therefore, their contact may be a normal facies change rather than a fault.

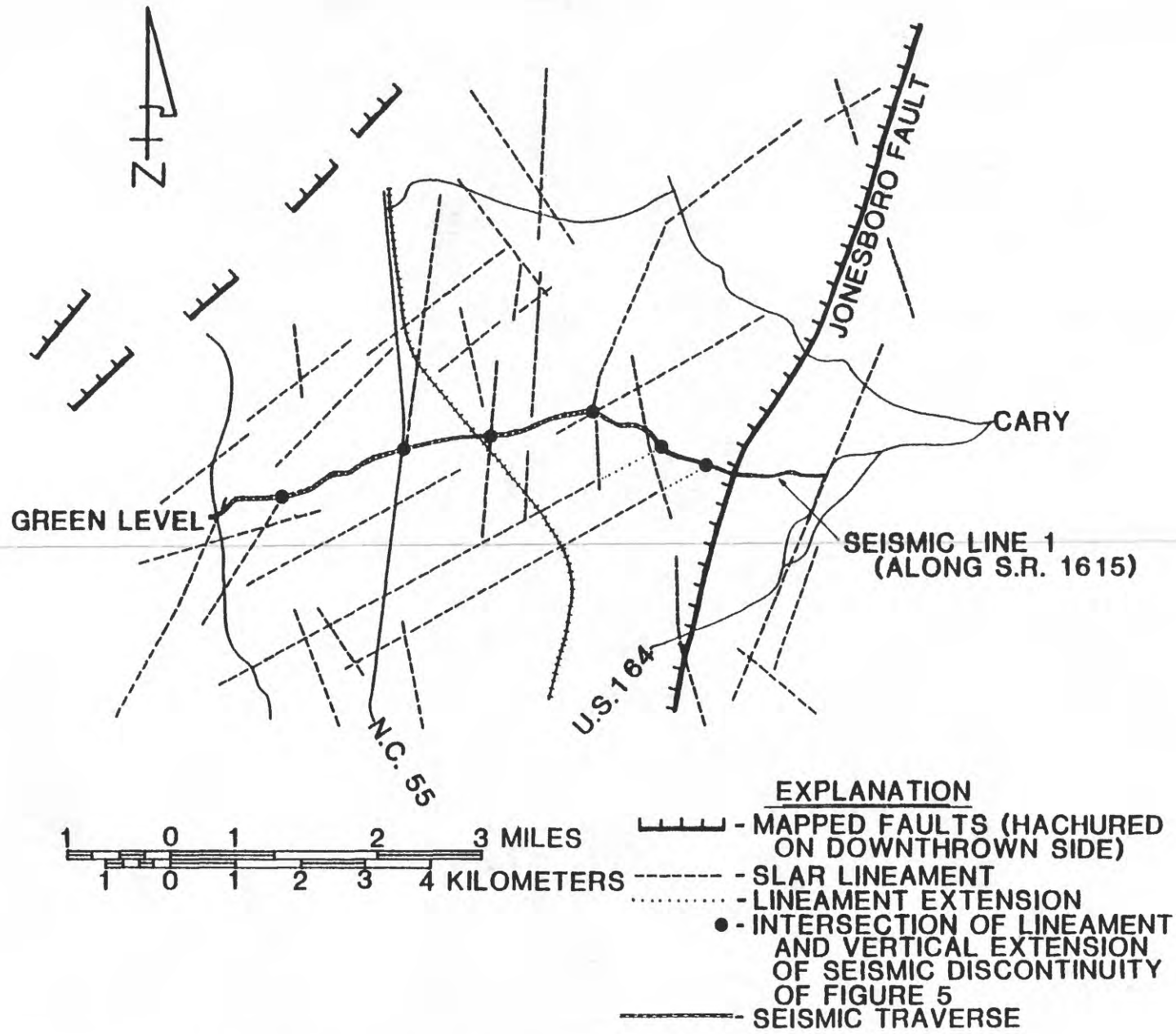

Figure 7. Side-looking airborne radar(SLAR) lineaments in the vicinity of seismic line 1

Seismic Lines 2 and 3

Seismic lines 2 and 3 (located on fig. 5) were recorded using the same equipment that was used on seismic line 1, but with only 100 percent coverage--that is, no stacking. The basement was shallow at this site, and the principal data were from refraction first breaks. However, some primary reflections were seen with two-way reflection times yielding similar depths as the refraction data. On several records, multiples were also seen which further corroborated the validity of the refraction analysis.

Figure 8 is the time-distance curve (line fitted by eye) for seismic lines 2 and 3 respectively. Gaps with no plotted points represent geophone failures. Plotted times are considered to be accurate to within $\pm$ 0.005 s. Calculated depths are referenced to a datum of 60 m above mean sea level (National Geodetic Vertical Datum of 1929).

Traverses 2 and 3 are near the present-day western border of the Durham Triassic basin. An outlier of "Slate Belt" type rocks lies immediately southwest of these traverses. From examination of field relationships, aerial photos, and SLAR lineaments this outlier of metasediment and metatuff appears to be an upthrown horst-block. Figure 9 shows the location of traverses 2 and 3 relative to known and suspected structural elements. Local Triassic lithologies include the argillite-graywacke-conglomerate and the red mudstone-siltstone-sandstone sequences intruded by northwest-trending diabase dikes. The sequences appear to be in fault contact. Both gravity and aeromagnetic data discussed in following chapters show a strong northeast-trending positive anomaly parallel to and just east of the fault labeled Bonsal-Morrisville on figure 9.

If the fault-block boundaries (see fig. 9) exist, the postdepositional structural history of the basin is even more complex. The sedimentary rocks here appear fractured by two sets of conjugate shears with rotation of most of the individual blocks to the southeast. Although the refraction data indicate the possibility of a fault separating the two traverses, no geologic lineament was observed in the field crossing the site in a north or northwesterly direction.

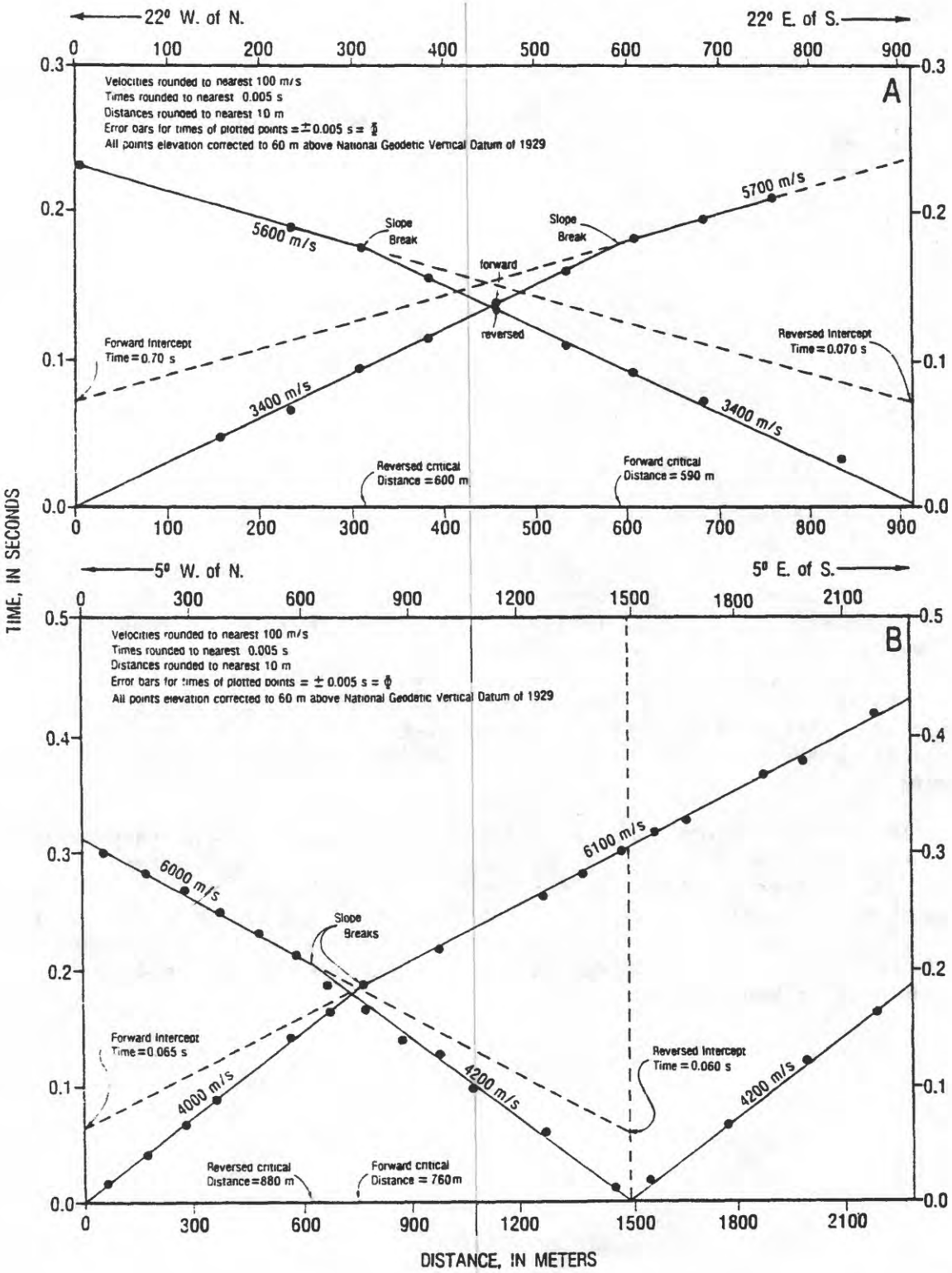

Figure 8. Refraction time-distance curves for (A) seismic line 3, (B) seismic line 2.

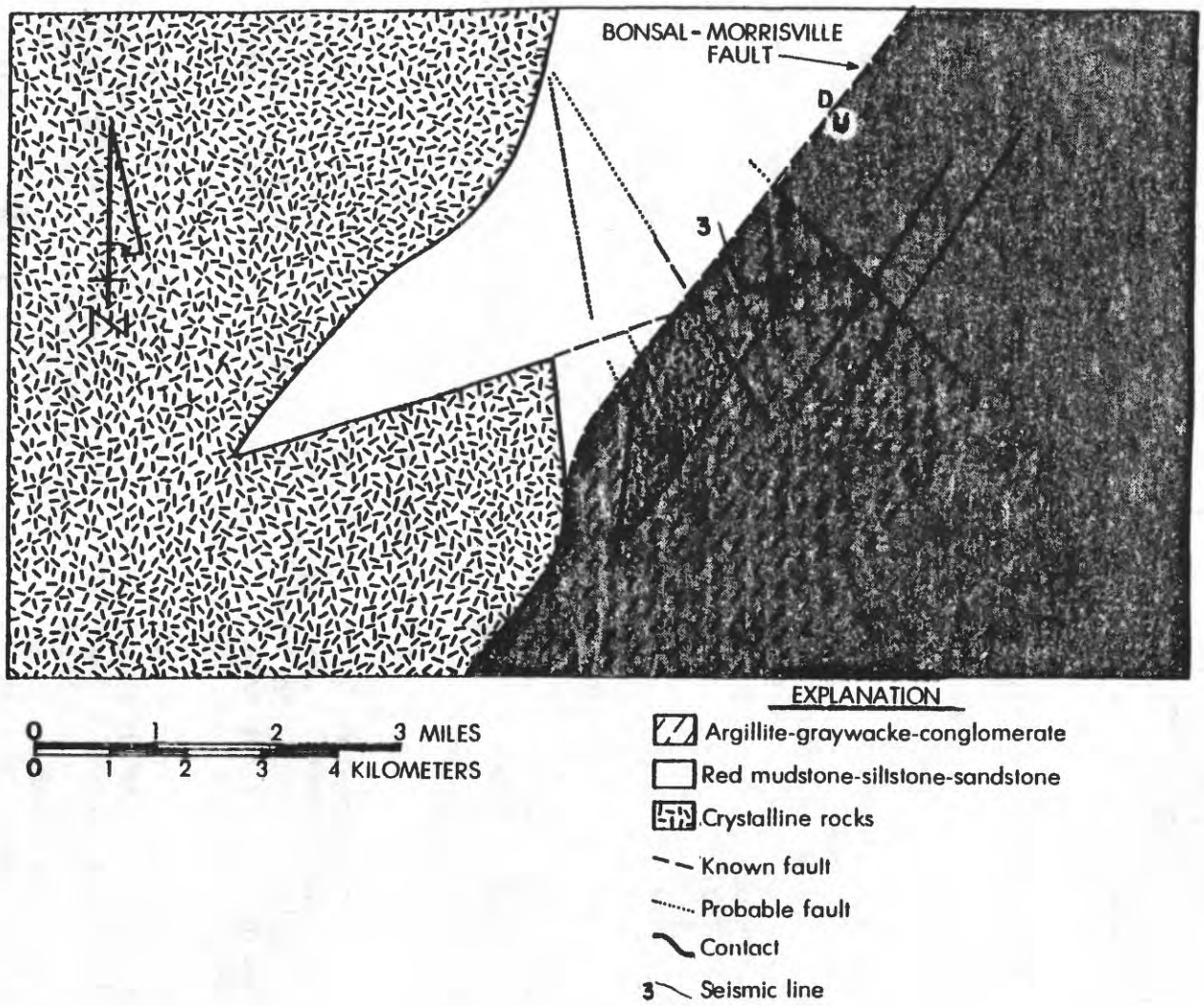

Figure 9. Generalized geologic map of seismic lines 2 and 3

Rounded to the nearest 10 m, calculated depths to basement for line 2 were 170 m on the north end and 180 m on the south end. Considering the possible errors in plotted times, determinations of critical distances, and intercept times, these depths are probably accurate to within ± 15 m. Hence, there may or may not be any real dip in the basement surface from north to south. Calculated depths for line 3 were all about 150 m regardless of which end of the traverse and which formula was used. Hence, although there is little or no dip along each line, there must either be some inclination in the basement surface or the basement is faulted.

Seismic Velocity of Triassic Rocks

The rocks of the Durham Triassic basin are typical of Triassic basins elsewhere - mostly sandstones and shales. The characteristic velocities of these rocks, however, are not typical of sandstone and shales from non-Triassic environments. Typical values for non-Triassic sandstones and shales (Birch, 1942) range from 1,800 to 3,600 m/s. The refraction data of lines 2 and 3 indicate seismic velocities ranging from 3,400 to 4,200 m/s. Sonic-log measurements taken by Marine (oral personal communication, 1977) in the buried Dunbarton basin in South Carolina, indicate velocities in excess of 5,800 m/s for Triassic rocks in that basin. Sonic-log velocities in a nearby test well drilled to 1143 m ranged from approximately 3,600 to 5,500 m/s below a depth of 152 m. Laboratory analysis of core from this test well under simulated overburden conditions indicated velocities ranging from 3,300 to 5,100 m/s. There is apparent but not conclusive evidence of a velocity anisotrophy within the Triassic rocks. Measurements made on three pieces of core at 120° spacings normal to the horizontal axes of the core indicated a maximum p-wave anisotrophy of 4 percent.

Airborne Magnetometer Survey

An airborne magnetometer survey of the Durham Triassic basin was made to determine the degree to which (1) the magnetic anomalies thus mapped would aid delineation of the lateral continuity of Triassic lithologies and subbasins and (2) the broad changes in magnetic susceptibility would be related to depth of sedimentary rocks.

The total magnetic intensity in and surrounding the Durham Triassic basin was mapped at 152 m above ground level with an airborne magnetometer with flight lines spaced 0.3 km apart. The mapping was a cooperative project of the U.S. Geological Survey, the North Carolina Department of Mineral Resources, and the Wake County Planning Commission. Figure 10 is a generalized contour map of the measured data, on which the magnetic reference field has been removed and the rectified data contoured at a 60-gamma contour interval. Removal of the magnetic reference field enhances the anomalies resulting from local inhomogeneities in the Earth's crust.

The areal distribution and shape of magnetic anomalies suggest a structural model of alternating intrabasin horsts and grabens that are alined in a 40° E. direction. The horst and grabens are crossfaulted, intruded by diabase dikes, predominantly rotated to the southeast, and stepped up toward the eastern boundary fault.

The depth to basement along the upthrown side of the Bonsal-Morrisville fault was estimated from half-slope and maximum-slope methods to range from 610 to 1,200 m. Depth to basement on the downthrown side was calculated to be 1,800 m, assuming an estimated magnetic susceptibility contrast across the fault of 0.0025. If the basement rocks are more basic, the computed throw and therefore the depth to basement on the downthrown side is somewhat less. The resistivity profile A-A' (fig. 20) indicates that depth to basement on the upthrown side is about 500 m and on the downthrown side is about 1,100 m. The same susceptibility contrast across the Jonesboro fault has been used to estimate maximum depth to basement along the eastern side of the Durham Triassic basin to be approximately 2,100 m near Apex. Note, however, that the magnetic pattern does not change appreciably across the fault between Apex and Holly Springs indicating very little susceptibility contrast across the fault or very shallow depths to basement. The Jonesboro fault is better defined on the aeromagnetic map (than on the gravity map) where rocks of apparent major differences in magnetic susceptibility are in contact.

Side-looking Radar Lineations

Side-looking airborne radar (SLAR) imagery was collected to ascertain effectiveness of this exploration technique to define faults and diabase dikes in the deeply weathered and heavily vegetated rocks of the Durham Triassic basin.

Radar energy effectively penetrates cloud cover, vegetation, and the upper few millimeters of soil. Part of the broadcasted radar energy is returned to the airborne radar recorder in proportion to the character of the ground and cultural features. In general, longer-wavelength radar imagery gives sharper definition of culture but poorer geologic information. Shorter-wavelength imagery gives better definition of geologic character but poorer cultural definition.

Imagery of the latter type has been collected by the Geological Survey over the Durham Triassic basin from Wadesboro to Oxford, North Carolina. The lineations observed on the radar imagery from the Durham area have been transposed to a corrected base and are shown in figure 12. The declination of these lineations is presented in figure 13 from each look direction and is combined on a Cartesian plot (fig. 24) of East Coast lineaments.

Lineations observed on the SLAR imagery as well as Landsat imagery can be identified in the field or from maps as diabase dikes, faults, lithologic contacts, streams, roads, power lines, pipelines, and field-edge corner reflectors. Power lines, pipelines, and most field-edge corner reflectors and roads can be defined on the imagery by their extreme linearity. Abandoned roads, logging trails, slightly sinuous roads, and property lines that trend in one direction (usually due north and due east) are more difficult to delineate.

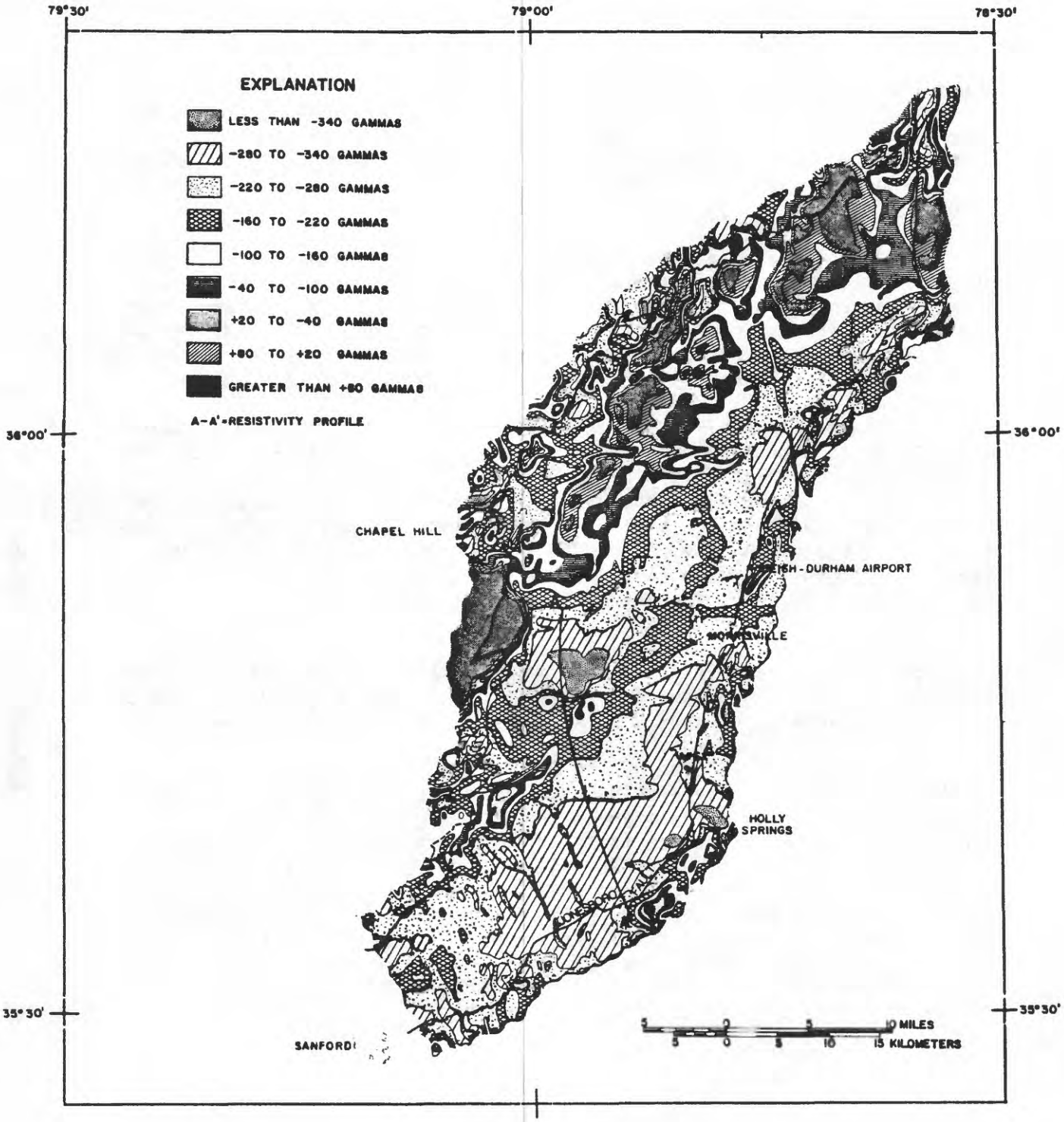

Figure 10. Aeromagnetic map for part of the Durham Triassic basin

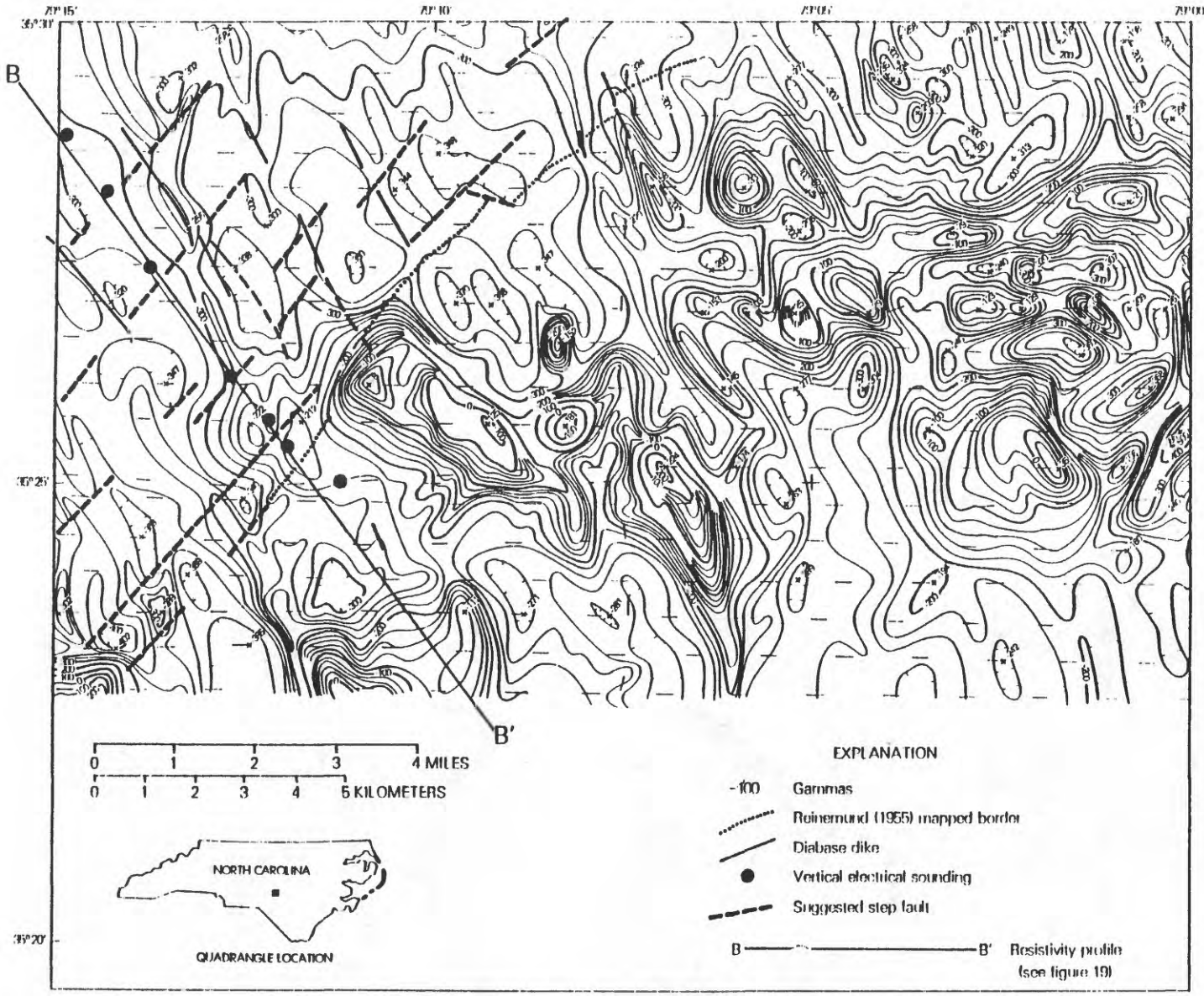

Figure 11. Aeromagnetic map of eastern border south of Sanford, N.C.

Of more importance to this study are the variations in shape and intensity of the magnetic field caused by local variations in the composition of the Earth's crust. Specifically, the rocks of the Triassic basins and the surrounding and underlying Piedmont complex differ in their magnetic susceptibility (ease of magnetization) and intrinsic magnetization. In general, sedimentary rocks are usually weakly magnetic as are most acidic igneous rocks. Mafic igneous rocks tend to be much more magnetic depending largely on their percentage composition of such iron-bearing minerals as magnetite, ilmenite, hematite, and pyrrhotite.

The detailed aeromagnetic map from which figure 10 was generalized reveals broad areas of alternating higher and lower magnetic grain trending northeast-southwest subparallel to the basin. Major exceptions are a large, intense oval-shaped magnetic high on the central western edge of the map and an arcuate, northwest-trending magnetic high truncating the regional structural grain at the southeast corner of the map.

The magnetic map gives somewhat better definition of basin boundaries and intrabasin structure than does the gravity. South of Sanford at the point where the resistivity profile B-B' crosses the east edge of the basin, (fig. 11), the amplitude and frequency of the magnetic anomalies indicate that basement is shallow at that point. In addition, the frequency, location, and trend of the step-fault slices are also revealed by the magnetic pattern. Because the dikes mapped by Reinemund (1955) are clearly right-laterally offset, the age of the step faults are at least post-diabase intrusive.

Farther northeast (fig. 10) the magnetic patterns indicate shallower basement along the Jonesboro fault near Holly Springs and Apex and the area along the basin edge between Morrisville and the Raleigh-Durham airport.

The entire western side of the Durham subbasin from Chapel Hill northward is underlain by highly magnetic basement rock or is intruded by thick diabase "sills." The major magnetic feature within the basin is a northeast-trending intrabasin fault appearing as a well-defined "positive" anomaly that bisects the basin and dies out to the northeast. As on the Bouguer and residual gravity maps (figs. 10 and 15), the positive magnetic anomaly over this fault is interpreted as downthrown to the northwest fault effectively separating the two areally smaller 100 mgal anomalies from the much larger one to the southeast (see also section A-A' of fig. 20). A basin similar to the one west of the Jonesboro fault is created on the northwest side of this intrabasin fault.

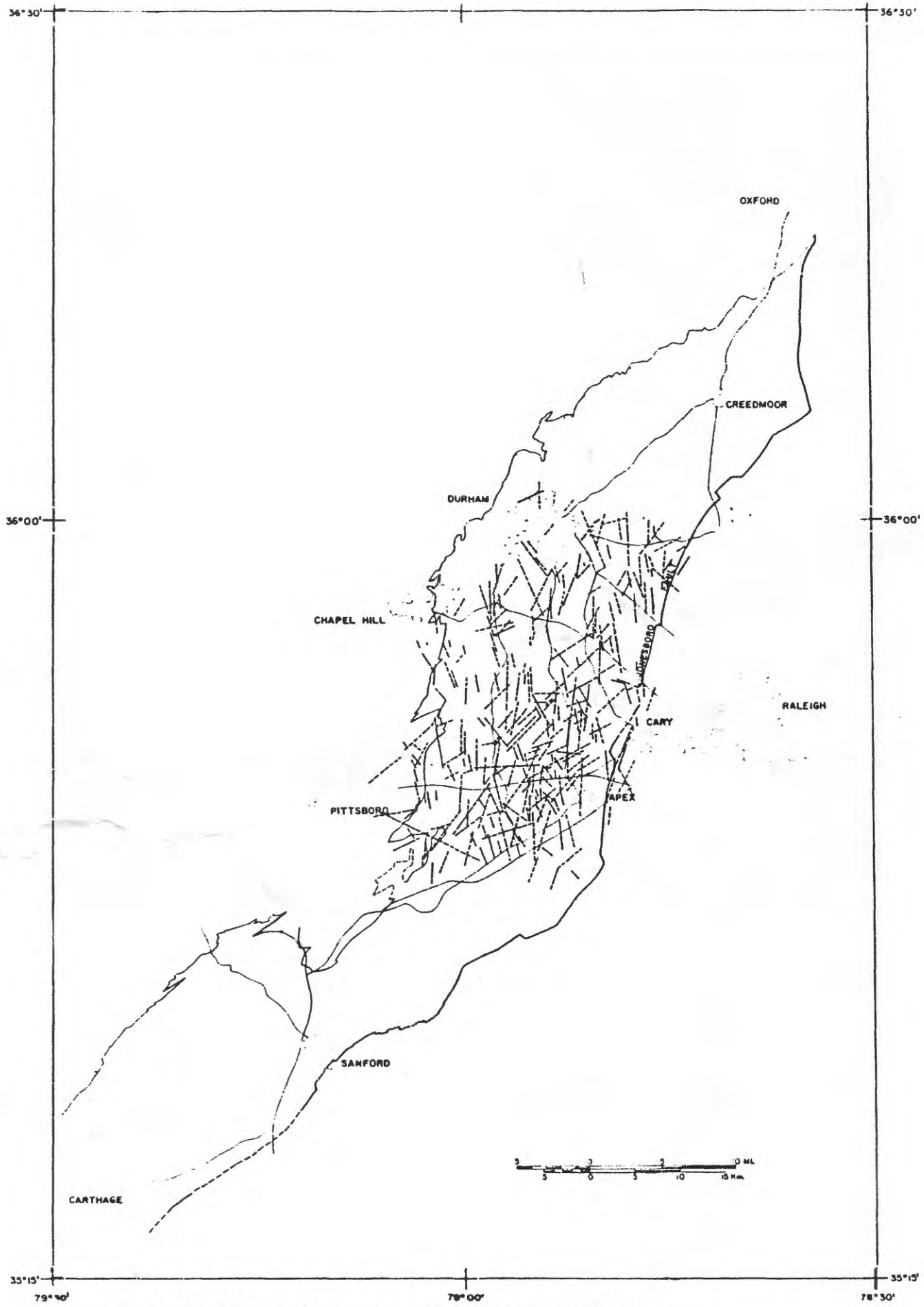

Figure 12. Side-looking airborne radar lineaments of the Durham Triassic basin.

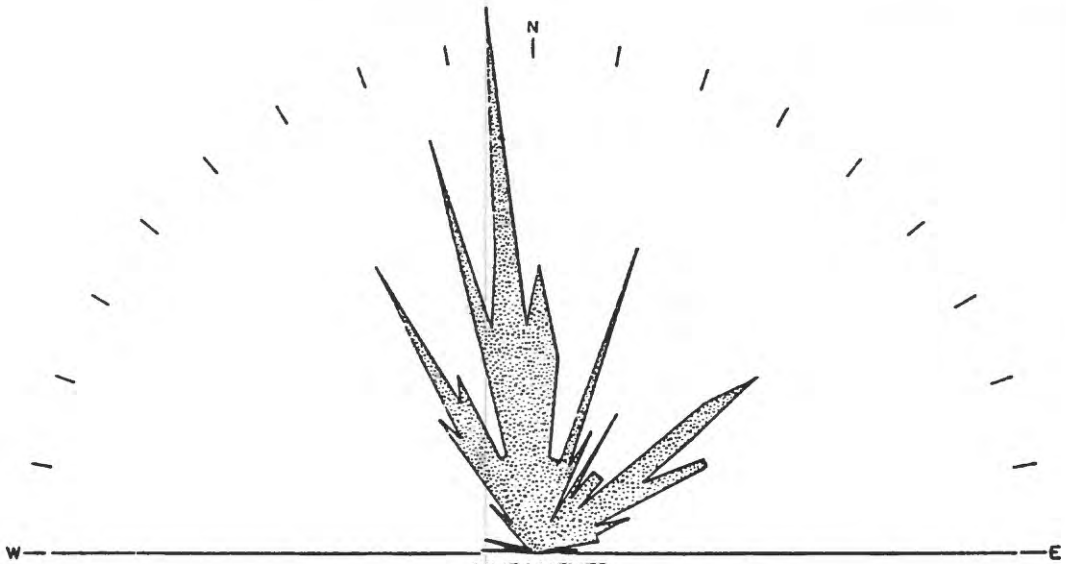

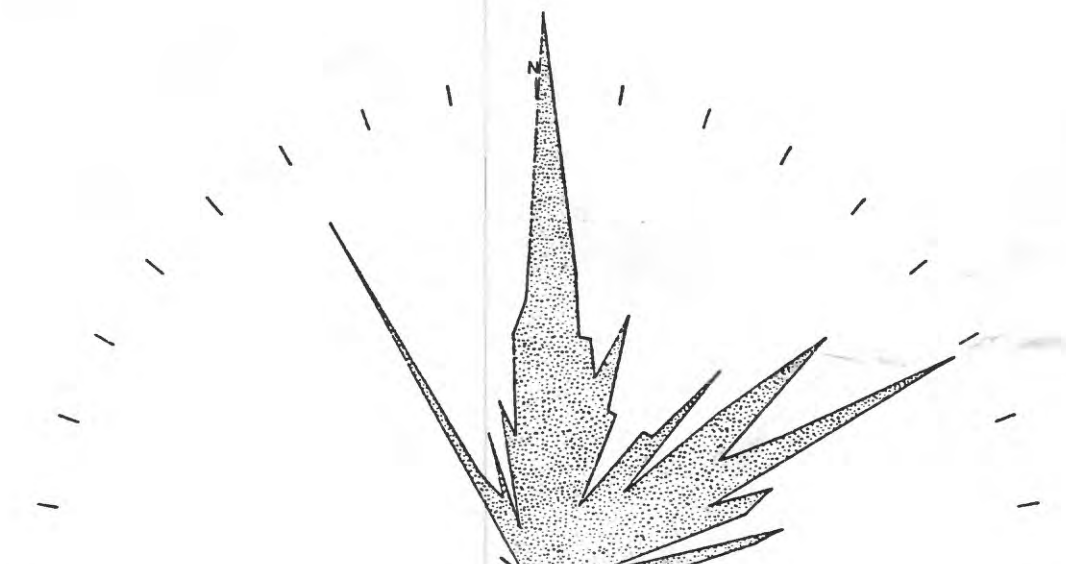

Figure 13. Rose diagrams showing strike of side-looking airborne radar lineaments.

Some observed lineations cannot be identified on the ground. However, some are parallel to known geologic elements and are therefore assumed to have some geologic significance.

Although not differentiated on the above figures, diabase dikes, which are discussed later, give unique raised outlines on SLAR imagery and are readily mapped as such where their length and thickness permits their resolution. Faults and fractures appear as linear depressions, or en echelon offsets. Roads and streams appear as linear depressions but the stream depression on radar imagery is generally broader in cross section.

The strike of observed radar lineaments cluster in narrow zones along N. 15° W. to N. 3° E., N. 50°-62° E., and N. 20°-30° W. Very few lineaments are observed in an east-west direction because this apparently was the "look direction" approximately perpendicular to the flight path.

The close agreement between radar lineations and magnetic anomalies is exhibited by figure 14. Major discontinuities in magnetic expression have a relationship to radar lineaments. Many of these radar lineaments have been identified on the ground as faults or dikes. Comparison of radar imagery to the residual gravity anomaly map shows the same general agreement (fig. 15). From comparison of these radar lineaments with gravity and magnetic anomalies and with the basin margins, most of the lineaments are related to geologic features. The analysis of radar lineaments has proven to be a valuable tool to refine and extend the structural-stratigraphic model produced from sparse outcrop data.

Gravity Measurements

A field gravity mapping program was started in the Durham Triassic basin during this project to obtain better definition of the Triassic subbasin and their individual depths.

The gravity data available for the Durham Triassic basin at the project's inception are published in Mann and Zablocki, 1961. Over 1,200 stations were measured in or near the Durham Triassic basin by Zablocki (1959) who produced Bouguer and residual anomaly maps and eight gravity profiles from the data. The Bouguer anomaly map shows a general ESE "descending" gradient across the basin of 20 to 35 mgal with local 3- to 10-mgal closures. Removal of the regional gradient by Mann and Zablocki produced a residual map with better definition of positive and negative gravity anomalies within the basin. The five major negative anomalies shown on the Mann-Zablocki map are presumed underlain by the thickest, less dense Triassic rocks. They are roughly elliptical in shape and have the steepest gradient on the southeast side.

The southeastern border of the Durham Triassic basin is broadly defined by the separation of anomalies on the residual gravity map. The border is not readily apparent on the Bouguer map. The deepest parts of the basin are inferred from the negative anomalies to occur through most of the central area of the Wadesboro basin, in the Sanford area of the Deep River subbasin, and between Moncure and Cary and in a long narrow area from Carpenter to Oxford in the Durham basin.

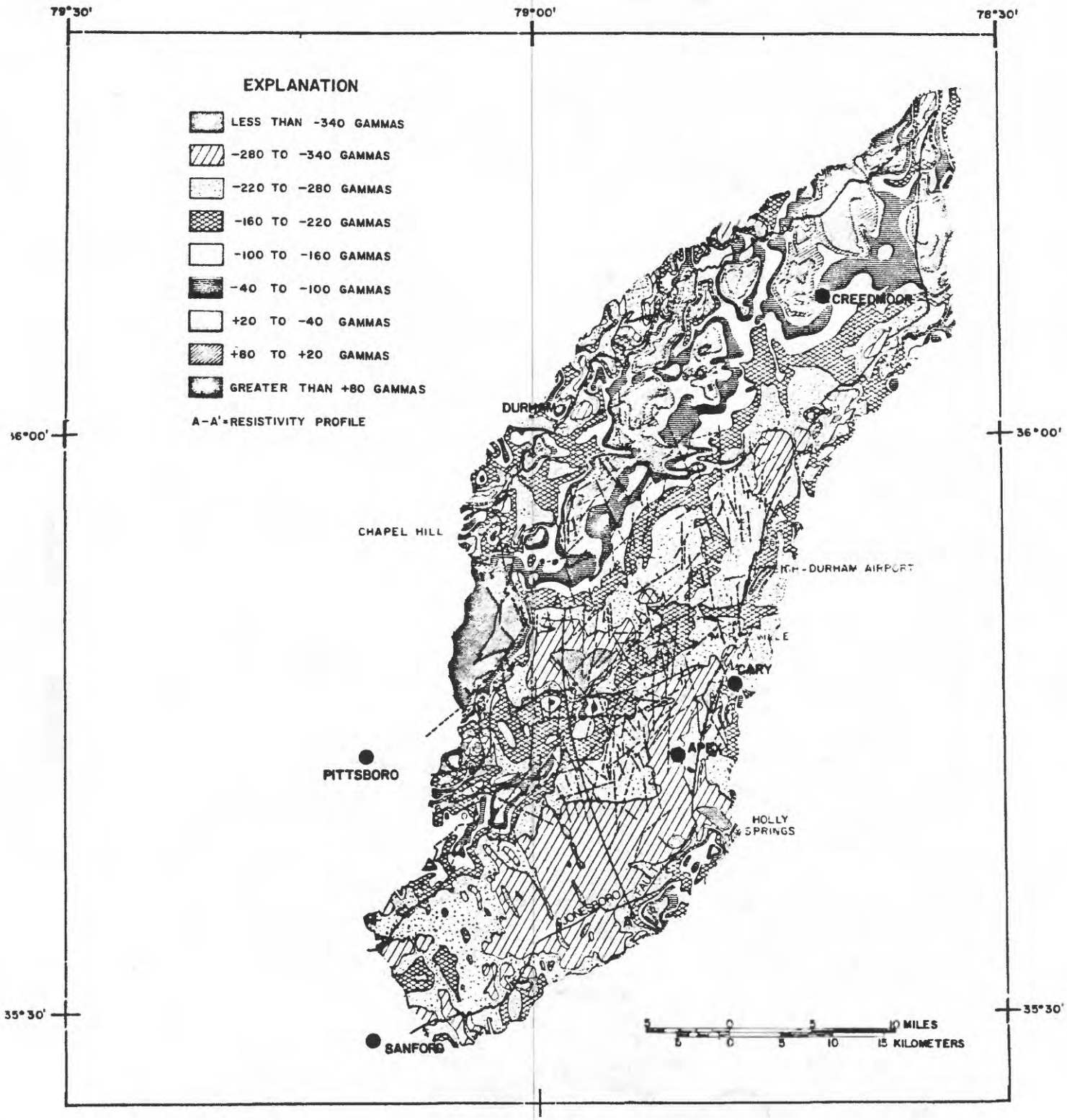

Figure 14. Side-looking airborne radar(SLAR) lineaments on the aeromagnetic map of the Durham Triassic basin

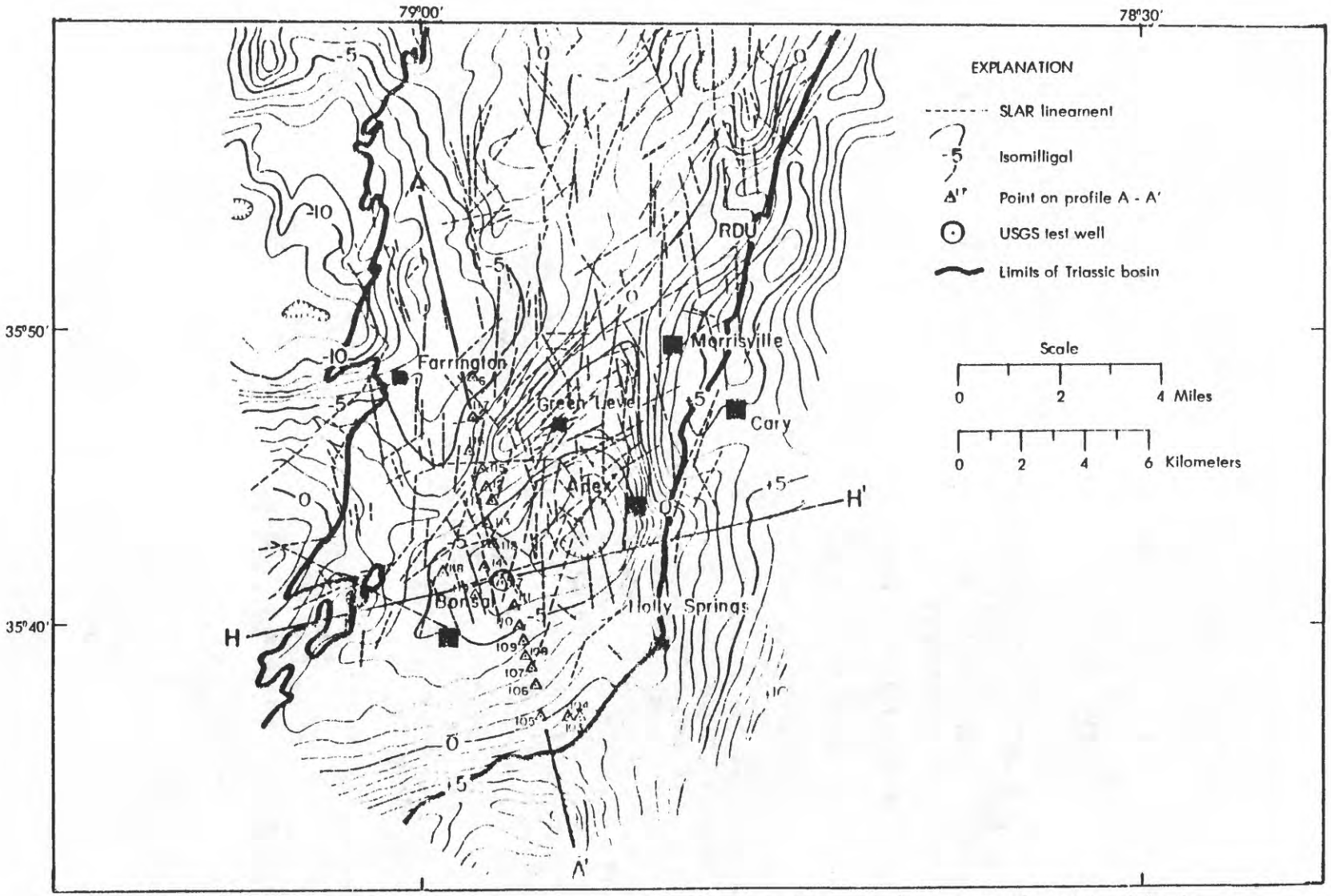

Figure 15. Side-looking airborne radar lineaments and residual-gravity anomaly map—Durham Triassic basin.

The eight gravity profiles presented were constructed by graphically removing the regional gradient. All profiles by Mann and Zablocki (1961) show some relief on the basement floor interpreted to be caused by faults or dikes. The southermost profiles show a faulted western border.

Estimates of the thickest parts of the Durham Triassic basin were calculated using an infinite-slab model and as assumed density contrast of 0.1 g/cm^3. Calculated depths at several locations were: 1,600 m depth east of Creedmore (5 mgal), 945 m depth between Durham and Raleigh (4.5 mgal), 1,980 m depth southwest of Cary (8.5 mgal), 610 m depth southeast of Moncure of the Colon cross structure (2.5 mgal), 1,770 m depth near Sanford (7.5 mgal), 1,860 m depth near Carthage (8 mgal), 2,350 m depth east of Candor beneath the Coastal Plain overlap (10 mgal), and 1,160 m depth near Wadesboro.

Additional gravity measurements were made in the Durham Triassic basin for this project to supplement the data set of Mann and Zablocki. An additional 600 gravity stations were measured to increase coverage.

The resulting more detailed Bouguer and residual gravity maps support the general subbasinal character of the Durham Triassic basin outlined by Mann and Zablocki, but they also reveal it to be structurally more complex than previously thought (see figs. 15 and 16). In particular the maps show that the gravity low in the Apex area is separated from the northern part of the basin by a northeast trending fault zone or horst in the basement. This horst or fault zone extends northeasterly from the Slate Belt "window" 3 km north of Moncure to at least the vicinity of Morrisville. The trend and attitude of the above structure is also supported by the resistivity, aeromagnetic, surface geology, and lineament studies and is further discussed in those sections. The more detailed maps also reveal an additional gravity and magnetic low on the northwest side of this structure which is interpreted to be a down-faulted wedge of Triassic rocks. The shape and gradient of the gravity anomalies along the eastern border of the basin indicate the possibility that there is much variation in depths to basement along it.

The regional gravity gradient was removed graphically along six sections across the Bouguer map of this project to determine the thickness and general geometry of the Triassic sedimentary deposits. The locations of these sections are shown in figure 16.

Section H-H' (see figs. 16 and 18) is approximately east-west from a point 3.2 km south of Apex on the eastern side. Use of the infinite-slab model and a density contrast of 0.117 g/cm^3 yields depth estimates consistent with depths determined by electrical sounding along this profile. Depth to basement at the New Hill well site is estimated from the residual anomaly profile to be 1,390 m and at the deepest point along the profile to be 1,695 m.

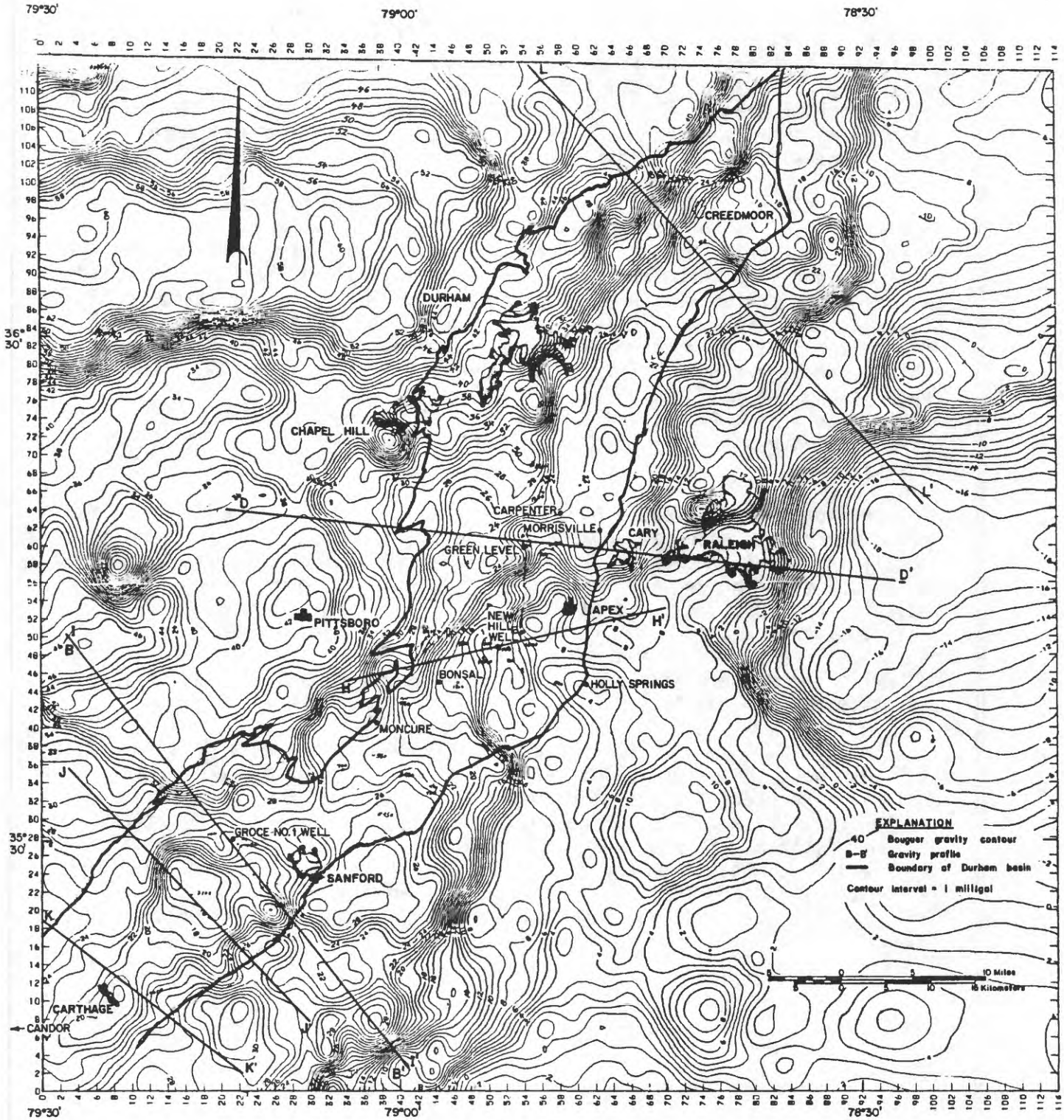

Figure 16. Bouguer gravity map with locations of gravity profiles in the Durham Triassic basin.

The average bulk density of the Durham Triassic rocks is 2.556 g/cm^3 based on 99 determinations from the Sears No. 1 well density log (fig. 28). Figure 17 illustrates the relationship of core densities to depth. The underlying crystalline rocks, then, have a density of slightly over 2.67 g/cm^3 --a reasonable density for acid igneous and pyroclastic rocks. Use of the 0.117 g/cm^3 gravity contrast in areas of the basin underlain by more basic rocks will result in estimates that are too deep.

Section A-A' (fig. 18) shows the Bouguer profile from the Chapel Hill area to a point on the border of the Durham basin 9 km southwest of Holly Springs. Note that both the Bouguer and residual gravity profiles show the basin divided into three negative gravity anomalies that become larger and more negative to the southeast. Geologically, they represent three fault slices on half grabens which are downthrown to the southeast. The Bonsal-Morrisville fault zone discussed above is represented by the sharp positive anomaly approximately in the center of the profile. Maximum depths along the profile are estimated from the gravity profile to be approximately 915, 1,224, and 1,677 m in each of the subbasins. The corresponding resistivity profile agrees in general shape with the residual gravity.

Section L-L' is along a NE-SE line across a negative anomaly south of Oxford where an electrical sounding has been made. The residual gravity anomaly indicates a depth of approximately 2,226 m at a point where the electrical sounding depth is estimated at 1,982 m. The maximum depth indicated by the 15 mgal anomaly is 3,050 m. Although the gravity depth estimates agree within about 10 percent with the electrical depth estimates, their correctness depends on the accuracy of the gravity contrast, the slope of the regional gravity gradient, and the validity of the infinite-slab model.

Section I-I' is a NW-SE line coinciding with resistivity profile B-B' south and west of Sanford. The residual gravity profile agrees reasonably well with the electrical sounding profile. Sounding 128 is at the site of the Chevron, U.S.A., Inc., Groce No. 1 well where basement was penetrated at about 1,555 m. The maximum depth of the Sanford subbasin along this profile is estimated from the residual gravity and resistivity values to be between 1,756 and 1,960 m. Both curves--particularly the resistivity--indicate that the basin is shallower (or steps up) near the eastern border fault.

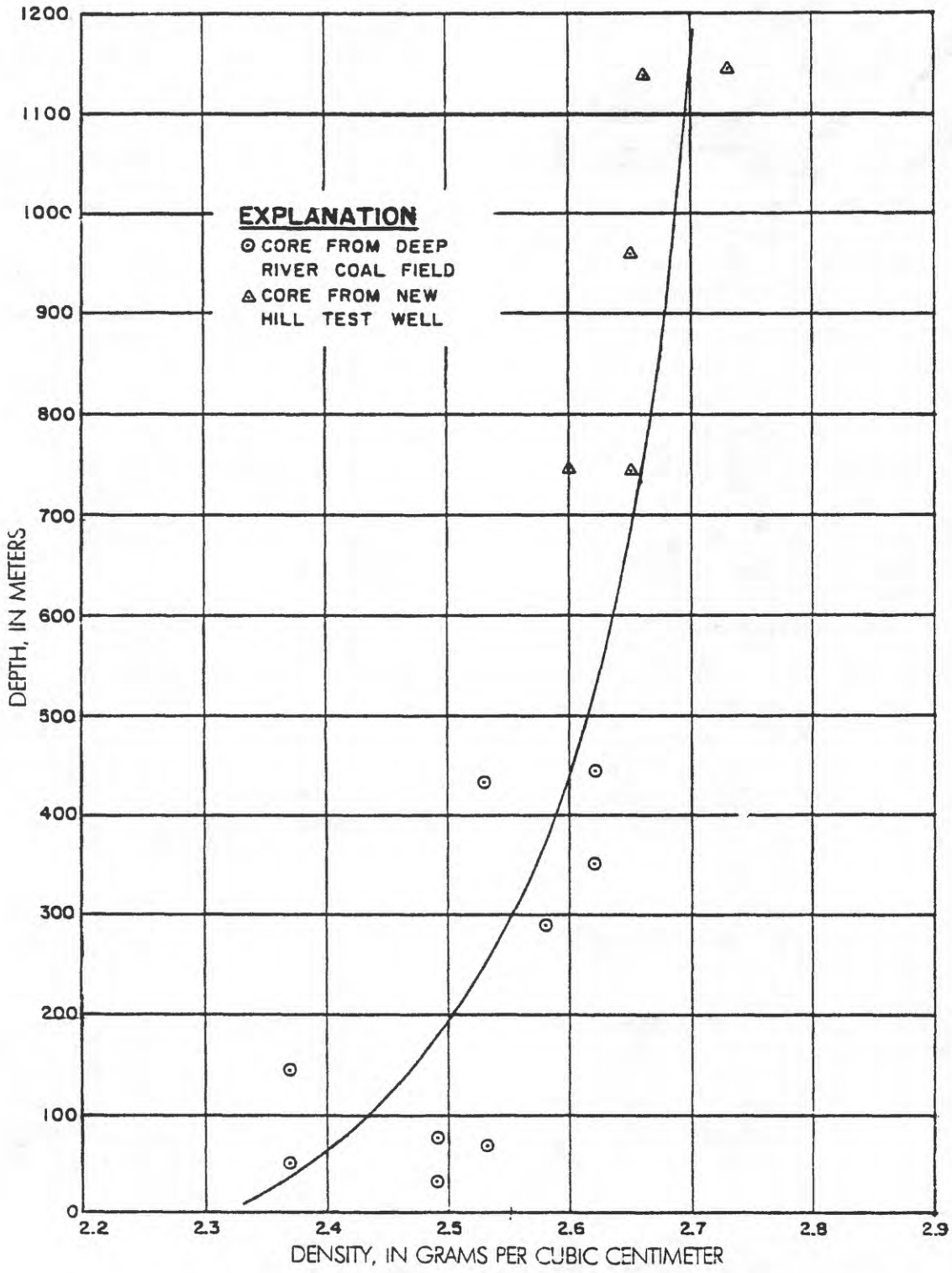

Figure 17. Bulk density of Triassic core versus depth.

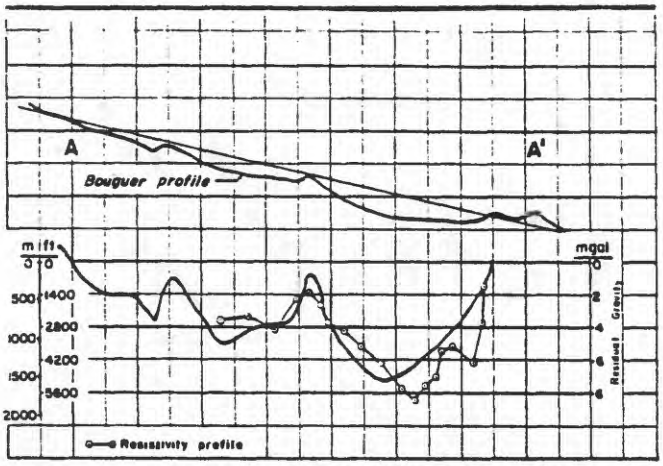

Residual profile AA' along resistivity profile AA'

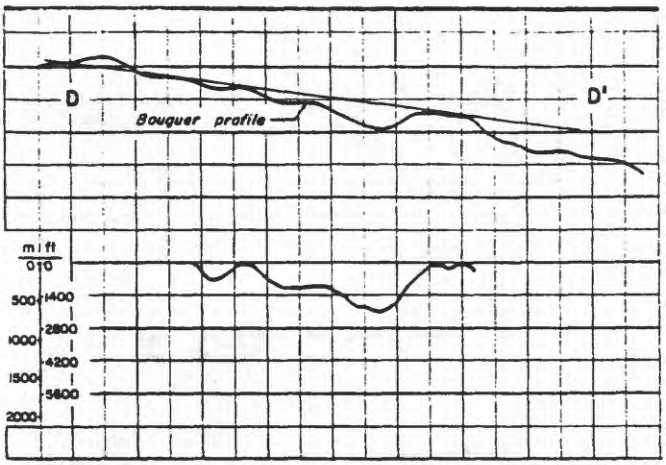

Residual profile DD'

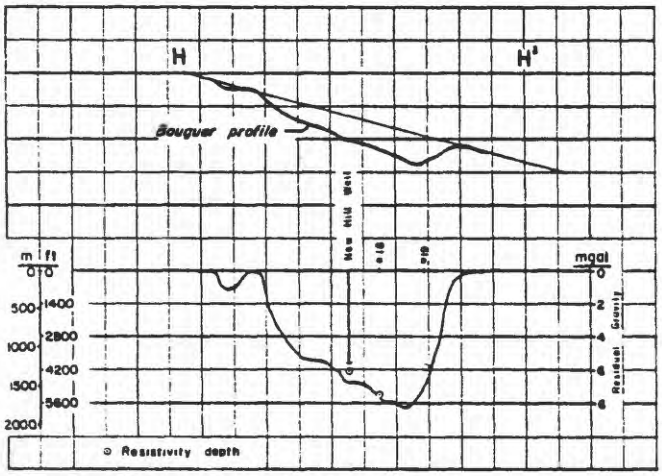

Residual profile HH'

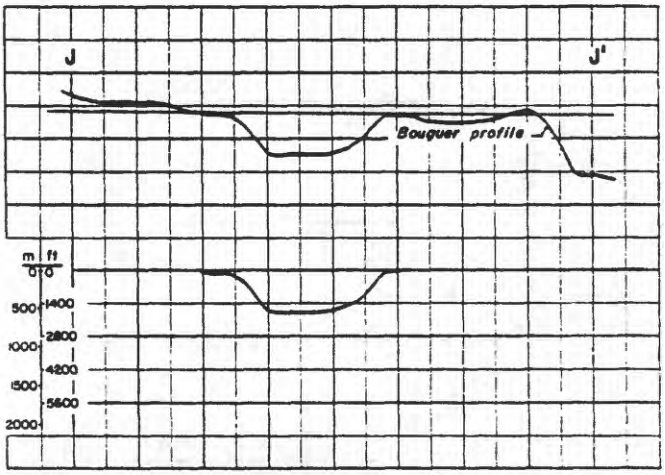

Residual profile JJ'

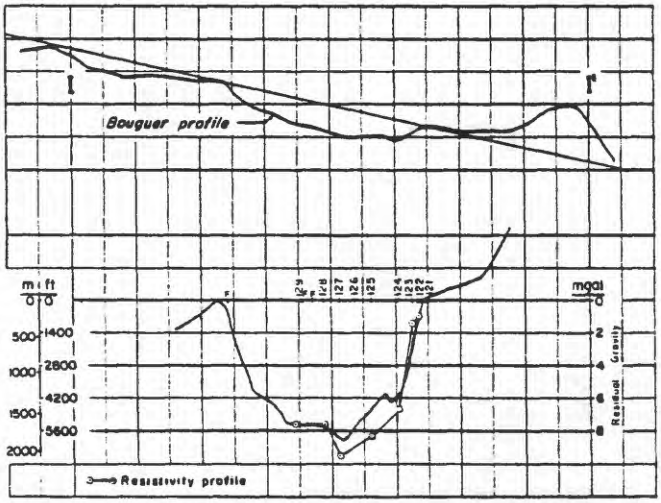

Residual profile II' along resistivity profile BB'

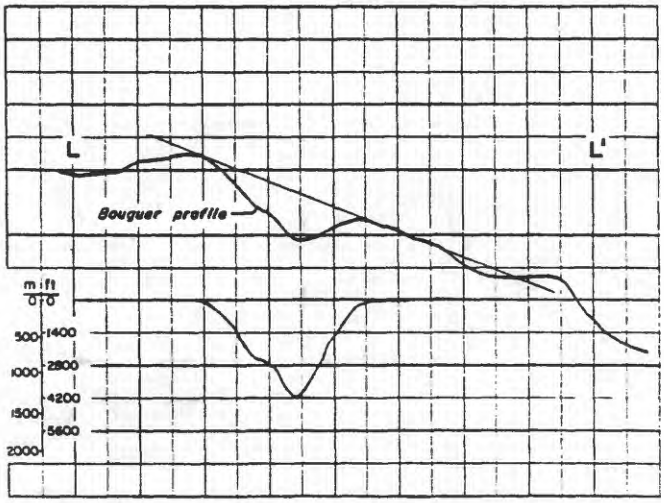

Residual profile LL'

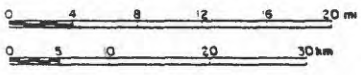

LOCATIONS OF PROFILES SHOWN IN FIGURE 16

Figure 18. Gravity profiles across the Durham Triassic basin

Section J-J' is a NW-SE line across the most negative part of the gravity low southwest of Sanford and is about 7.2 km southwest of section I-I'. The deepest part of the basin here is about 2,652 m deep and is on the northwestern side. The basin shallows to approximately 1,220 m at a point 12.8 km farther to the southwest. Section D-D' is a combined resistivity, gravity, and seismic profile from Green Level to Cary. The correlation between the resistivity and seismic depths is good and their correlation with the residual gravity profile is fair.

The point along the profile where the basin is deepest is about 2.6 km from the end showing Green Level. Both the seismic and resistivity depth estimates indicates that the depth is approximately 1,524 m. The shallow steplike character of the basement at the eastern border is shown by the seismic profile and perhaps corroborated by the convex charcter of the gravity profile on the eastern side.

Resistivity Profiles

The direct-current electrical resistivity method was used in the Durham Triassic basin to determine if sufficient resistivity contrast existed between the Triassic sedimentary rocks and among the individual units of that fill to make the resistivity method an effective exploration tool.

Subsurface exploration using the resistivity or electrical sounding method depends on the contrast in electrical conductivity of earth materials and their thicknesses relative to their depth. Best results are obtained where the geologic units are thick and their resistivity contrasts large. Interpretative precision decreases with depth as well as with decreases in bed thickness and resistivity contrast. Differences in porosity, clay content, and chemistry of interstitial water are the primary causes of contrasting electrical resistivity. Sixty-two Schlumberger electrical soundings were made along roads in the Durham Triassic basin in an effort to determine basin geometry, the depth of the sedimentary infill, and the spatial distribution of individual facies. Figure 19 shows the distribution of these soundings and the location of the resistivity profiles.

The symmetric quadrapole method was used wherein a pulsed direct current of up to 2 amperes is fed into the earth through two outer current electrodes, and the resulting potential difference is observed between two closely spaced inner electrodes at the center of the array (Ackermann and others, 1976). Maximum current electrode half-spacings were increased until plotted apparent resistivities clearly indicated the effects on basement rocks.

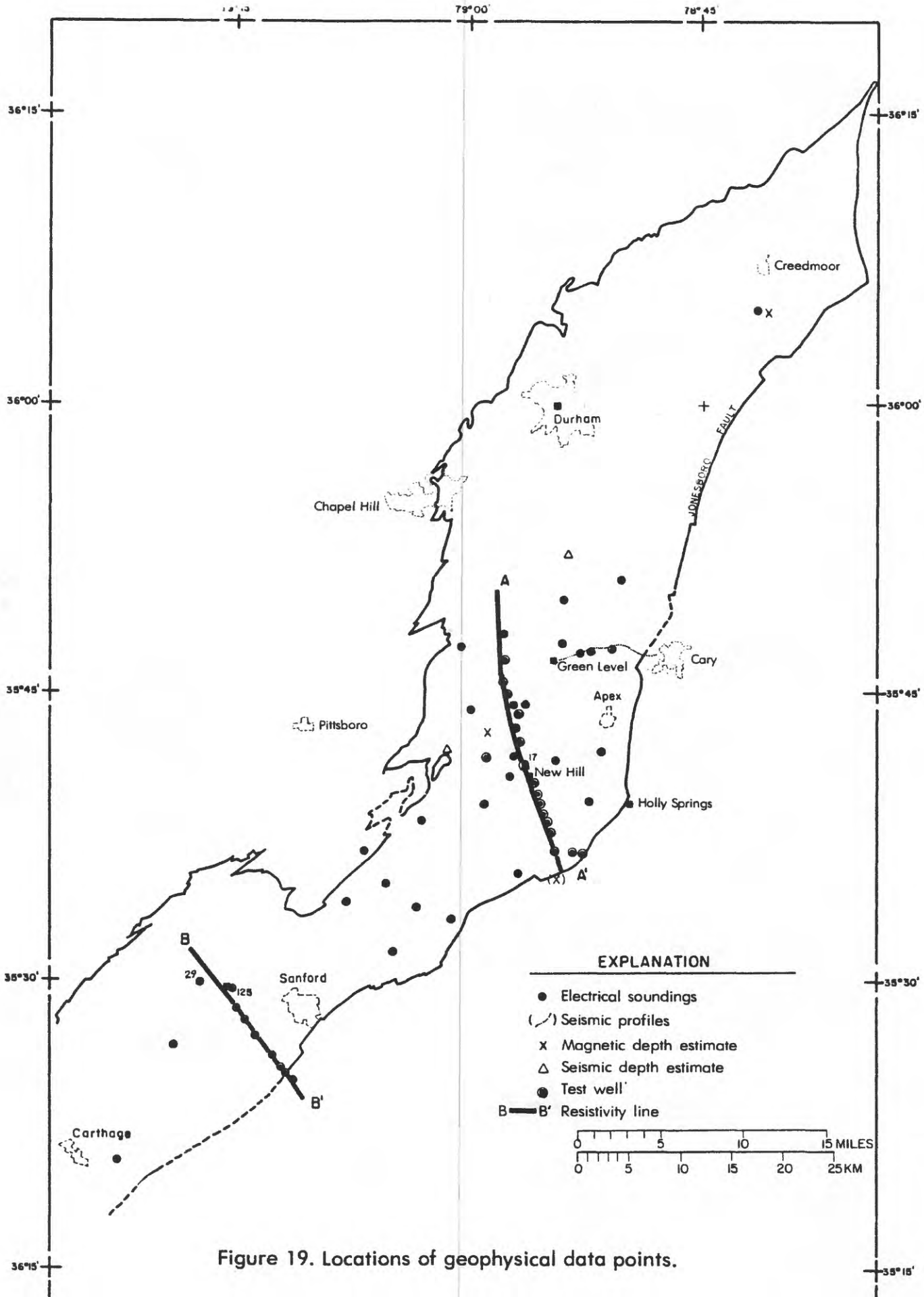

Figure 19. Locations of geophysical data points.

Field measurements in the Durham area showed a range in resistivity of 1,000 to 7,000 ohm-meters for the resistivity of the Piedmont crystalline rocks. Subsequent measurements in the Triassic rocks indicated that resistivities characteristically range from 30 to 350 ohm-meters and that the underlying basement rocks have resistivities similar to those for rocks measured outside the basin.

The individual smoothed sounding curves (apparent resistivity versus distance) were interpreted by inverting them into units of certain thicknesses and resistivities using a digital computer (see Zohdy and Bisdorf (1975) and Zohdy (1974)).

To restrict the range of possible solutions and to obtain an acceptable model, several geologic and electrical constraints were applied from knowledge of the local geology and of the characteristic rock resistivities. Contraints on known geological and geophysical interpretation included a single basement depth from an exploratory oil well (Groce No. 1) at sounding 128, resistivity logs from this well, and Geological Survey well data (Sears No. 1) at sounding 17. In addition to restricting resistivities greater than 1,000 ohm-meters to the Piedmont crystalline rocks and those less than 350 to the Triassic rocks, the layer immediately overlying basement was limited to a resistivity range of 250 to 350 ohm-meters. Additional constraints were applied to shallower layers to minimize differences in lateral resistivities, thereby improving correlation between soundings. Lateral changes still remaining are those that could not be removed easily and therefore most probably represent faulting and facies changes.

Section A-A'

To better illustrate the vertical and lateral distribution of resistivity across the basin, cross sections or resistivity profiles were constructed from the individual soundings (figs. 20 and 21). Figure 20 is a section trending NNW for 23 km from a point 7 km southwest of Holly Springs through New Hill to a point 6 km NW of Green Level. The horst and graben character of the basement floor and of the overlying sedimentary rocks is clearly displayed. Movement of the Bonsal-Morrisville fault has caused apparent vertical separation of the overlying Triassic rocks of up to 600 m. The southeastern edge of the basin is not defined on this section by a single master fault, but by a fault zone several km wide which causes the crystalline basement floor to "step down" into the basin. As a result the geoelectrical section has a synclinal shape. Near Green Level the basin shallows to approximately 380 m at sounding 12. The deepest part of the basin along this profile is predicted at sounding 110 to be 1,800 m.

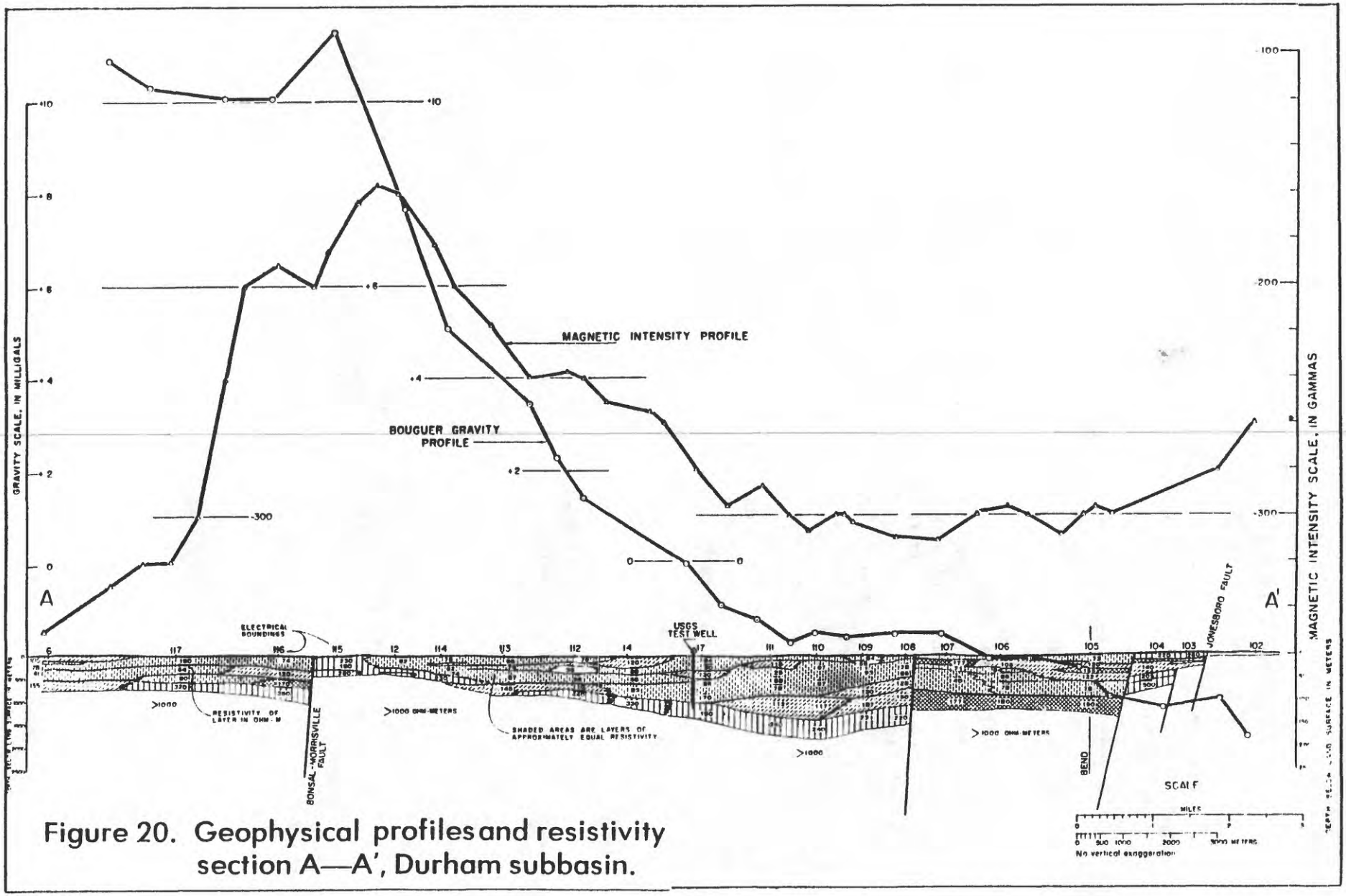

Figure 20. Geophysical profiles and resistivity section A—A', Durham subbasin.

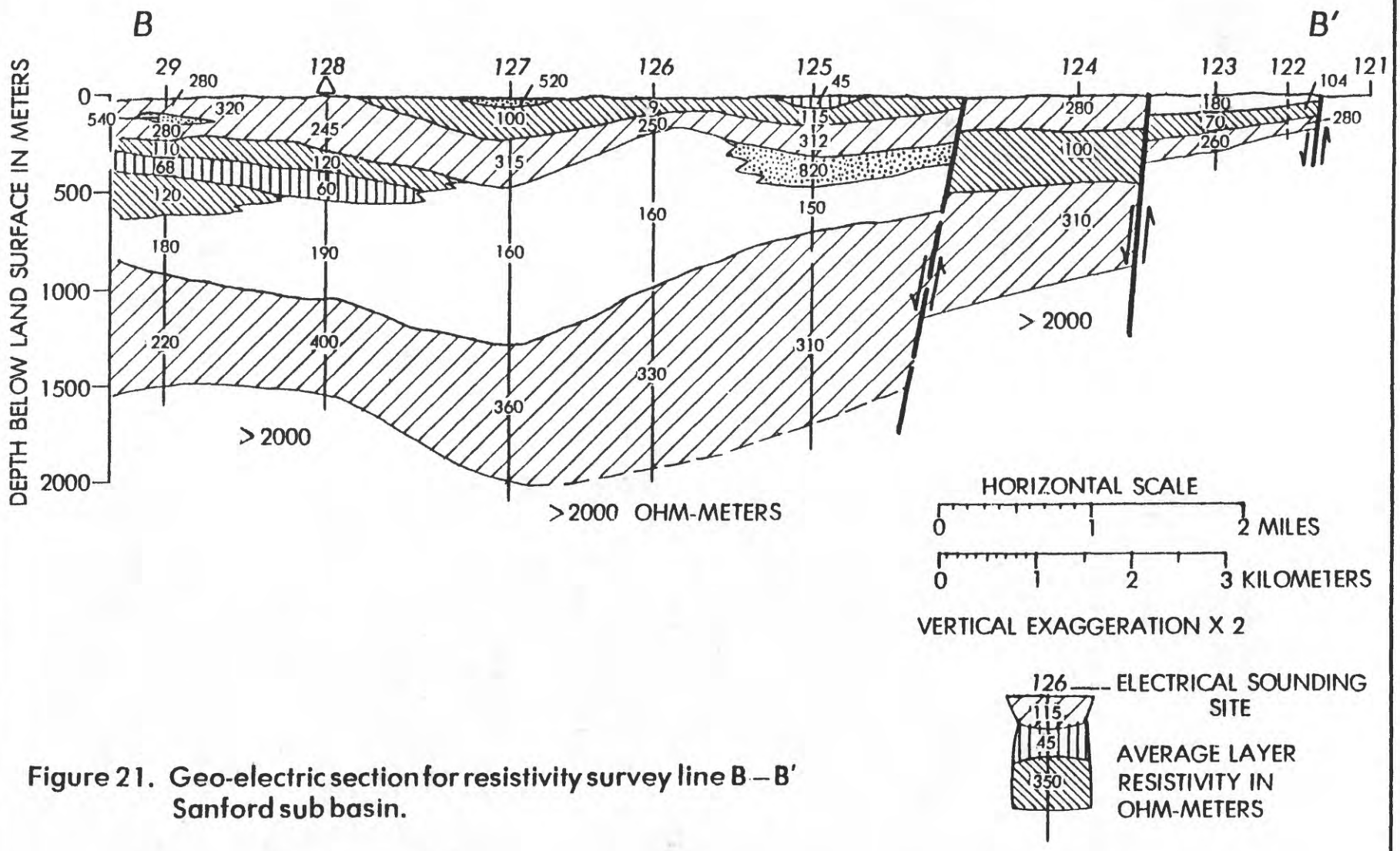

Figure 21. Geo-electric section for resistivity survey line B—B' Sanford sub basin.

The following data support the conclusion that the resistivity sections are similar to the actual geologic sections.

1. A basement depth interpreted from sounding 128 compared within 4 percent with the basement depth from the Groce No. 1 well near Sanford (fig. 21).

2. The interpretation of sounding 17 at the site of the Sears No. 1 well predicted a basement depth of 1,350 m. The well was completed to a total depth of 1,142 m in Triassic sedimentary rocks indicating that basement is at least greater than 1,142 m at that point.

3. The known location and sense of displacement of the Bonsal-Morrisville fault was correctly shown by the electrical section A-A'.

4. The eastern limit of the Triassic basin along both sections A-A' and B-B' agrees with known locations of the Jonesboro fault.

5. The depths on the electrical sections agree with the estimates obtained from aeromagnetic, gravity, and seismic data.

To construct the profile in figure 20, vertically adjacent electrical units of relatively similar resistivity were combined into larger units of more convenient ranges. The individual electrical units may or may not correspond to Triassic rock units. In general, rocks are formed of quartz, feldspar, and other silicates which are relatively poor conductors. The resistivity of such rocks is a function of two independent variables, (1) the shape, size, and degree of interconnection (F) of the pore spaces and (2) the resistivity of their contained fluid (Guyod, 1944). Thus, variations in conductivity of water from the Traissic rocks may mask vertical and lateral changes in resistivity caused by facies changes.

Aside from the overall increase in resistivity with depth caused by the normal decrease in liquid filled pores, an electrical inversion is noted between 100 and 1,000 m on most soundings. That is, resistivity decreases with depth between 100 and 1,000 m below which resistivity increases progressively to the bottom of the section. This inversion may reflect an increase in ground-water conductivity (salinity) with depth. The point at which the vertical trend changes (from decreasing resistivity to increasing resistivity with depth) may represent the point where the rocks do not contain uncombined water.

Section B-B'

Figure 21 is a resistivity section 13 km in length trending NW-SE, beginning at a point 10 km due west of Sanford, and ending 7 km due south of that city just east of the basin edge (fig. 19). This section also exhibits the lateral discontinuities in resistivity seen in profile A-A' that are due either to faulting, facies changes, differences in porosity, or differences in water quality.

Sounding 128, located on the west edge of this section, is at the site of the Groce No. 1 well where the depth to basement (1,550 m) is known. This section shows that to the east of sounding 128 the basement floor and the overlying Triassic rock dip progressively eastward. However, the eastern edge of the section shows different characteristics. There is no resistivity evidence for a master Jonesboro fault with 1,500 to 2,200 m of throw. Rather, the basement floor exhibits a steplike pattern within 2 to 5 km of the eastern edge, and the cumulative throw is distributed among the fault slices. As erosion proceeds in future millennia, the location of the Jonesboro fault will appear to move westward as successive basement steps of this fault zone are exhumed. There should be faults lying immediately east of and parallel to the Durham Triassic basin that mark the edges of fault slices or basement steps previously exhumed. The occurrence of quartz dikes parallel and east of the Durham subbasin near the Raleigh-Durham airport described by Shearer (1927) and Prouty (1931) may indicate that quartz dikes mark the traces of such fault lines.

Landsat Lineations

High-altitude multispectral Landsat imagery of the Durham Triassic basin was studied to determine if it could be used successfully for identification and recognition of Triassic geologic elements not necessarily visible from the ground surface (see, for example, Hogson and others (1974)). Landsat images of the Durham area show a complex tonal grain, some of the elements of which can be resolved into individual lineaments. The lineaments are particularly apparent on data from MSS (multispectral scanning) Band 7 (0.8 to 1.1 γm) at low sun angle. Some of the apparent lineaments are not geological but can be identified as roads, pipe lines, or other cultural elements. However, many of the linear tonal characteristics apparently are related to differences in vegetation, soil water content, soil type, fracture frequency, and changes in rock type. They are thereby useful in deciphering the geology of the area.

Figure 22 shows the location of lineaments observed on the January 11 and 12, 1973, imagery of the central Piedmont of North Carolina in the vicinity of the Durham and Danville Triassic basins. Although on these images there are large cloud-effected areas due to a passing snowstorm, there are sufficient areas without cloud effects to show the correspondence of some lineaments to the present-day outlines of the basins. The NNE and NE lineaments outline the notches in the western border of the Durham basin particularly well. The character of the intersecting lineaments along the Gold Hill fault about 13 km southeast of Lexington is very similar to the pattern of notches along the western edge of the Durham Triassic basin between Moncure and Chapel Hill where northeast trending lineaments pass through and on either side of the Farrington Pluton.

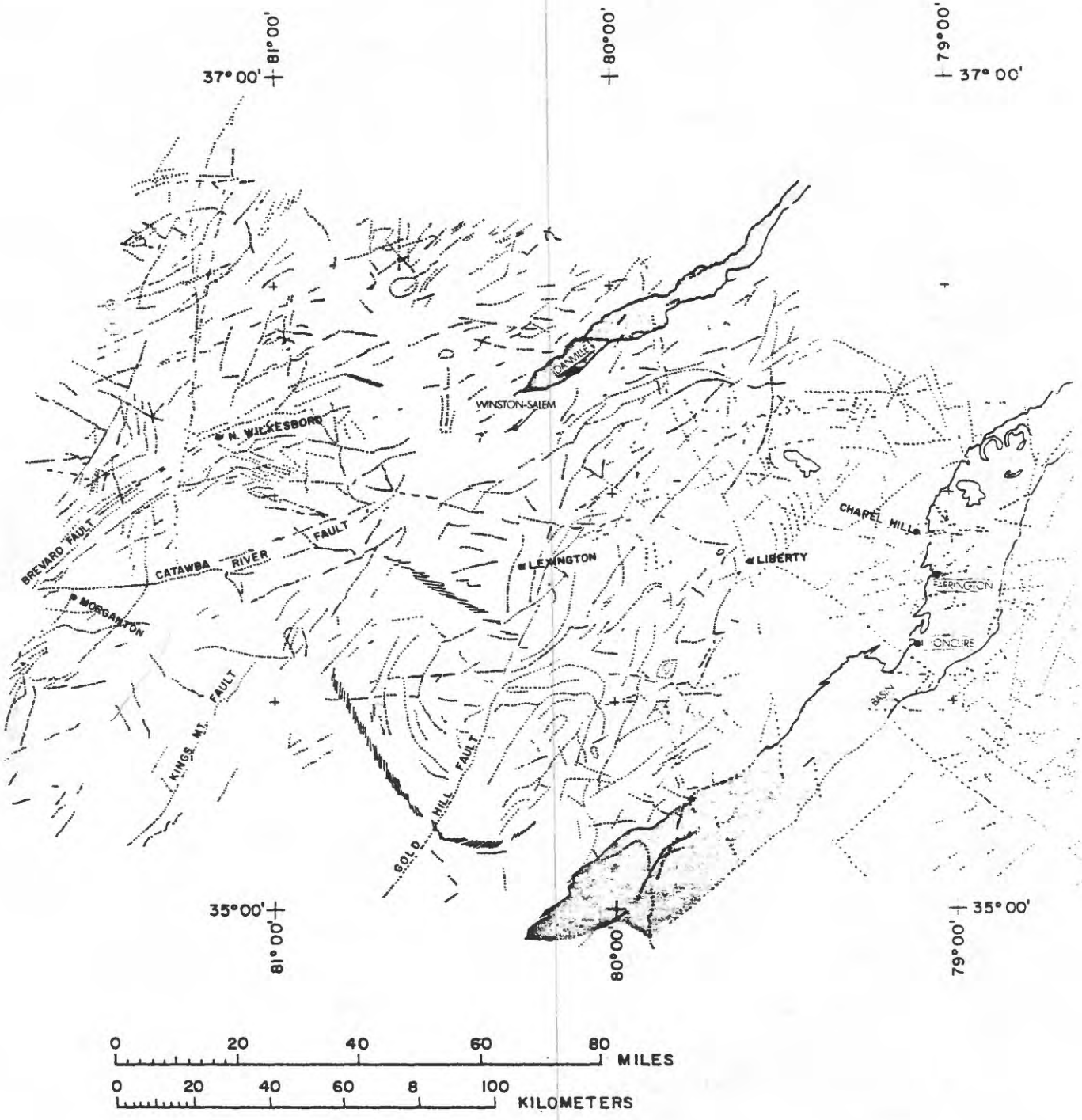

Figure 22. Landsat lineations in the vicinity of the Durham and Danville Triassic basins

The principal observed lineament directions are N. 70° W., N. 20°-30° W., N. 65° E., and N. 15-30° E. The former two directions and the latter two form two sets of apparent orthogonal fracture systems (see figs. 23 and 24). The N. 55-65° E. linear is associated with the northeastern extension of the Brevard and its Catawba River--Winston-Salem splay. The N. 70° W. lineament direction is parallel to the direction of the swarm of east-west fractures near North Wilkesboro that extend to the vicinity of Liberty in northwest Randolph County. The southernmost of this group of lineaments appears to cross the Brevard zone near Morganton, North Carolina, follow the Catawba River--Winston-Salem fracture swarm, and pass the northern end of the Durham Triassic basin. Still farther south a lineament beginning west of Atlanta, Georgia, near the southern tip of the Sequatchie anticline crosses Georgia and South Carolina in a east-northeasterly direction passing south of the Kings Mountain structure, Gold Hill fault, and Durham Triassic basin.

The similar-en echelon-parallelism of the northern one-half of the Durham Triassic basin to the Gold Hill fault and Kings Mountain structure appears to have some tectonic significance. Of the two longest regional lineaments, the Catawba River--Winston-Salem trend has the most obvious genetic relationship to the Gold Hill fault. The Kings Mountain structure, the Henderson granite gneiss, the Gold Hill fault, the Durham Triassic basin all terminate in or south of this 16-km-wide zone. This zone also effectively separates the northwest dipping Danville and other Virginia Triassic basins to the north from the southeast tilted Durham Triassic basin. The Kings Mountain and Gold Hill lineaments also appear terminated to the south by a N. 70° E. trending lineament parallel to the Brevard and Catawba--Winston-Salem zones on an East Coast mosaic discussed later.

There are numerous other obvious examples on the Landsat photos where the observed lineaments lie parallel to, border, or otherwise coincide with known geologic or geophysical elements. But more importantly, the lineations occur in patterns and directions which are helpful in deciphering the tectonic development of the Durham Triassic basin, and therefore the intrabasin structure and probable spatial distribution of sedimentary facies.

Moody and Hill (1956), Anderson (1951), Hubbert (1951), Hafner (1951), Wilcox and others (1973), McKinstry (1953), Chinnery (1966) and many others have shown that the angular relationships of such fractures are predictive in a wrench fault system and are useful in recognizing first- and second-order shear sets and fracture patterns associated with a uniaxial stress axis (see fig. 23).

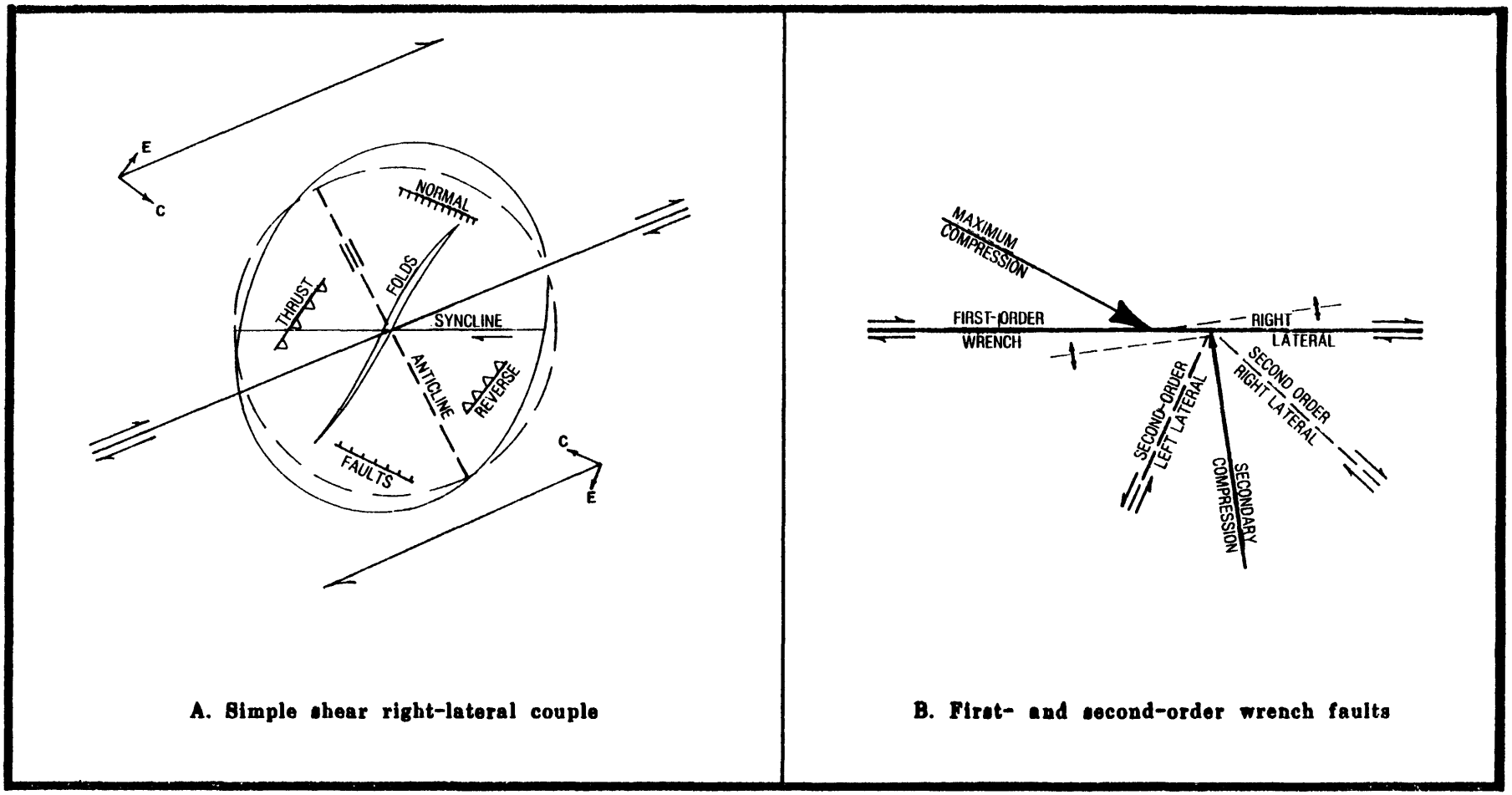

A. Simple shear right-lateral couple

B. First- and second-order wrench faults

Figure 23. Diagram showing angular relationship of stress direction to first- and second-order wrench faulting .

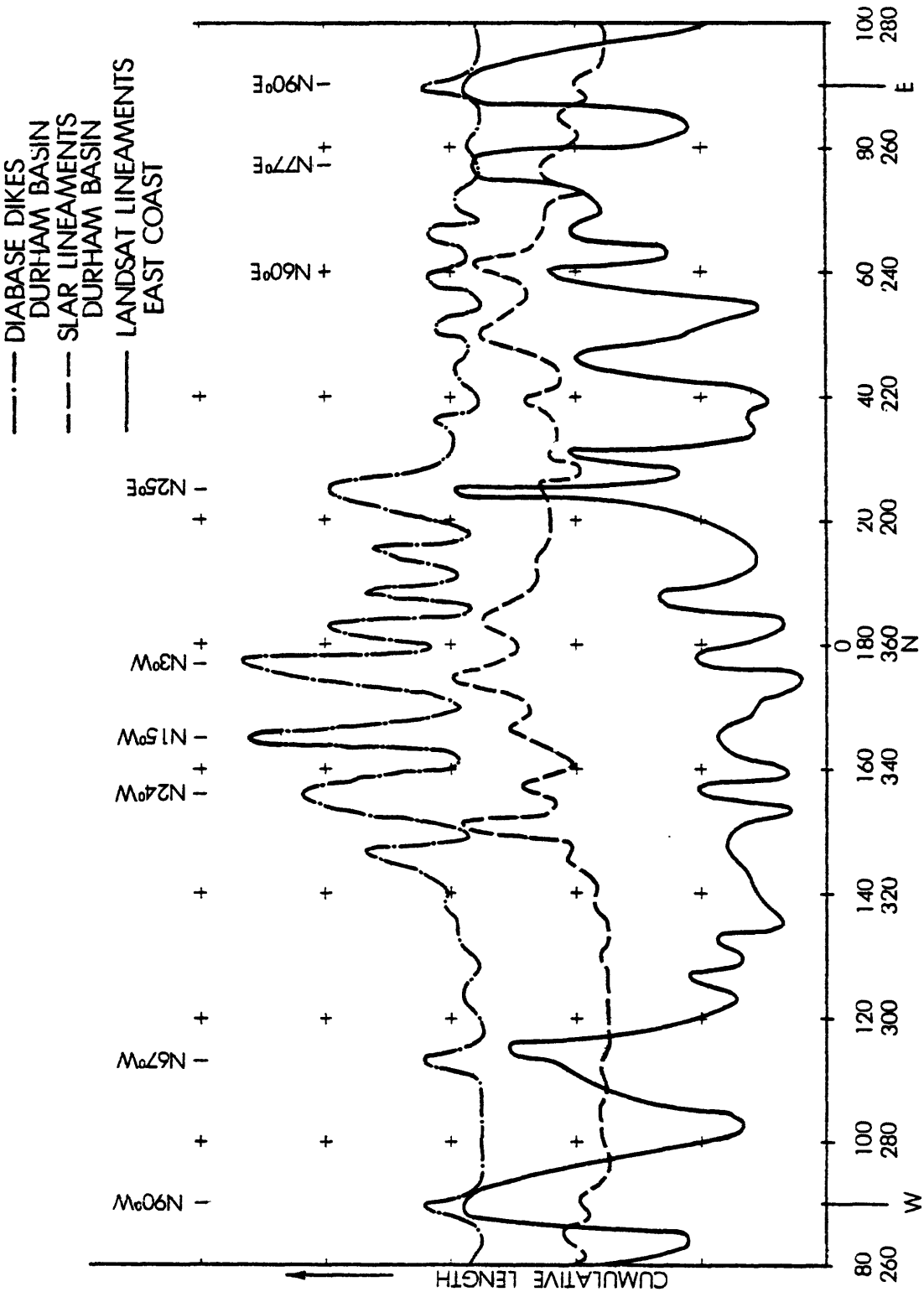

Figure 24. Cartesian plot of side-looking airborne radar and Landsat lineaments and diabase dikes.

Figure 24 is a cartesian plot of the azimuths versus cumulative length of lineaments observed on the Landsat mosaic of the eastern United States. A sampling interval of 3° was used with the 75° and 80° west meridians serving as base lines. The traverse east-northeast lineaments previously mentioned cluster about the 76° and 89° points on this graph--the north-northeasterly ones cluster about the 24° and 30° points.

The strikes of side-looking radar lineaments from a northeast oriented flight over the Durham subbasin are also plotted (the middle dashed curve). The plot at the top of this graph represents the Durham subbasin diabase dike directions weighted by length. The N. 70° W. and N. 15°-30° E. orthogonal set is still represented. The N. 20°-30° W. and N. 65° E. is less obvious.

Thus, even in the comparatively small area of the Durham subbasin there is good agreement between some of its lineament strike directions and those of the entire East Coast. Randazzo, Soper, and Waskom (personal commmunication, 1976) found three regional joints sets in the Slate Belt at N. 60° E., N. 30° W., and N. 65° W.

Most of the East Coast Triassic grabens trend N. 45° E. parallel to the Brevard trend south of Pennsylvania but range from due north to due east to the northeast in orientation (fig. 1). They exhibit a clockwise offset pattern and are subparallel to the folded Appalachians. If most are tension structures under pure shear parallel to a maximum compression along N. 45° E., conjugate shears should occur at approximately N. 75° E. (left lateral) and N. 15° E. (right lateral). If produced by a couple in the simple-shear system, N. 45° E. tension structures should result from an east-west left-lateral couple or a north-south right-lateral couple (fig. 23). In both orientations, the conjugate shears would be approximately at N. 75° E. (left lateral) and N. 15° E. (right lateral).

Structural Significance of Diabase Intrusives

The Triassic basins as well as the surrounding Piedmont and New England provinces of the Eastern United States were intruded by swarms of diabase dikes in Late Triassic (?) and Jurassic time.

Their attitude and outcrop pattern (fig. 25) indicates that these tholeiitic magmas were injected along two sets of fracture systems in Late Triassic (?) and Early Jurassic time after sediment lithification and subbasin rotation. Their location and frequency are an important aspect of the waste disposal evaluation of the Triassic basins because their inherent difference in permeability and the shearing that attended intrusion tend to compartmentalize the basins sediments into small hydrologic regimes.

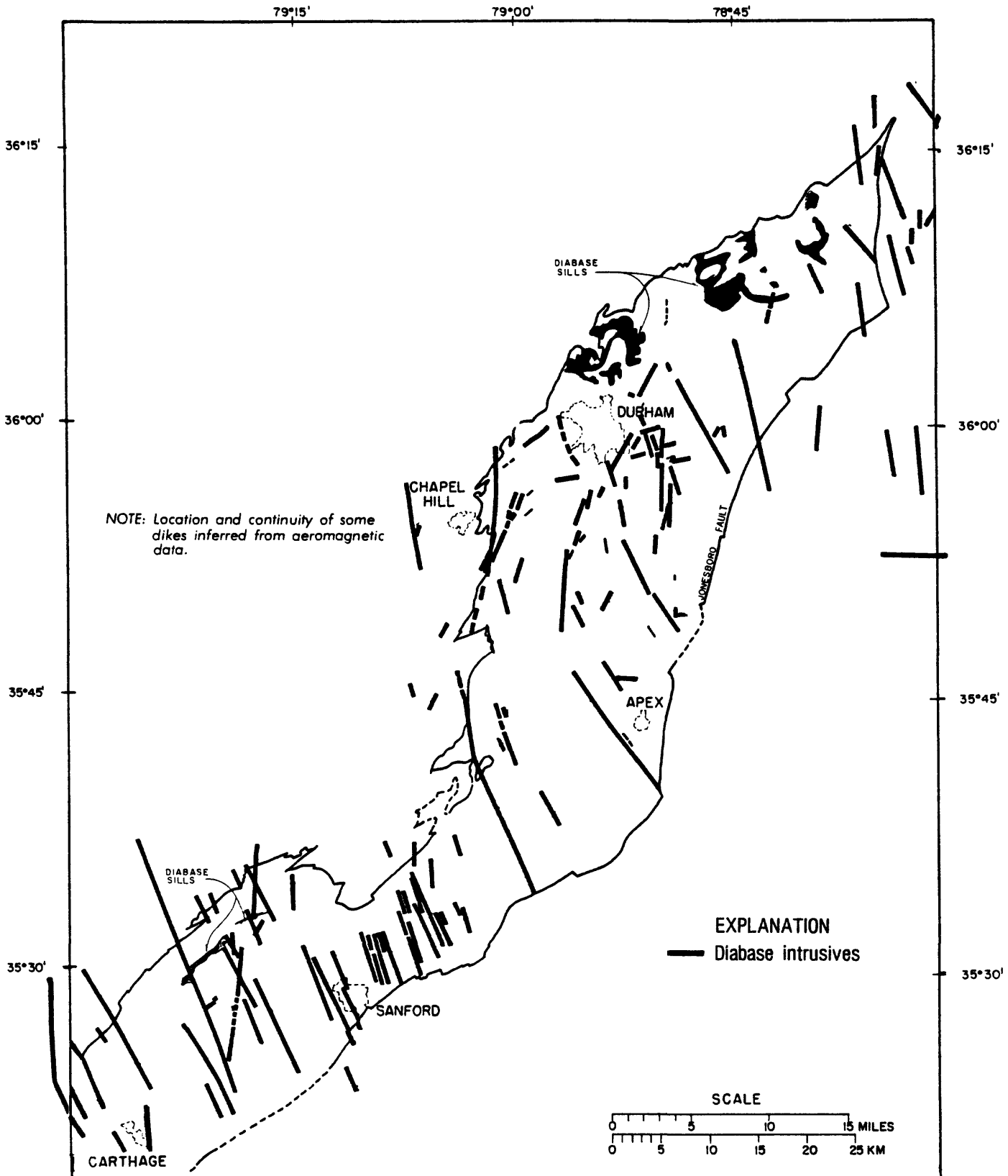

Figure 25. Diabase intrusives of the Durham Triassic basin.

The diabase dikes are deep crustal tholeiites changing composition from predominately olivine normative in the south to high and low titanium quartz normative in the north. The older diabase dikes appear to be in the south with a progressive change to younger age to the north. The diabase dikes change trend from NW in the southern Piedmont to nearly NE in New England. Most of the dikes in the Durham area trend between due north and northwest directions. Their outcrop pattern presumably represents a fossil tensional stress system(s) of Late Triassic (?) and Early Jurassic time.

Diabase dikes cross the Durham as well as the other Triassic basins (fig. 25) without change in trend, and although widespread in the east, their westward occurrence ends abruptly as if confined to a specific crustal zone. They are much more difficult to distinguish from the rocks of the Piedmont, but the aeromagnetic map from which figure 10 is derived indicates that they are just as numerous in the surrounding crystalline rocks. They are discernable on the SLAR images by their unique raised outline, and their parallelism to Landsat lineations is evident in figure 24.

THE TRIASSIC CONTINENTAL ENVIRONMENT

A knowledge of the nature, distribution, and thickness of the various rock types in a sedimentary basin is a prerequisite to its evaluation for waste storage purposes because of the obvious clues to the occurrence of suitably porous and permeable reservoir rock and rock seals. Similarly, an understanding of the special tectonic and climatic environment present at the depositional loci leads to a predictable sedimentary facies model.

As pointed out in the "structural geometry" section, the literature on East Coast Triassic basins contains many different tectonic, climatic, and depositional models not necessarily supported by the actual rock associations--a problem no doubt caused in part by the general lack of subsurface data. The lithologic variety and associations, mineralogy, and depositional structures preserved in the Durham Triassic basin were examined specifically for clues to more accurate tectonic, paleotopographic, climatic, and sediment dispersal models.

The alluvial fans, the angularity of the sand, the poor sorting of the fines, the size of the boulders in the fanglomerates, and the freshness of the feldspar in the Durham Triassic basin all point to short transport distance from an elevated source area to a nearby valley floor or graben of low relief. The depositional environment was not unlike deposition in the low intermontane basins of the Basin and Range Province or in the Salton Trough of Southern California.

Typically in this environment alluvial fans form as a direct result of a sharp break in slope and a corresponding decrease in stream competency. The decrease in stream competency is further aggravated by loss of water through the permeable alluvium by "sieving." The resulting high ratio of rock detritus to water at the fan surface creates shallow braided streams that slowly prograde the coarse proximal fan deposits over the finer distal ones. Individual facies within the fan are quite localized and are caused by intermittant faulting and attendant increased relief, by meandering bifurcating channels, and by variability of stream discharge.

Braided streams on the fan surface create longitudinal and traverse bars which migrate downstream. Sedimentary features of both the upper and lower flow regime are characteristic; that is, parallel laminae, thin lenticular shales, many interclastics, cut-and-fill structures, and planar and trough cross stratification (Smith, 1970). There is a general down-the-fan-slope increase in the ratio of planar over horizontal cross stratification due to the decrease in flow regime. Longitudinal bars consisting of coarse, poorly sorted debris are most common in the upper reaches of the braided stream. Transverse bars containing finer, better sorted material are most common at the distal end of the fan.

The finer grained sediment at the distal end of the fan is carried onto the basin floor into a playa, bolson, or lake or is further distributed in the floodplain of through-flowing longitudinal streams.

Springs and seep lines, which develop in the valley floor near the boundary fault(s) of these fault-controlled intermontane valleys, support local swamps and peat bogs. Swamps also form in shallow water in low-lying sites remote from active deposition such as exist parallel to natural levees of through-flowing streams of low gradient and along the edge of ponds and lakes. Organic matter accumulates on the lake or bog floor to form peat where a reducing environment prevents its biologic destruction.

Preservation of organic rich mud produces a black or brown shale, the laminations of which record periodic or seasonal changes in sediment or vegetative supply. Preservation and compaction of peat produces coal.

Where evaporation exceeds precipitation because of either seasonal or perennial aridity, such as exists in a playa environment, dissolved salts are concentrated in starved lakes, and large expanses of salt flats develop. Various chemical deposits accumulate on the lake floor including normal carbonate, chert, anhydrite and gypsum, glauberite, and salt either in discrete beds or in fine dispersal in the bottom muds. Chert precipitates where there is a seasonal fluctuation in alkalinity and an abundance of detrital silica. Silica which is taken into solution at pH 9 and greater is precipitated when the pH is rapidly reduced by the rotting vegetation caused by drying of the lake (Peterson and Borch, 1965). Analcime is sometimes formed in the bottom muds of those lacustrine environments marked by seasonal aridity and soda-rich sediment (Van Houten, 1977).

Comparison of Areal Geology to Depositional Model

The surface Triassic geology in the Durham area was mapped at a reconnaissance scale to gain insight into basin geometry, type and geometry of lithofacies, and degree of faulting. The geologic map that evolved reflects depositional environments modified by later faulting (fig. 3).

The fanglomerate-conglomerate association shown in figure 3 marks the locations of greatest relief of the land and least transportation of the sediments. This unit which is associated with the border faults is principally developed on the east side in the Durham subbasin and on the west side in the Wadesboro subbasin. The fanglomerates represent scree and mud-flow deposits from the steep terrain along the bounding fault scarps. Fanglomerates and conglomerates also mark the points where major intermittent (?) streams entering the basin dropped their bedload. The presence of conglomerates in thinner beds near the middle of the Durham subbasin record the locations of major braided stream channels and times of movement on the boundary faults. There is no known evidence that longitudinal or transverse growth faults were active during sedimentation to produce midbasin conglomerates.

The fanglomerate-conglomerate association on both sides of the basin contains clasts identical in compostion to the crystalline rocks immediately adjacent, attesting to the process of local infill from both sides. Mixed with the clasts, especially along the western border in the argillite-graywacke-conglomerate facies (fig. 3), however, are rounded to subrounded quartz pebbles and cobbles which indicate greater transport distance and or a mixed supply.

The coarse tan feldspathic sandstone facies (granite wash) best developed between Carpenter and Apex and north and east of Creedmoor represents the midfan braided stream deposits of one such alluvial fan. This particular facies is the uppermost unit penetrated in the Sears No. 1 test well and is approximately 610 m thick at that point. It grades laterally and vertically into the red and grey, finer, less sorted deposits.

Although possibly not the same rock stratigraphic unit, this midfan facies is also represented on the western side of the basin between Durham and Chapel Hill (fig. 3), on the western side of the Sanford subbasin in the subsurface, and throughout much of the Wadesboro subbasin. The general lack of red color is due to the absence of hematitic cement probably caused by the winnowing of the hematitic muds or its general absence from the source materials. Fluvial conditions along probable longitudinal streams are indicated by channel and point-bar sands and overbank muds. Coarse cut-and-fill channel sandstones record where distributary channels cut through fine deltaic muds. The poorly sorted overbank and distal fan deposits into which the above facies grade are represented by mudstones, siltstones, and massive argillites in a down-fan direction and by bimodal coarser sandstones in an upfan direction. They are best represented in the Durham subbasin (fig. 3) in the area south of Apex and West of Holly Springs toward Brickhaven, from the Raleigh-Durham airport north to Oak Grove and southwest from that point toward Farrington. In the Sanford area, they are characteristic of both the Pekin and Sanford Formations indicating that this particular facies was being deposited somewhere in the basin throughout the Late Triassic. Locally this facies is unquestionably lacustrine.

Triassic lakes are represented by limy, evaporitic, red mudstones, flaggy micaceous sandstones, red and black fossiliferous shale, and chert. Limy redbeds, thin nodular limestones, and chert are generally confined to the interfan areas. Lacustine conditions occurred in at least two places in the basin at different times. In the Pekin Formation on the Colon cross-structure (fig. 3) and southward at the base, flaggy sandstone and freshwater fossilbearing argillite occur, overlain by chert. Reinemund (1955) also reports limy shales, coal, and chert in the Sanford area.

Farther north and somewhat later, lacustrine and paludal conditions are marked in the Oak Grove-Bethesda-Research Triangle-Morrisville area by thin-bedded micaceous sandstone which is overlain by two thin beds of red to black fossiliferous shale succeeded by a thick section of limy redbeds containing widespread chert beds. One additional fossiliferous zone is present in this facies, higher in the section, between the Olive Branch Church community and the Raleigh-Durham airport.

The grey to buff paludal shales and thin coal zones in the Pekin Formation from west of Sanford to north of Moncure (Olive Chapel), the relatively thick coal and humic shale of the Cumnock Formation of the Sanford area and its thinner equivalents near Brickhaven, and the thin black shales centered around the Research Triangle Park occur in the same geographic area as the lacustrine facies and are interbedded with them. They are obviously products of the same tectonic environment within the basin. Coal, shale, limy redbeds, or chert formed in swamp, lake, or playa in response to different combinations of climate, water depth, and sediment supply.

Paleocurrent Studies

Few studies have attempted to determine the specific source area or character of the Durham Triassic basin parent material or its redistribution within the basin. Whitehead (1962) concluded from a study of the major rock types exposed at the surface in the Sanford subbasin that the grain composition indicated a source consisting of metamorphosed Precambrian rocks now largely eroded away. More specifically, he proposed that the source lithology consisted predominately of moderate-grade metamorphic rocks interbedded with lesser amounts of low grade metamorphic granitic and volcanic rock. Klein (1969) proposed that the sediment source was from both sides of the basin based on K-Ar and paleocurrent measurements.

The paleocurrent direction of the coarse tan feldspathic sandstone facies (granite wash), previously described as an example of midfan braided stream deposits of an alluvial fan, was studied in some detail. Paleostream direction data of Custer (1967) indicate that this particular deposit may have originated from the southeast side--perhaps south and west of Holly Springs. The macroscopic petrography, however, indicated a plutonic source. Although there is a small granite pluton south and west of Holly Springs, the volume and general lack of metamorphic clasts indicate a larger, mostly granitic source such as the Rolesville pluton to the northeast. Contrary to Custer's conclusion, paleocurrent data gathered by Dittman (1979) for this project do indicate that the prevalent paleostream direction in this facies is toward the south and southwest both in the Carpenter-Apex area and in the Creedmoor-Oxford area.

Paleocurrent data gathered elsewhere by Dittman (fig. 26) show that basin-margin streams flowed into the basin normal to the edge and that midbasin or longitudinal streams flowed almost universally to the south-southwest parallel to the basin trend. Patterson (1969) also indicated a strong southwest direction across the Colon cross-structure.

Figure 26. Paleocurrent directions in the Durham sub-basin.

Reinemund (1955) found that the basal conglomerate and sandstone in the Sanford subbasin contain clasts identical to metamorphic rock types in the Slate Belt west of the basin. Crossbedded arkosic sandstone containing schist-arenite channel deposits indicated that streams flowed from the west and northwest into the basin on the west side (base of section) and from the southeast in the middle and upper part of the section. He also noted an increase in coarseness in the Sanford Formation to the southeast, an increase in arkose toward a Carboniferous granite pluton to the southeast, and an abundance of muscovite from rock types exposed on the east side of the basin.

Bell and others (1974) reported that the Wadesboro subbasin shows no coarsening of the sediments toward the southeast, although an arkosic conglomerate clearly derived from a granite along the eastern border occurs near the western border. Randazzo and others (1970) found that arkose (K feldspar) increases to the east in the Wadesboro subbasin. It is therefore obvious only that there was coarse sediment contribution from both sides of the Durham Triassic basin, that streams depositing the alluvial fans flowed into the basin more or less at right angles to the borders, and further sediment dispensal and reworking was parallel to the basin by through-flowing probably intermittant streams.

Palynology and Stratigraphic Correlation

Lateral correlation of chronostratigraphic units in the Durham subbasin is complicated by the rapid facies changes described above and extensive faulting which has placed units of different ages into juxtaposition. Most workers have proposed a tripartate division of the rocks in the Durham Triassic basin solely on the basis of a coal and black shale occurrence in the Cumnock Formation in the Sanford area near the middle of the section. According to this system, the Cumnock Formation is overlain by the Sanford and underlain by the Pekin Formations. Cross section (A-B) showing facies correlation in figure 3 is an attempt to illustrate the vertical and lateral facies relationship that is thought to exist between the Durham and Sanford subbasins based on the latest structural models, paleocurrent directions, palynology, and surface geology.

The coal and the black shale of the Cumnock Formation near Sanford and their thinner equivalent near Brickhaven, the grey shales and thin coal zones of the Pekin Formation on the Colon cross-structure and the thin black shales of the Research Triangle Park-Bethesda area all contain plant remains and freshwater biota--ostracods, fish bones and scales, and branchiopoda. Fossil collections from these rocks are adequately described in Emmons (1856), Jones (1862), Redfield (1856), Fontaine (1883), Ward (1899), Murray, Jr. (1938), Prouty (1931), Hope and Patterson (1969), Delevoryas and Hope (1971), and Swain and Brown (1972). Many of the same fossils are represented in all the shales. Almost without exception they indicate a Late Triassic age. Unfortunately, their age ranges are too long to be very diagnostic of specific horizons within the Durham Triassic basin.

Recent work by Cornet and Traverse (1975) and Cornet (1977) on the palynoflorules of the rocks of the East Coast Triassic basins demonstrates that spores and seeds can be used not only to correlate between the basins, but also to establish temporal zones within the basins. As a direct result of their work, coal from the Copper Creek prospect near Moncure formerly placed in the Cumnock Formation is now found to belong to the Pekin Formation. The reassignment has greatly simplified the stratigraphic problems of the Moncure area. Chert in the Moncure area, which is an apparent down-strike equivalent of the Copper Creek prospect, cannot be traced laterally across the Bonsal-Morrisville fault zone into the chert of the Research Triangle Park. Chert and the associated black shales in the Research Triangle Park area are thought now to be slightly younger than the Cumnock Formation on the basis of the faunal evidence. The other possibility--that the two chert beds were age equivalents--requires that the entire west and northwest part of the Durham subbasin be older than Pekin or the basal part of the Colon cross-structure be a Cumnock equivalent.

Cornet's (1977) facies correlations between the basins indicate sedimentation began first in the North Carolina and Virginia basins in Late Triassic time (Middle Carnian) and then progressed to the northern basins. Cornet's facies correlations between the basins and to the facies correlation section (fig. 3) indicate that lacustrine and paludal conditions occurred in different basins at different times, probably in response to a combination of tectonic framework and climate. This means that the traditional assumption that the lacustrine-paludal facies postion near the middle of the basins indicates middle postion in the simple, monoclinal, half-graben model used (Bain, 1973, and Sumner, 1977) is in error.

The data presented in this report indicate that the triparte division used in the Sanford subbasin is not applicable to the remainder of the Durham Triassic basin. The chert at Moncure was not penetrated in the Sears No. 1 test well at New Hill (fig. 3) even though correlation of the basal 350 m of the Sears well with the basal section of the Groce No. 1 well west of Sanford shows that the Sears well was within 90 m of penetrating the entire section of the Pekin Formation. Although the lower section of the Sears well correlates with the lower section of the Groce No. 1 well, the Cumnock is very thin or absent in the Sears well. The Sanford Formation is also absent in the Sears well; therefore, the upper section of both wells are in entirely different facies.

The position of the fanglomerate at the surface along the downfaulted side of the Durham and other subbasins is frequently cited as evidence for continued periodic movement along the downthrown side. Recent resistivity, gravity, and aeromagnetic evidence show that the basin floor "steps up" near the border fault causing exposure of some of the basal fanglomerates. Thus, the evidence for or against continued movement throughout the time of deposition in the Durham Triassic basin is eroded away. In fact, part of the eastern side of the Sanford subbasin now mapped as Sanford Formation is most probably Pekin in age. The presence of the basal conglomerate does indicate strong initial relief and may indicate only the time of maximum local relief between Piedmont and basin floor.

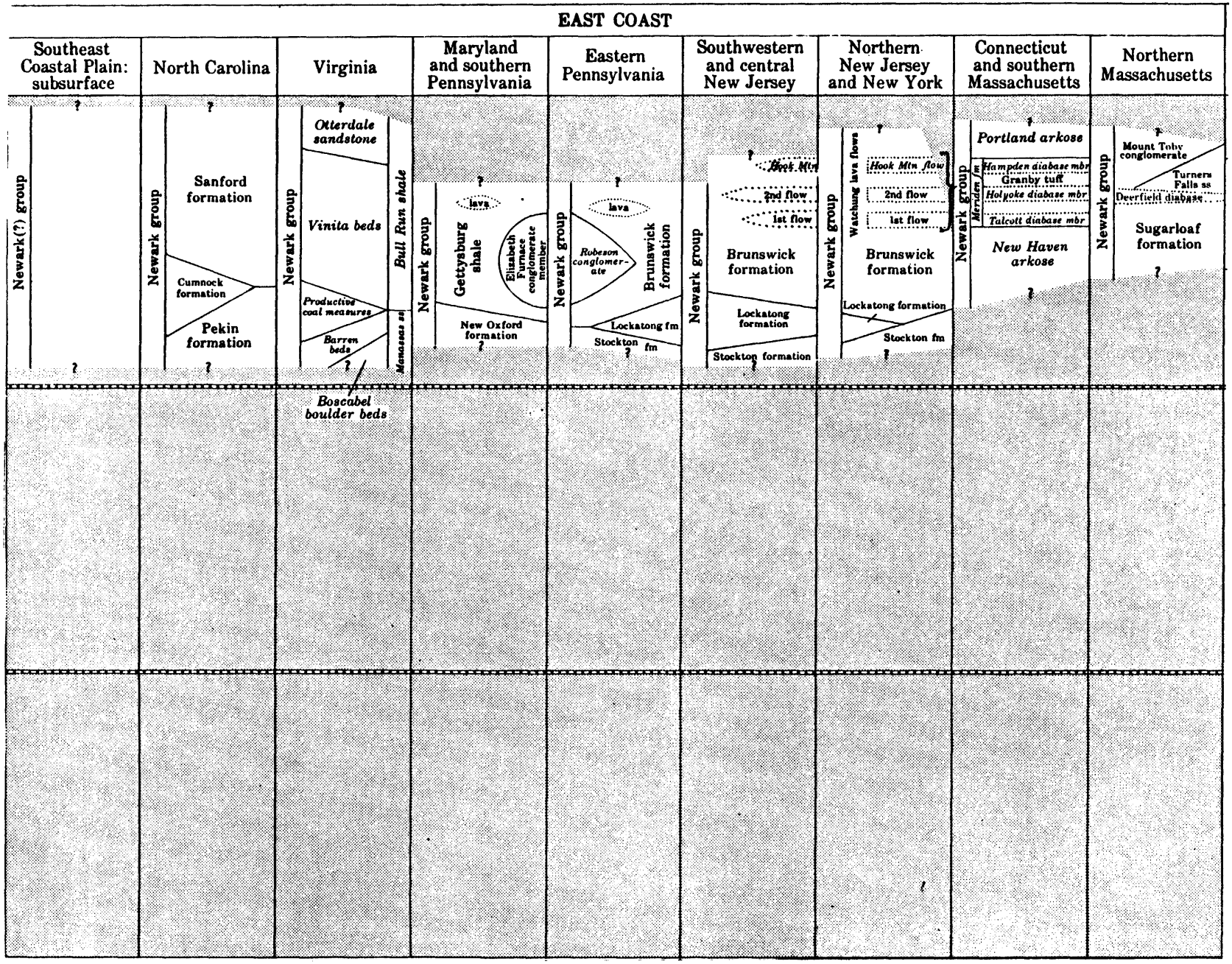

Figure 27.--Generalized stratigraphic correlation chart of the East Coast Triassic (Modified from McKee and others, 1959)

TEST DRILLING AND BOREHOLE GEOPHYSICS

A deep test well was drilled to 1142 m in the early part of 1976 in the Durham subbasin near New Hill, on the property of W. H. Sears (Sears No. 1) by the Geological Survey. The test well was specifically designed and drilled to:

1. Calibrate surface and airborne project geophysical data; seismic reflection, gravity, aeromagnetic, and electrical sounding data.

2. Test the validity of structural and stratigraphic models developed from surface reconnaissance studies.

3. Obtain core samples from deep lithologic units for measurements of porosity and permeability.

4. Obtain samples of formation fluids to determine water chemistry.

5. Obtain continuous drilling samples to determine the vertical distribution of the sedimentary sequence.

6. Determine aquifer characteristics of reservoir rock penetrated.

Drill cuttings were sampled at 1.5 m intervals from which the lithologic log of plate 1 was prepared. Cores were taken at five different intervals for physical property determinations. Results of physical property tests are described below and are summarized in table 1. Borehole logs obtained at completion of drilling (plate 1) include temperature, neutron porosity, gamma ray, gamma-gamma density, sonic, dual-induction laterolog, microlaterolog, microlog, caliper, and borehole televiewer. Two zones in the test well were isolated with hydraulic packers to collect reservoir fluids for chemical analysis and to determine aquifer characteristics.

General Lithology

The Triassic strata penetrated in the Sears No. 1 well can be grouped into at least three rock stratigraphic units. They are--from bottom to top: (1) a basal argillite-greywacke-conglomerate facies at least 122 m in thickness, (2) succeeded by a 670 m sequence of massive mudstone, argillite, and quartz conglomerate, and (3) overlain at the top by 640 m of arkosic sandstone, siltstone, and mudstone. This interval becomes predominatly more sandy toward the surface by a decrease in mudstone and an increase in thickness and frequency of arkosic sandstones in the bottom 340 m. These units do not necessarily conform to the traditional boundaries of the Pekin, Cumnock, and Sanford Formations of the Sanford subbasin.

The rocks penetrated have inherent low porosity and permeability, above average density, high acoustic velocity, high resistivity, low gravity in contrast to the Piedmont crystallines, and drill slowly because they are indurated and poorly sorted.

Table 1 - Physical Properties of Core Samples from the Sears No. 1 Well

Sample depth (meters)	Lithology	Bulk density (g/cm^3)	Water content (percent)	Gas porosity (percent)	Permeability Liquid (Millidarcys)	Permeability Air (Millidarcys)	Velocity (km/s) Longitudinal	Velocity (km/s) Shear	Resistivity ---R_O (ohm-meters)	Formation Factor $F = R_O / R_W$	Unconfined Strength (kPa x 10^4)	Porosity (percent) from neutron log at indicated depth
154	Sandstone			5	.00000046	.11			1/ 58	2/ 2.74		13-14 at 156.6
154	-do-			2.3			4/3.73					15-18 at 153.4
157	-do-			8.9	2.2	11			1/422	2/24.1		13-14 at 158.7
157	-do-			12.0			4/3.82					
329	Grey arg.			1.3			4/3.28					1.6-9 at 326.5
329	-do-			--	Sample failed	.01						4-15 at 329.0
330	Siltstone			4.7	.0000049	.02			1/ 80	2/ 3.64		7-18 at 329.3
330	-do-			2.2								1-24 at 331.7
330	-do-			2.8			4/4.26					
744		2.65	0.6	0.9	.000002		4.50	2.37	72	3/ 6.5	8.8	0-16 from 742.7-745.1
745	Red Ss.	2.60	1.1	6.2	.000017		4.71	2.60	130	12	11.4	
961	Cong.	2.65	0.5	2.8	.000005		5.14	3.04	1060	3/96	13.9	
1138	-do-	2.66	0.1	2.5	.000007		5.14	3.02	736	3/67	11.1	
1142	Arg.gryw.	2.73	0.1	0.9	.000004	.0001	4.55	2.36	195	3/18	12.2	

1/ Calculated from $R_O = F_f \times R_W$.
2/ Measured at 15169 kPa.
3/ At overburden pressure.
4/ At 13790 kPa.

Spontaneous Potential Log

The SP or spontaneous potential log measures the natural electric current potential between the borehole fluid and the surrounding rock. Generally, the conductivity of the borehole fluid is less than that of the surrounding rock causing apparent negative SP deflections to the left opposite clean sand and to the right opposite shale. The SP log of the Sears No. 1 well shows a number of zones above 640 m where negative anomalies up to 40 millivolts mark the occurrence of more permeable sandstones.

Between depth of 640 and 990 m, the SP log shows little contrast between the rock and borehole fluid and indicates shaliness. The lithologic log shows this zone to consist of mudstone, massive argillite, and minor occurrences of conglomerate. Thus, the subdued character of the SP in this interval is caused by the shale content of the rock. A similar but much thinner facies occurs between 308 and 338 m. The negative SP anomalies below 990 m occur opposite conglomerate on the lithic log.

The SP contrast between borehole and formation fluids is used elsewhere in this paper to predict dissolved-solids content of the formation waters. The general subdued character of the SP curve indicates formation fluids are not much more saline than the fluid in the borehole. Dissolved-solids content in the drilling mud was less than 300 mg/L throughout the drilling. From all indications, the New Hill well did not penetrate rock containing brine.

Resistivity Logs

The resistivity of a rock depends on the resistivity of the rock-mineral matrix and its contained fluid. Rocks that are composed primarily of quartz and feldspar, which are poor conductors, contain water that is usually a better conductor. Thus, the resistivity of a sandstone generally depends only on the geometry of its pore space and the resistivity (or salinity) of its contained fluid. As permeability and porosity decrease, resistivity increases with no change in formation fluid.

Five separate resistivity logs were run in the Sears No. 1 well; they are: a microlog, microlaterolog, laterolog, and a medium and deep induction log. Resistivity on these logs is expressed in ohm-meter^2/meter.

The log response to the difference in resistivity of different lithologies is useful in determining the vertical distribution and thickness of rock types. Conventionally, some type of resistivity curve (plate 1) is recorded with the SP log. The SP-resistivity log combination is useful in ground-water investigations to identify the more permeable, water-yielding zones. Normally, in an area of saline ground water such a zone has a sizeable negative deflection on the SP curve and a right deflection (more resistive) on the resistivity curve. Examples of such opposing deflections occur at 192, 229, and 250 m in the Sears No. 1 well (plate 1).

In permeable zones, drilling mud invades the formations and displaces the native fluid because of the higher hydrostatic head maintained on the drilling mud. Thus, the depth of mud invasion is a qualitative measure of permeability. The five types of logs have different depths of investigation. The dual induction-laterolog combination is specifically designed to determine the depth of mud invasion. In table 2 the known effect of mud invasion on the true resistivity (Rt) of the formation is compensated for through the application of the ratios of Rild (deep-induction tool), Rilm (medium-induction tool), and R118 (laterolog 8) to each other.

In the first four zones (154 m to 248 m) the radius of the invaded zone is so large that a meaningful measure of Rt from the Rild curve is not possible (that is, invasion is deeper than the depth of investigation of the tool). Below 248 m a reasonable accurate formation resistance can be calculated from the Rild log response or read directly from it. Above a depth of 396 m invasion is evident (see R118, Rilm, Rild) in the more permeable sandstones and is negligible from 396 m to 1,006 m. Below 1,006 m evidence of shallow invasion by the drilling mud indicates some permeability to 1,130 m.

The resistivity logs reveal a cyclic or alternating sequence of sandstones and massive shales. The average resistivity of "shale" on the deep induction curve is about 40 to 50 m^2/m throughout the well. The sandstones and conglomerates, however, are typically 5 to 10 times more resistive. One sandstone or conglomerate is as thick as 10 m near a depth of 793 m, but the vast majority of the sandy zones are 0.67 to 3 m in thickness. If the lithologies of the well are arbitrarily divided into sandstone and shale, the ratio of sandstone to shale is approximately 2:3.

The sample log and the gamma-ray logs also exhibit a cyclic pattern. This pattern is most pronounced on the microlaterolog particularly between 732 and 793 m and between 915 and 960 m where it has an inverted stairstep character. Cycle frequency is about 5.5 m, and resistivity amplitude is about one order of magnitude. The cycles start at the bottom of the well with a highly resistive conglomerate which fines progressively upward into massive red argillite or mudstone. The fining-upwards cycles are also apparent higher in the hole such as at 518 m and 427 m.

Cycles having a frequency of 3 m to 6 m can also be identified in the upper more sandy portion of the hole. Here, however, the change from coarse to fine is much more abrupt, and the geologic material is obviously better sorted.

The conglomerate-massive argillite is probably a consequence of the normal settling out of sedimentary debris from periodic influxes of coarse sediment into standing water as might be caused by fault movement or storms. The abrupt change from coarse to fine in the upper part of the hole results from braided-stream, cut-and-fill, erosion and deposition through overbank or distal-fan deposits.

Table 2 - Selected log data from the Sears No. 1 well

Dual Induction-LL 8 Depth	Rt or Rild	Sonic Velocity Δt	Density ρ	Porosity ϕ
Center of Zone (meters)	(Ω m)	(km/s)	(g/cm^3)	(percent)
353	95	4.12	2.45	12
350	75	4.18	2.65	2
339	65	4.42	2.5	8
273	25	3.81	2.4	15.5
262	53	4.23	2.5	11
259	40	3.91	2.45	13
258	45	3.81	2.50	11
250	45	3.67	2.46	13
248	28	3.46	2.42	16
242	55	4.12	2.55	8
233	50	3.86	2.45	13
229	120	3.72	2.45	13.4
220	200	3.91	2.46	13
192	220	3.72	2.48	10.2
1119	150	4.92	2.65	1.8
1111	85	5.00	2.65	1.5
1103	160	5.00	2.75	-3
1102	150	5.12	2.72	-2
1098	95	4.69	2.73	-3
1096	63	4.62	2.70	-1
1089	48	4.18	--	
1085	65	4.18	--	
1080	160	4.88	2.67	0
1077	45	3.86	2.74	-4
1062	70	4.55	2.70	0

Table 2 - Selected log data from the Sears No. 1 well
Continued

Dual Induction-LL 8 Depth	Rt or Rild	Sonic Velocity Δt	Density ρ	Porosity ϕ
Center of Zone (meters)	(Ω m)	(km/s)	(g/cm^3)	(percent)
1056	375	5.40	2.68	0
1046	390	5.54	2.68	0
1044	400	5.49	2.71	-2
1041	250	5.35	2.67	-.1
1026	110	5.12	2.72	-3
155	140	3.79	2.45	14
279	39	3.57	2.42	16
282	47	3.93	2.5	11
289	64	4.18	2.46	13
307	75	--	2.47	11
378	38	4.23	2.48	10.1
399	64	4.12	2.46	13.6
414	65	4.26	2.56	8.3
440	90	4.48	2.50	10
477	47	4.45	2.45	13
479	55	4.76	2.57	7
508	190	4.84	2.58	5
527	120	4.88	2.60	3
570	100	4.84	2.57	6
583	140	4.84	2.57	7
610	170	5.00	2.70	-1
633	130	4.92	2.55	8
999	100	5.17	2.67	0.6
1020	150	5.21	2.68	0
1082	160	5.54	2.69	-1.5
1105	200	5.00	2.72	-3

Density-Porosity Log

The gamma-gamma density tool measures the apparent density of the borehole environment by recording the loss of gamma radiation caused by collision with electrons of the rock matrix and contained fluids. The attenuation of gamma radiation from the tool source depends on the electron density of the formation. Bulk density in grams per cubic centimeter (g/cc) depends, then, on porosity and the electron density of the rock matrix and fluid. In practice a shielded gamma ray source is pressed against and moved along the borehole wall. The attenuated radiation is received at two points at different distances from the source in order to adjust for the effect of mud thickness and irregular hole diameter. The density-porosity curve of plate 1 has been adjusted electronically for mud thickness and hole diameter changes except where there are extreme washouts.

The density log confirms the dense, generally low porosity character of the Triassic sedimentary rocks. Recorded densities range from an average 2.55 at 152 m to nearly 2.70 g/cc below 610 m. Above 610 m the densest beds are the massive argillaceous rocks. Below this depth the sandstones and siltstones appear to be as dense if not denser than the argillaceous rocks.

Bulk densities and corresponding porosities have been selected from the density log at points where the borehole is relatively free of washouts. These values are presented in table 3 for direct comparison with porosities from the neutron and sonic logs.

The density log indicates that there is very little primary porosity between 655 and 905 m. Sandstones and conglomerate at 833, 911, 1,020, 954, 1,110, and 1,131 m have apparent density porosities up to 4 percent. Reference to the SP log at these points indicate that formation fluids are present.

Neutron Porosity Log

The neutron logging tool responds to the amount of hydrogen in the borehole environment which includes hydrogen bound up in water and in the rock matrix. In clean (nonshaly) formations, the neutron log is a measure of liquid filled porosity. For shaly formations and minerals such as gypsum ($CASO_4 \cdot 2H_2O$) the indicated porosity is erroneous because this tool also measures the hydrogen associated with bound water and water of crystallization.

In principle, high energy, electrically neutral particles are emitted from a radioactive source which collide with the nuclei of the surrounding environment. Greatest loss of energy occurs when the neutrons collide with particles of their own mass such as hydrogen. The neutron tool is generally designed to count either thermal neutrons or the gamma radiation resulting from neutron capture by hydrogen (Schlumberger, 1972b).

Table 3 - Log Crossplot Data - Sears No. 1 Well

ell log depth (m)	R LLS	ILD	HD	γAPI	φD	ρb	Δt	φN	M $\frac{189-\Delta t}{\rho b-1.0}$ x.01	N $\frac{1.0-\phi N}{\rho b-1.0}$	Δtlog	$\phi = \frac{\Delta t log - \Delta tma}{\Delta t_f - \Delta tma}$ Ma=4.7 km/s	Ma=5.3 km/s	Ma=6.0 km/s	Remarks
3.6	1800	45	--	120	14	2.45	81	14	0.74	0.59	81	12.9	18.2	21.7	Positive
53.3	?	?	--	100	18	2.43	84	16	0.73	0.59	84	15.3	20.5	23.9	
58.6	125	70	--	80	14	2.45	81	13	0.74	0.60	81	12.9	18.2	21.7	
60.0	80	40	--	175	5	2.60	69	14	0.75	0.54	69	03.2	09.1	08.7	Limy?
63.2	120	50	--	100-120	9	2.55	76	13	0.73	0.56	76	08.9	14.4	18.1	Fractured?
66.4	55	60	--	110	-1.5	2.7	71	8	0.69	0.54	71	04.8	10.6	14.5	
70.7	40	40	--	120	3	2.64	72	12	0.71	0.54	72	05.6	11.4	15.2	
72.2	48	30	--	100	16	2.42	85	17	0.73	0.58	85	16.1	21.2	24.6	
81.2	40	20	--	222	18?	2.37	103	31	0.63	0.50	103	30.6	34.8	37.7	Anhydrite? Fractured.
84.4	75	55	--	120	15	2.43	81	14	0.76	0.60	81	12.9	18.2	21.7	
87.4	65	95	--	260	8.5	2.54	93	13	0.62	0.56	93	22.6	27.3	30.4	
91.1	950	210	--	80	11	2.47	98	12	0.62	0.60	98	26.6	31.0	34.0	
97.5	40	40	--	105	17	2.40	85	15	0.74	0.61	85	16.1	21.2	24.6	
00.5	30	30	--	225	0	2.69?	79	10	0.65	0.53	79	11.3	16.7	20.2	Anhydrite?
06.0	70	30	--	140	10	2.50	100+	15	<.59	0.57	100+	28.2	32.6	35.5	

- Resistance in ohm-meters
  LLS - Laterlog 8
  ILD - Deep induction
D - Hole diameter, in inches
API - Gamma radiation, in API units
D - Density log porosity, in percent

Δt - Sonic velocity, in microsecond/ft
ρb - Bulk density, in gm/cm^3
φM - Neutron log porosity, in percent
Ma - Matrix, in percent
M, N - Symbols for values used in mineral cross plots (fig. 32)

Table 3 - Log Crossplot Data - Sears No. 1 Well
Continued

Well log depth (m)	R LLS	ILD	HD	γAPI	φD	ρb	Δt	φN	M $\frac{189-\Delta t}{\rho b-1.0}$ x.01	N $\frac{1.0-\phi N}{\rho b-1.0}$	Δtlog	$\phi = \frac{\Delta t log - \Delta tma}{\Delta t_f - \Delta tma}$ Ma=4.7 km/s	Ma=5.3 km/s	Ma=6.0 km/s	Remarks
208.5	240	80	--	80	11	2.49	80	10	0.73	0.60	80	12.1	17.4	21.0	
215.2	80	90	--	140	4	2.60	64	5	0.78	0.59	64	-00.8	05.3	09.4	Limy?
220.0	700	700	--	80	13	2.46	80	9.5	0.75	0.62	80	12.1	17.4	21.0	
221.6	60	60	7.8	180	4	2.60	78	12.5	0.69	0.55	75/ 78	08.1/ 10.5	13.6/ 15.9	17.4/ 19.6	Shale
224.0	60	60	7.6	220	2	2.64	70	9.5	0.73	0.55	70	04.0	09.8	13.8	Low SP, High γ
228.6	1200	120	7.4	85	13.5	2.46	82	11	0.73	0.61	82	13.7	18.9	22.5	Sandstone
239.6	280	60	7.5	110	11	2.50	75	09	0.76	0.61	75	08.1	13.6	17.4	Do.
249.0	350	45	--	80	14	2.47	86	12	0.70	0.60	86	16.9	22.0	25.4	High Sp, Clean Sandstone
271.3	35	30	--	215	4	2.60	82	18	0.67	0.51	82	13.7	18.9	22.5	High γ
275.7	30	45	9.8	180	18.5	2.23	87	31	0.83	0.56	87	17.7	22.7	26.1	Gypsum?
289.2	900	70	7.4	54	12	2.48	73	12.5	0.78	0.59	73	06.5	12.1	15.9	Lowest γ Sandstone
296.6	22	50	9-13	190	10	2.50	101	32	0.59	0.45	101	29.0	33.3	36.2	Thin fracture, Low SP
279.2	24	40	8.8	80	17	2.39	83	16	0.76	0.60	83	14.5	19.7	23.2	Sandstone, Low SP
306.9	80	800	7.6	73	10	2.50	102	12.6	0.58	0.58	102	29.8	34.0	37.0	Sandstone, Anhydrite?
326.4	45	60	8.3	110	8	2.55	67	9	0.79	0.59	67	01.6	07.6	11.6	
328.9	40	40	8.5	140	4	2.62	76	15	0.70	0.52	76	08.9	14.4	18.1	Shale
329.2	50	40	8.3	120	10	2.51	74	18	0.76	0.54	74	07.3	12.9	16.7	Shale

Table 3 - Log Crossplot Data - Sears No. 1 Well
Continued

$$\phi = \frac{\Delta t\log - \Delta tma}{\Delta t_f - \Delta tma}$$

Well log depth (m)	R LLS	ILD	HD	γAPI	φD	ρb	Δt	φN	M $\frac{189-\Delta t}{\rho b-1.0}$ x.01	N $\frac{1.0-\phi N}{\rho b-1.0}$	Δtlog	Ma=4.7 km/s	Ma=5.3 km/s	Ma=6.0 km/s	Remarks
331.6	50	50	9.4	150	01	2.52	75	24	0.75	0.50	75	08.1	13.6	17.4	Shale
334.0	40	40	8.7	95	14-16	2.35	76	09	0.84	0.67	76	08.9	14.4	18.1	Sandstone
335.9	60	60	8.5	110	-2	2.70	68	11	0.71	0.52	68	02.4	08.3	12.3	Shale
338.9	65	190	7.5	110	09	2.52	69	12	0.79	0.58	69	03.2	09.0	12.0	Sandstone
342.0	100	60	7.5	80	08	2.55	73	7.5	0.75	0.60	73	06.5	12.1	15.9	Siltstone
344.4	100	80	7.5	115	06	2.57	66	05	0.78	0.60	66	00.8	06.8	10.9	
352.0	800	85	7.5	50	14	2.44	75	13	0.79	0.60	75	08.1	13.6	17.4	Sandstone, High SP
357.8	45	45	8.8	165	02	2.64	76	15	0.69	0.52	76	08.9	14.4	18.1	Shale
360.0	90	60	7.9	95	12	2.48	70	12	0.80	0.59	70	04.0	09.8	13.8	Thin sandstone
377.6	130	40	8.0	65	11	2.48	73	11	0.78	0.60	73	06.5	06.0	15.9	
394.1	180	70	7.6	65	09	2.52	69	6.5	0.79	0.62	69	03.2	09.0	12.0	Cycle skip just beneath.
398.0	500	80	7.5	150	13	2.46	72	12	0.80	0.60	72	05.6	11.4	15.2	Radioactive Sandstone
417.9	80	80	7.7	250	03	2.72	64	06	0.73	0.55	64	-00.8	05.3	09.4	
419.4	80	60	7.7	325	03	2.72	65	07	0.72	0.54	65	0	06.0	10.1	
440.4	90	70	7.6	55	10	2.50	69	09	0.80	0.61	69	03.2	09.0	13.0	
449.2	50	60	8.6	60	14	2.45	75	14	0.79	0.59	75	08.1	13.6	17.4	Low SP, Sandstone
465.1	80	80	8.0	80	05	2.60	64	07	0.78	0.58	64	-00.8	05.3	09.4	

Table 3 - Log Crossplot Data - Sears No. 1 Well
Continued

Well log depth (m)	R LLS	ILD	HD	γAPI	φD	ρb	Δt	φN	M $\frac{189-\Delta t}{\rho b-1.0}x.01$	N $\frac{1.0-\phi N}{\rho b-1.0}$	Δtlog	$\phi = \frac{\Delta tlog - \Delta tma}{\Delta t_f - \Delta tma}$ Ma=4.7 km/s	Ma=5.3 km/s	Ma=6.0 km/s	Remarks
488.9	60	50	7.5	70	11	2.49	67	10.5	0.82	0.60	67	01.6	07.6	11.6	Sandstone
495.9	50	60	7.8	150	02	2.64	67	13	0.74	0.53	67	01.6	07.6	11.6	Shale
498.9	80	90	7.1	230	09	2.53	67	07	0.80	0.61	67	01.6	07.6	11.6	Sandstone?
500.8	80	60	7.1	76	09	2.52	63	07	0.83	0.61	63	-01.6	04.5	08.7	Sandstone
508.4	120	120	7.1	90	0-02	2.6-2.7	59	04	0.76-0.81	0.56-0.60	59	-04.8	01.5	05.9	Limy sandstone
526.1	70	100	7.1	220	0	2.68	64	08	0.74	0.55	64	-00.8	05.3	09.4	High γ
534.6	70	90	7.5	90	10	2.54	65	06	0.80	0.61	65	0	06.0	10.1	Sandstone
549.8	50	50	7.5	60	12	2.49	64	11	0.84	0.60	64	-00.8	05.3	09.4	Sandstone
550.4	300	60	12	140	22	1.85	82	45	1.27	0.67	82	13.7	18.9	22.5	Fractured
569.3	90	90	7.6	215	02	2.63	67	11	0.75	0.55	67	01.6	07.6	11.6	High γ
570.9	100	100	7.2	250	16?	2.42?	72	15	0.82	0.60	72	05.6	11.4	15.2	High γ
576.3	70	80	7.4	225	01	2.65	64	07	0.76	0.56	64	-00.8	05.3	09.4	High γ
581.5	60	70	7.1	90	09	2.52	66	06	0.81	0.62	66	00.8	06.8	10.9	Siltstone
585.2	120	125	7	220	09	2.54	62	05	0.82	0.62	62	-02.4	03.8	08.0	Sandstone
596.8	200	140	7.3	80	08	2.55	61	09	0.83	0.59	61	-03.2	03.0	07.2	Siltstone
609.6	300	170	7.0	70	-2	2.70	57	03	0.78	0.57	57	-06.5	0	04.3	
619.3	50	55	7.7	140	0-01	2.68	73	10	0.69	0.54	73	06.5	12.1	15.9	Shale

Table 3 - Log Crossplot Data - Sears No. 1 Well
Continued

Well log depth (m)	R LLS	ILD	HD	γAPI	φD	ρb	Δt	φN	M $\frac{189-\Delta t}{\rho b-1.0}\times.01$	N $\frac{1.0-\phi N}{\rho b-1.0}$	Δtlog	$\phi=\frac{\Delta t\log-\Delta tma}{\Delta t_f-\Delta tma}$ Ma=4.7 km/s	Ma=5.3 km/s	Ma=6.0 km/s	Remarks
624.5	70	80	7.1	75	08	2.54	65	07	0.80	0.60	65	0	06.0	10.1	Sandstone
639.4	50	60	7.2	130	0	2.67	70	12	0.71	0.53	70	04.0	09.8	13.8	Shale
638.2	200	130	7.2	80-100	0	2.70	59	3.5	0.76	0.57	59	-04.8	01.5	05.8	
641.9	100	105	--	70	07	2.58	61	05	0.81	0.60	61	-03.2	03.0	07.2	Very low SP, Sandstone
654.7	70	90	--	100	-1	2.70	62	06	0.75	0.55	62	-02.4	03.8	08.0	Siltstone?
670.5	120	120	6.8	70	0-01	2.67	59	5.5	0.78	0.57	59	-04.8	01.5	05.8	Conglomerate
694.9	70	65	7.7	100	0-01	2.68	68	14	0.72	0.51	68	02.4	08.3	12.3	Shale
696.7	180	90	7.1	65	02	2.65	59	05	0.79	0.58	59	-04.8	01.5	05.8	Conglomerate
715.6	80	65	8.0	90	04	2.6	63	09	0.79	0.57	63	-01.6	04.5	08.7	Calcareous shale
742.5	50	50	8.0	95	06	2.55	72	16	0.75	0.54	72	05.6	11.4	15.2	Shale
743.1	35	45	8.4	100	0	2.65	71	15	0.72	0.52	71	04.8	10.6	14.5	Shale
743.7	50	50	7.6	85	0	2.68	65	12	0.74	0.52	65	0	06.0	10.1	Shale?
744.3	70	70	7.4	85	0	2.68	62	08	0.76	0.55	62	-02.4	03.8	08.0	
744.9	100	100	7.2	60	03	2.62	64	08	0.77	0.57	64	-00.8	05.3	09.4	
788.9	150	120	7.0	60	01	2.66	60	05	0.78	0.57	60	-04.0	02.2	06.5	Conglomerate
828.4	110	110	6.8	60	01	2.66	59	06	0.78	0.57	59	-04.8	01.5	05.8	Conglomerate
853.4	70	80	7.2	90	-1	2.70	64	9.5	0.74	0.53	64	-00.8	05.3	09.4	

Table 3 - Log Crossplot Data - Sears No. 1 Well
Continued

Well log depth (m)	R LLS	ILD	HD	γAPI	φD	ρb	Δt	φN	M $\frac{189-\Delta t}{\rho b-1.0}$ x.01	N $\frac{1.0-\phi N}{\rho b-1.0}$	Δtlog	$\phi = \frac{\Delta t log - \Delta tma}{\Delta t_f - \Delta tma}$ Ma=4.7 km/s	Ma=5.3 km/s	Ma=6.0 km/s	Remarks
882.7	160	70	6.6	70	03	2.52	59	06	0.86	0.62	59	-04.8	01.5	05.8	
894.2		?	7												
907.0	100	80	6.8	60	04	2.61	59	09	0.81	0.57	59	-04.8	01.5	05.8	
917.1	50	50	7	95	0	2.70	65	9.5	0.73	0.53	65	0	06.0	10.1	
925.3	190	110	6.8	60	05	2.60	57	04	0.82	0.60	57	-06.5	0	04.3	Conglomerate
936.9	50	60	--	100	-1	2.69	66	10	0.73	0.53	66	00.8	06.8	10.9	
946.1	500	210	--	60	01	2.66	57	04	0.80	0.58	57	-0.65	0	04.3	
976.8	40	30	--	105	<50	1.65	76	42	1.74	0.89	76	08.9	14.3	18.1	
1019.2	600	150	--	70	0	2.68	59	07	0.77	0.55	59	-04.8	01.5	05.8	
1039.3	1200	240	--	70	0	2.68	56	06	0.79	0.56	56	-0.73	-00.8	03.6	
1061.3	90	70	--	125	-4	2.74	67	14	0.70	0.49	67	01.6	07.6	11.6	
1055.2	1200	40	6.6	70	-1	2.69	55	05	0.79	0.56	55	-08.1	-01.5	02.9	
1079.2	?	120	6.6	80	03	2.63	63	7.5	0.77	0.57	63	-01.6	04.5	08.7	
1109.1	?	160	6.5	70	03	2.63	61	07	0.78	0.57	61	-03.2	03.0	07.2	
1115.5	?	105	6.5	135	-3	2.72	66	12	0.72	0.51	66	-00.8	06.8	10.9	Shale?
1125.3	?	100	6.5	175	-3	2.72	72	16	0.68	0.49	72	05.6	11.4	15.2	
1130.8	?	200	6.4	?	4.5	2.60	62-63	5.5	0.79	0.59	62-63	-02.4/-01.6	03.8/04.5	07.8/08.7	Cycle skip

In practice the SNP (sidewall neutron porosity) tool consists of a neutron source and a shielded neutron detector that is pressed against and moved along the borehole wall.

The neutron porosity log presented in plate 1 is scaled linearly in percent porosity. The tool and the automatic porosity compensation system is designed to calculate a porosity from the tool signal that would result if the borehole environment were water filled limestone. The recorded porosity must be corrected for other lithologies, fluids, and gases.

Uncorrected apparent limestone porosities are presented in Table 3. Care was taken to select porosity values from the neutron log opposite points in the borehole when the caliper log indicated the hole was reasonably smooth. Much of the shift toward higher apparent porosities in zones such as at 305 to 335, 445 to 949, 662 to 726, and 796 to 826 m is due to formation shaliness. Extreme high porosity spikes caused by poor logging tool contact with the borehole wall occur opposite fractures and washouts. However, high porosity spikes at 181, 201, and 274 m occurring opposite high gamma-ray anomalies probably indicate the location of radioactive, evaporite-rich beds. There is a slight but overall decrease in minimum porosity with depth. The lowest porosity value, however, occurs at 610 m opposite a dense, 1.8-m thick bed which appears to be cherty and quartzose from the cuttings. Minimum neutron porosities average 4 percent in sandstones thought to be non-porous. This apparent discrepancy is probably caused by the increased shale content of the sandstones.

Sonic Log

The speed of sound in rock is determined principally by the lithology and porosity of the rock. Indurated sandstones, limestones, and dolomite have high compressional velocities. Salt, gas, and water have relatively low velocities. The sonic log on plate 1 is a recording of the travel time of a compressional wave through the rock parallel to the well bore. The log is recorded in microseconds per foot which is the reciprocal of the compressional wave velocity and called the interval transit time.

Since sonic log response is dependent on porosity and independent of fluid content for lower porosities, it is an excellent porosity log. Shaliness tends to increase interval transit time (Δt) because the characteristic velocity of shale matrix is slower than that of sandstone. Thus, porosities calculated for shaly sandstones assuming a clean sandstone matrix velocity are too high.

Wyllie and others (1956) and Wyllie (1958) have developed a formula that relates porosity to interval transit time in clean sandstone.

$$\phi \text{ sandstone} = \frac{\Delta t - \Delta t_{ma}}{\Delta t_f - \Delta t_{ma}}$$

where:

Δt = the interval transit time from the sonic log in microseconds/foot.

Δtma = the inherent interval transit time of the rock matrix.

Δt_f = the interval transit time of water.

Porosities were calculated from the sonic log by the Wyllie formula for selected intervals of the Sears No. 1 well and are presented in table 3. The accuracy of these calculated porosities is dependent on the accuracy of estimated matrix velocity. An error of 1.0 microsecond/foot changes the computer porosity about 0.5 percent.

Crossplots of sonic velocity-bulk density, sonic velocity-neutron porosity, bulk density, and apparent limestone porosity (figs. 28, 29, 30) have been made to gain insight into the applicable matrix velocities of the Sears No. 1 well lithologies. It is readily apparent from these figures that a major portion of these points plot in the limestone-sandstone range having matrix velocities between 5,500 and 6,400 m/s (∇t_{ma} = 55.6 to 47.6 s/ft). It is equally obvious that many if not most of the points on the density-sonic crossplot plot in the dolomite range. Many of these points are identified as mudstones and argillites, and their displacement into the dolomite region of the chart is not the result of their having a dolomite matrix, but rather a result of their high density and low matrix velocity (higher ∇t_{ma}). The measured high densities also indicate that the shales penetrated in the New Hill well are not overpressured.

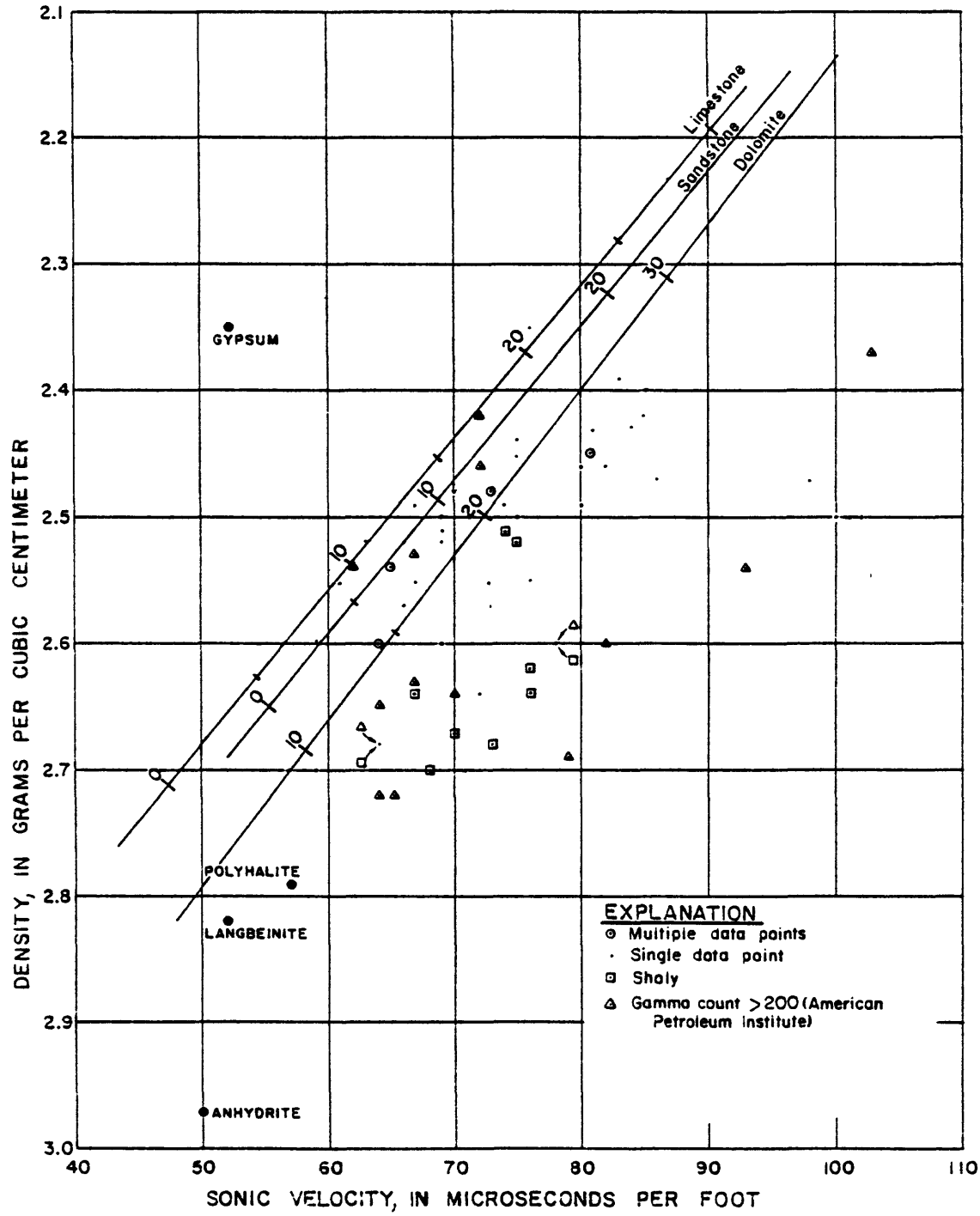

Figure 28. Bulk density versus sonic velocity for Triassic rocks in the Sears No. 1 Well.

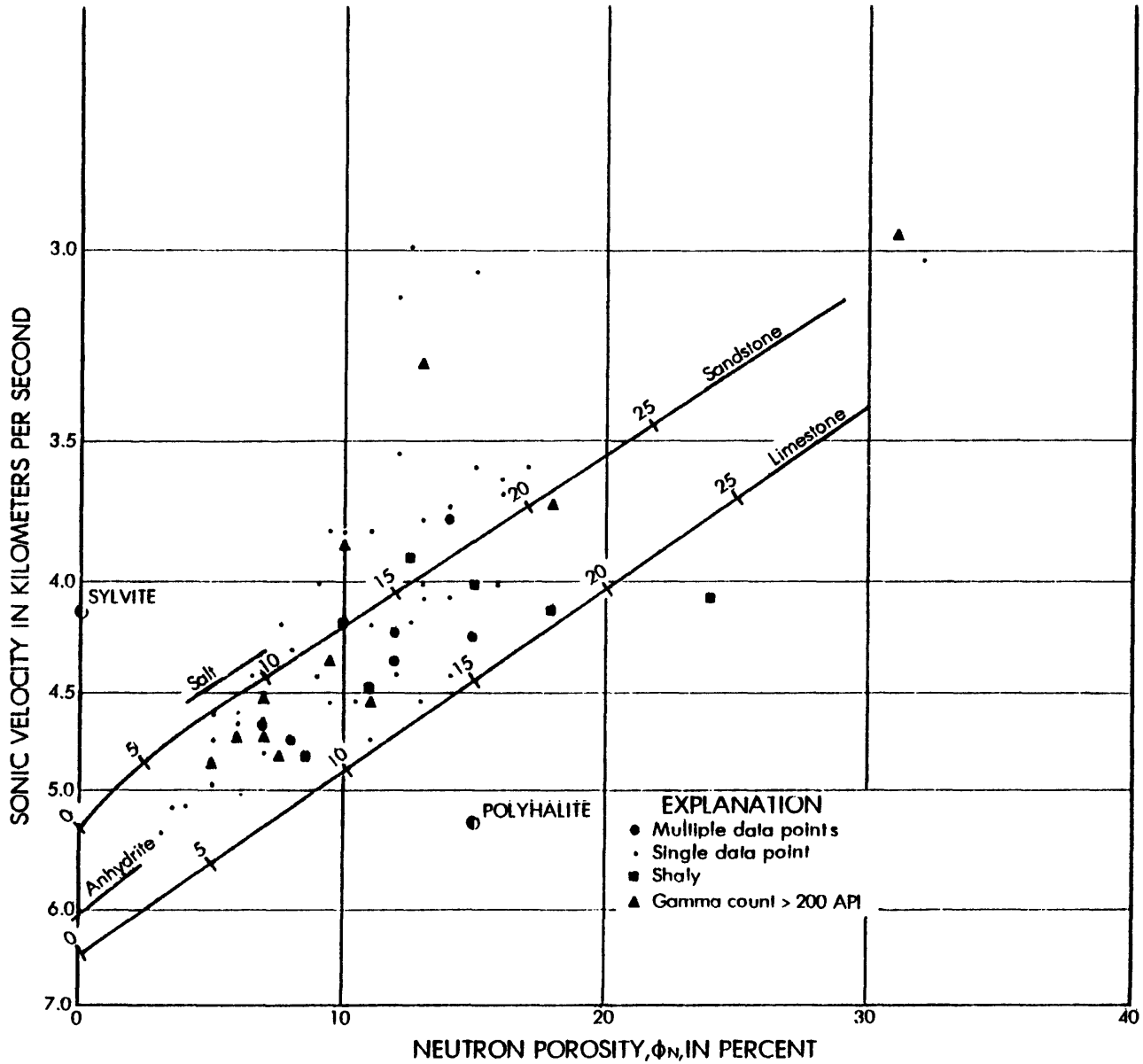

Figure 29. Neutron porosity versus sonic velocity for Triassic rocks in the Sears No. 1 Well.

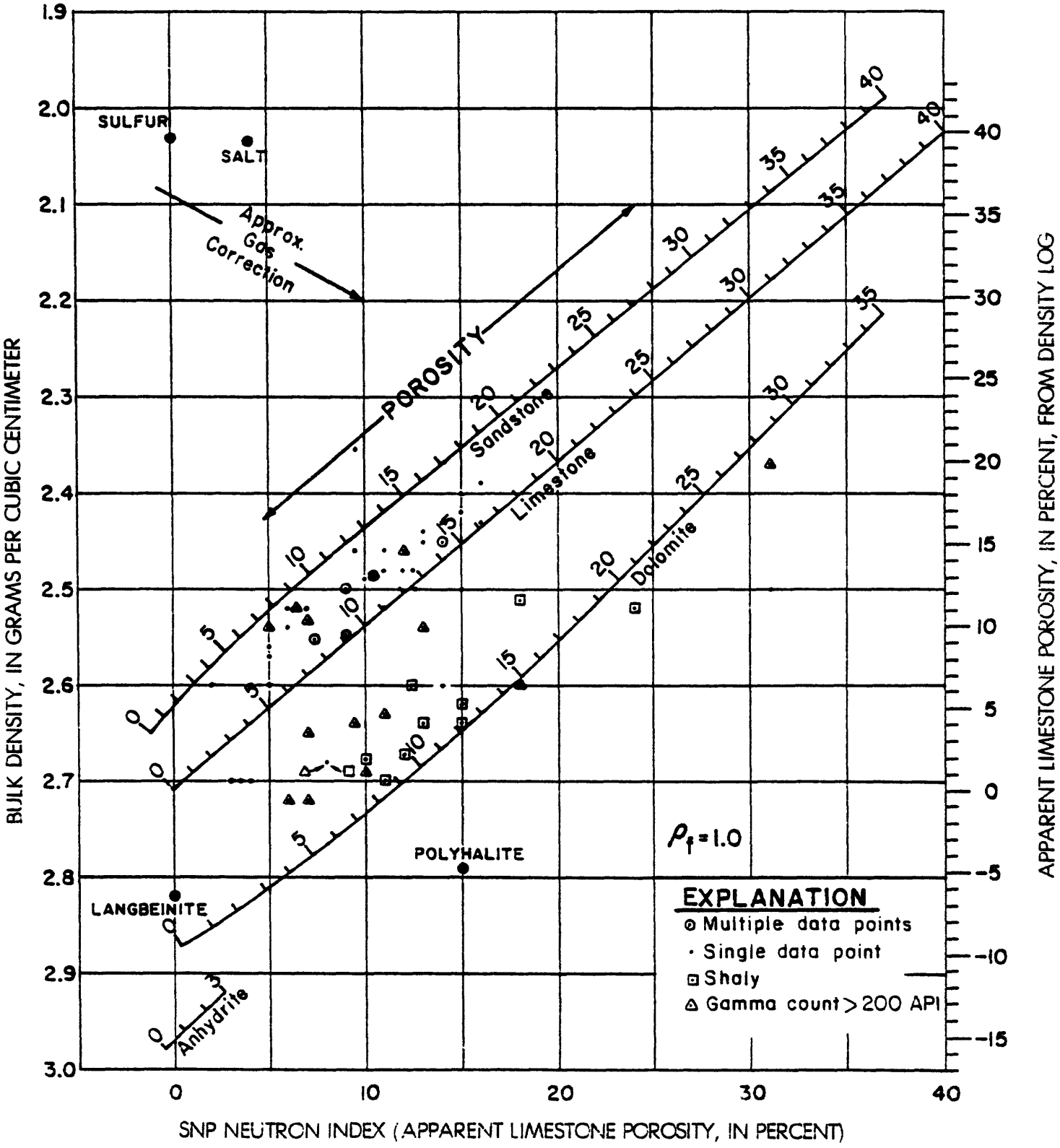

Figure 30. Bulk density versus apparent limestone porosity for rocks in the Sears No. 1 Well.

Figure 31 is a sonic-density crossplot of sandstones from the New Hill well. Figure 31 and figure 32 both reveal that all of the lithologic points plot above a ∇t of 56.5 microseconds/ft. and below a density of 2.73 gm/cm^3.

The sonic logging tool has two transmitters that are pulsed alternately. The received signals are integrated to give the recorded interval transit time and integrated travel time. The travel time between any two depths in the hole may be computed by totaling each millisecond pulse between the desired depths.

The first signal arriving at the sonic receiver is generally the compressional wave that has traveled through the rock adjacent to the borehole. However, if that signal is attenuated by gas, salt, or fractures in the formations, the receiver will record some later arrival. The result is a large displacement of the log curve to the left toward lower velocities (higher Δt) called "cycle skipping." Examples of this problem in the Sears No. 1 well occur at approximately 1,003, 887, 729, and 393 m. Cycle skipping can be caused also by badly washed out hole conditions. Although the occurrence of small amounts of gas cannot be ruled out in the Sears No. 1 well, the caliper log indicates that these cycle skips occur opposite greatly enlarged parts of the well bore.

The sonic log also has several sharp spikes or deflections to the right below 848 m. Although these could represent thin-bedded anhydrite zones, the recorded transit time is faster than is normal for anhydrite; therefore, these high velocity spikes are assumed to be noise spikes caused by cable and tool noise triggering the sonic receiver in a low signal area of the borehole.

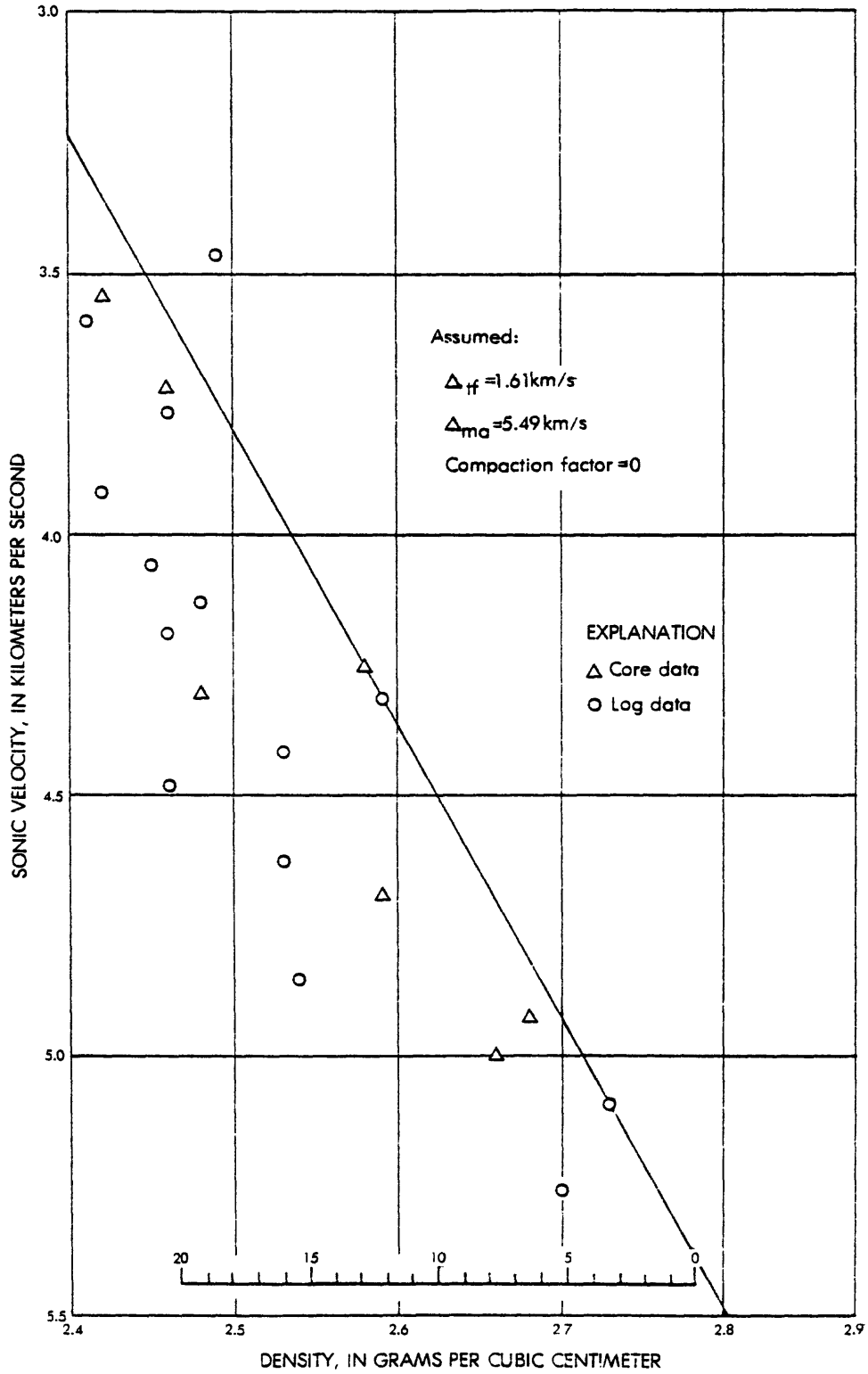

Figure 31. Density versus sonic velocity of cores and selected clean sandstones.

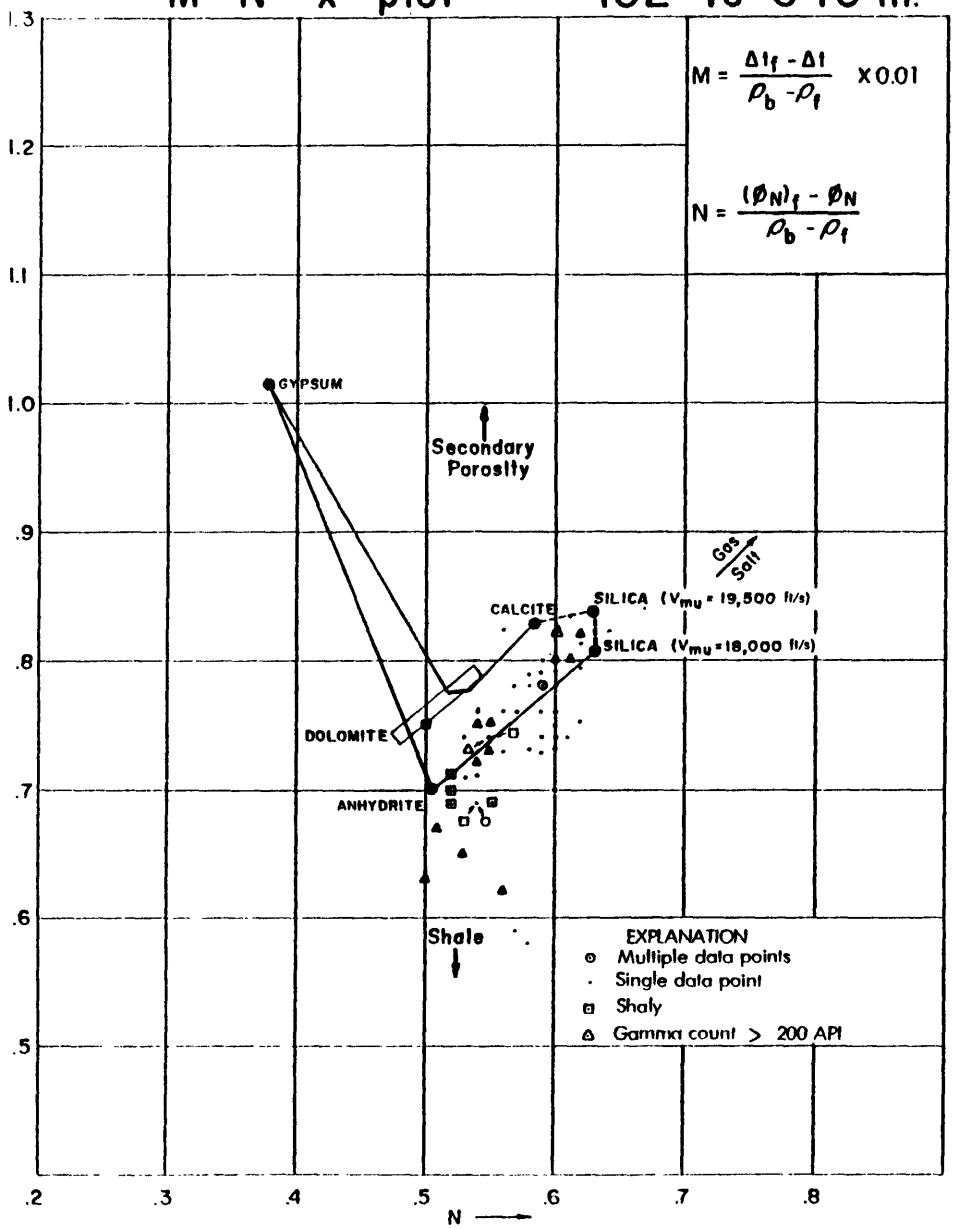

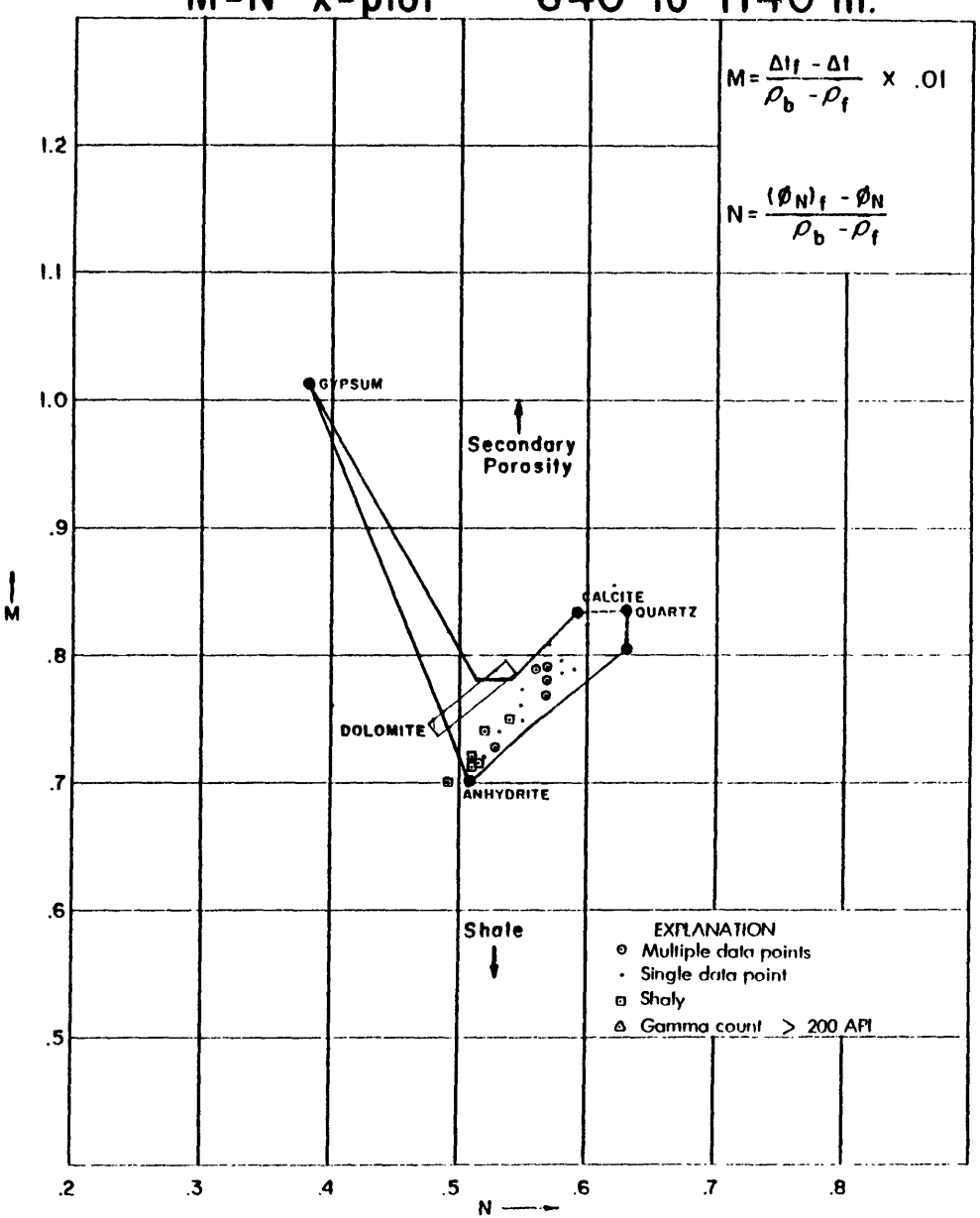

Figure 32. Mineral crossplots derived from geophysical logs.

The sonic log, being matrix-velocity dependent, is a good lithology tool and is commonly used for correlation purposes. The overall character of the Sears No. 1 sonic log confirms the cyclic character of the sedimentary rocks and the 793 to 1,134 m interval correlates quite well with the 1,174 m to 1,524 m interval of the Groce No. 1 well.

The data from sonic, density, and neutron logs are sometimes crossplotted to give additional information on mineral composition of the rocks penetrated. Figure 32 is an M-N crossplot (Schlumberger, 1972) of the above logs from the Sears No. 1 well

where:

$$M = \frac{\Delta t_f - \Delta t}{\rho b - \rho t} \times 0.01$$

$$N = \frac{(\phi n)_f - \phi n}{\rho b - \rho f}$$

and:

Δt_f = interval transit time of the fluid.

Δt = interval transit time of the logged interval.

ρb = bulk density of the logged interval.

ρf = density of the fluid.

$(\phi n)_f$ = 1.0

(ϕn) = percentage neutron porosity of the logged interval.

The plotted points are lithology dependent. Thus, binary mineral mixtures under ideal conditions should plot along lines connecting any two minerals and trinary mixtures should plot in the triangular areas connecting their respective end points. In practice gas and salty mud cause a shift of the data plot to the upper right, and shaliness causes a shift to the lower center. Figure 33 indicates that the upper 640 m of the Sears No. 1 hole is a relatively clean mixture of quartz, calcite, and anhydrite but below that point there is a major displacement of the data field downward toward the shale region. This interpretation corresponds to the sample data (plate 1).

Gamma Ray Log

The gamma ray tool measures the natural emmission of gamma-ray particles by the borehole environment resulting from the decay of radioactive minerals. Measurement is generally made with a borehole scintillation counter and recorded in American Petroleum Institute (API) units as in plate 1. Gamma-ray radiation is random; therefore, a time constant and logging speed is chosen to give a good average measurement.

The gamma-ray curve illustrates, as do the resistivity and sonic logs, the alternating sandstone-shale, cyclic nature of the Triassic rocks at Sears No. 1 well in the Durham subbasin. The "cleaner" sandstones occur at 289, 351, 537, and 782 m and have radiation values of 50 to 55 API units. Most of the units identified on the sample log as sandstones have radiation levels between 60 to 80 API units. The SP curve opposite the sandstone zones has a higher negative deflection indicating that they are water filled and more permeable. The lack of a good SP deflection opposite the 782 m zone indicates that if it contains water its chemistry is close to that of the drilling mud and/or that this sandstone is nonpermeable. The gamma-gamma density log indicates that it has a porosity no greater than 2 percent.

The shaly sediments in the Sears No. 1 well consist predominately of massive argillite and mudstone. There is little evidence of thin laminated fissile shale in the cuttings. The grey massive argillaceous unit between 308 m and 338 m is a good example of the "shale" radiation level of the upper part of the Sears No. 1 well. The red mudstone and argillite facies below 640 m, however, has a lower radiation level of around 100 API units.

The upper 610 m of this log have a number of thin gamma-ray anomaly peaks having intensities greater than 200 API units. The largest of these occurs at 420 m. That part of the gamma-ray log run in the cased part of the hole (0 to 151 m) apparently has 3 or 4 zones having gamma-ray intensities greater than 200 API units. Adjustment of the larger anomalies in the cased part for attenuation increases the 140 API measurements to about 225 API units.

The gamma-ray log anomalies at 161, 188, 398, 499, 571, and 585 m appear from sample logs and log crossplots to occur in sandstone. Some anomalies definitely occur at the base of the sandstones. The sandstone at 161 m is calcareous. Anomalies at 181, 271, 418, and 420 m are probably in shale. The anomaly at 201 m is perhaps in siltstone. Some of the anomalies such as at 181 and 188 m are opposite washed out parts of the hole.

Temperature and Borehole Televiewer Logs

A thermal gradient exists between the Earth's core and crust. The temperature gradient near the surface is generally about 1°C/55 m. Departure from this average gradient is caused by differences in the thermal conductivity of rocks, the degree of meteoric water circulation, and the depth to magmatic activity.

Borehole-temperature logging is usually accomplished with a sonde having a thermistor whose internal resistance changes in response to temperature change (Keys and McCary, 1971). In addition to determining gross thermal gradients the temperature log is used to detect entry and flow of liquids and gases in the borehole, thermal conductivity of individual beds, and the location of new cement grout behind casings.

The temperature logs of the Sears No. 1 well are presented in plate 1 and figure 33. The Geological Survey and Schlumberger logs in figure 33 are plotted beside the caliper and sample logs to facilitate examination of the temperature anomalies. The Schlumberger and Geological Survey temperature logs in plate 1 are not exactly at the same scale, thus it is difficult to compare temperature differences. The temperature gradient at the Sears No. 1 well was 1°C/66 m, but at the Groce No. 1 well near Sanford the gradient ranged from 1°C/16 m for the upper 366 m to 1°C/36 m from 366 to 1,616 m.

The Geological Survey log records a temperature of 20.7°C at a point where the Schlumberger log records 21.7°C. The maximum temperature recorded by the Geological Survey log is 30.7°C, and the thermal gradient as recorded by the Geological Survey log is steeper. The difference is thought to be caused by the circulation of colder drilling fluid with the warmer borehole environment prior to the Geological Survey temperature logging. Despite the differences in logging sondes, logging dates, and elapsed times since circulation, both the Geological Survey and Schlumberger logs, with few exceptions, show the same temperature anomalies at the same depths.

Most of the temperature anomalies occurring above 500 m appear caused by cooler water moving down the well bore and outward opposite more permeable sandstones. Most of the anomalies below that point appear opposite points identified on the caliper log as fractures. The small anomaly at 550 m appears caused by warmer water moving up the hole and discharging into the fracture at that point. The low temperature gradient of this well probably indicates deep circulation of ground water.

In addition, an acoustic televiewer logging tool was used to examine the detailed physical character of the borehole opposite recorded temperature and caliper anomalies. Figure 34 illustrates the apparent fractures and washouts observed between the depths of 590 to 620 m and 650 to 660 m that are typical for parts of the borehole. Vertical drilling tool marks and horizontal and dipping fractures or partings can be observed on the televiewer log. Most caliper anomalies and televiewer borehole enlargements occur opposite corresponding temperature anomalies (Keys and others, 1979) in this borehole.

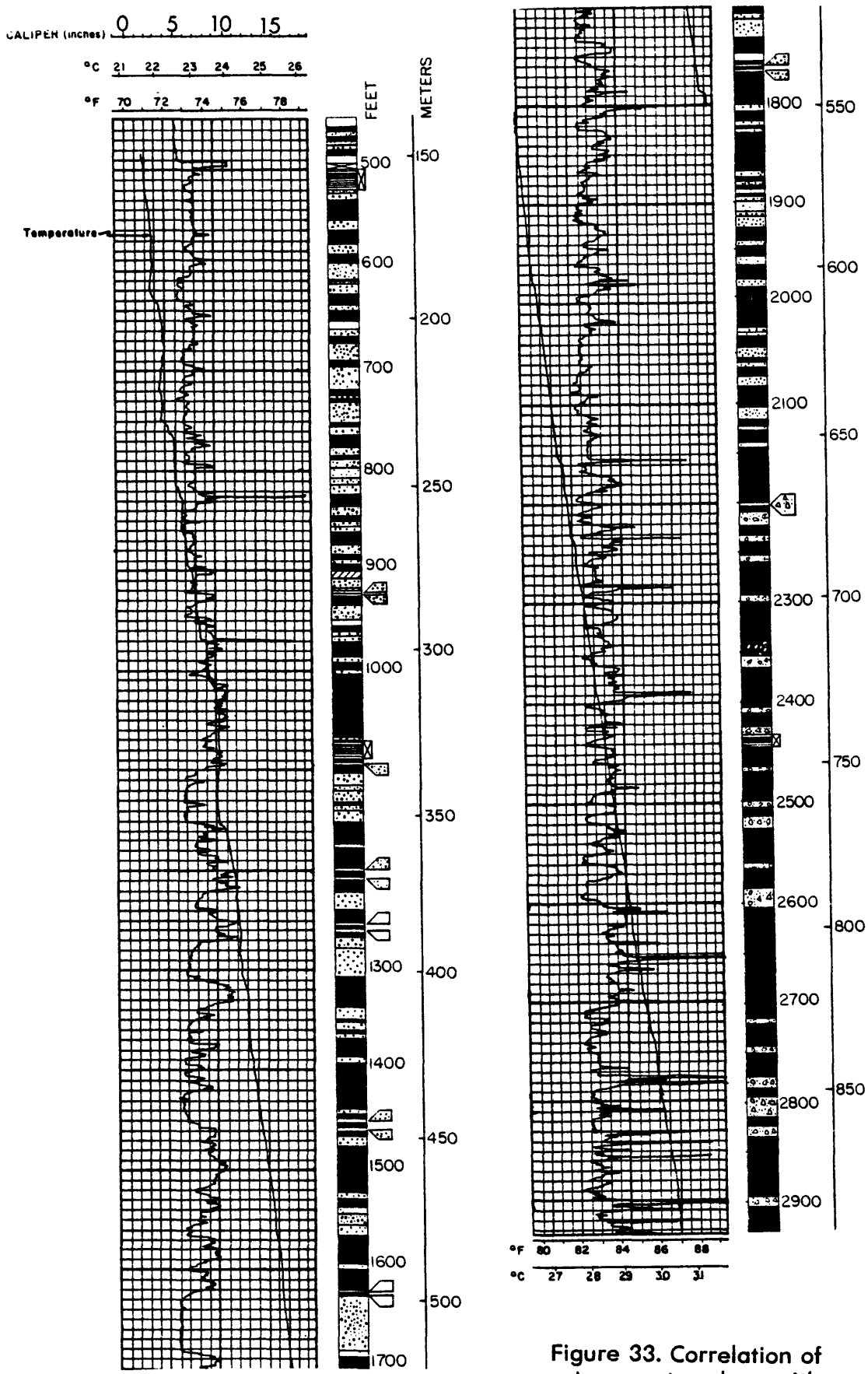

Figure 33. Correlation of temperature logs with caliper and sample logs.

Correlation with Groce No. 1 Well

The basal 350 m of the Sears No. 1 well is correlated with the basal 396 m of the Pekin Formation in the Groce No. 1 well of the Sanford area because of similar log response in plate 1 where the dual induction laterologs of the two wells are displayed. There is some suggestion from these logs that as much as 590 m of the basal part of the Sears No. 1 well may correlate with the basal 640 m of the Groce No. 1 well. There is no indication that a unit equivalent to the carbonaceous, coal and oil-shale bearing Cumnock Formation or one equivalent to the Sanford Formation of the Groce No. 1 well is present in the Sears No. 1.

The stratigraphic relationships between the two wells suggest (see fig. 3) that the environments of deposition were similar in both the Durham and Sanford areas during Pekin time and possible into early Cumnock time. Thereafter a stable, swampy, reducing, low sediment-input environment was created in the Sanford area at the same time that a higher energy environment was creating channel sands and point bars in the finer alluvial fan deposits of the New Hill area. In the Sanford area the paludal deposits were succeeded by red, poorly sorted sands and mudstones. In the New Hill area a different source area contributed increasingly greater amounts of grey to buff granite wash to the sediment pile.

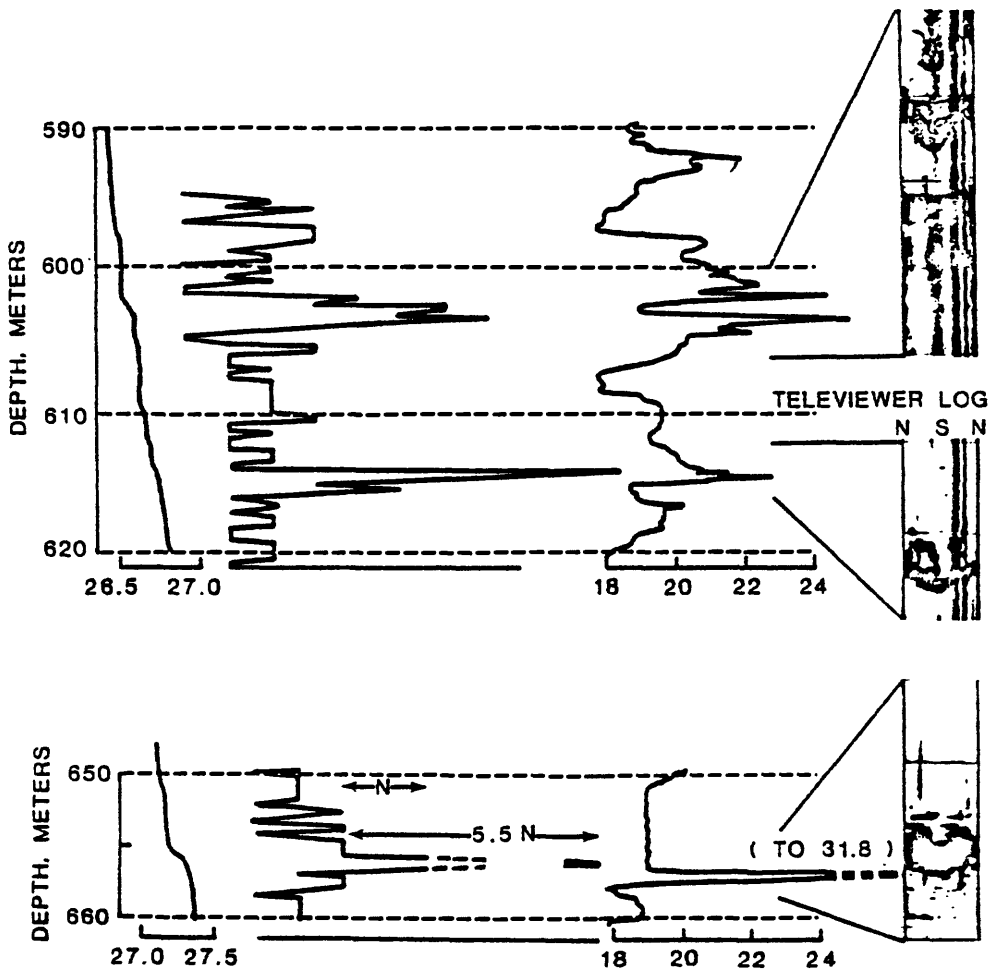

Figure 34. Graph showing temperature, differential temperature, caliper, and acoustic televiewer logs, Sears No. 1 well, Raleigh, N.C. (From Keys, and others, 1979)

HYDROLOGIC TESTING

The Triassic rocks of the Durham Triassic basin have inherent low porosity and permeability as stated previously, because they are continental type sediments which are not well sorted. Much of the initial or primary porosity has been lost through diagenesis, lithification, and compaction. Consequently ground-water yields are low--generally below 2.6 L/s in the shallow domestic wells (Bain and Thomas, 1966).

The ability of a subsurface rock formation to accept waste depends primarily on its porosity and permeability and the compatibility of the native fluid with the injected wastes. A subsurface geological horizon having large permeability and porosity values is therefore desirable. Injection into formations having reduced porosity and permeability not only reduces the amount and rate of injections, but raises the risk of fracturing the reservoir rock because of the increased higher head normally used to maintain reasonable injection rates. However, where waste toxicity is high and volumes low, the "tight" formation may be worthy of consideration.

Porosity

Laboratory porosity and permeability tests on representative core samples from the Deep River coal study (Reinemund, 1955) in the Sanford area and on core from the Sears No. 1 test well are presented in tables 1 and 4. Continuous porosity values for the Sears No. 1 well are available from the neutron porosity and gamma-gamma density logs of plate 1. In addition porosity values calculated for matrix velocities of 4.7, 5.3, and 6.0 km/s are presented in table 3.

The porosities determined from the geophysical logs show little relation to laboratory porosity values on core from equivalent depth. There is little consistency between the density, neutron, and acoustic porosity values in table 3. The Sears No. 1 well was badly washed out and the resulting hole diameter effects on the log porosity values are obvious. The neutron-log response is particularly vulnerable to the shaly matrix of the Triassic rocks.

Log values presented in table 3 were picked at depths where the hole was reasonably smooth and not washed out. Explanations for the apparent inconsistencies among the log porosities are given in the "Remarks" column of table 3. In sandstone the gamma-gamma and neutron-porosity values generally agree within 15 percent, and the corresponding acoustic porosity is found in the higher matrix-velocity columns. If the lithology is shale, the neutron value is erroneously high. The more nearly correct acoustic porosity value and the value closer to the gamma-gamma value is found in the lowest matrix-velocity column.

Table 4 - Physical Properties of Core from the Deep River Coal Field

Well No.	Specimen No.	Depth (m)	Density (S.G.) (g/cm^3)	Density Bulk (g/cm^3)	Porosity Ø (pct.)	Permeability μm^2	Tensile strength (kPa)
DH-2[4]/	1	290	2.64	2.58	2.04	4.9×10^{-5}	12170
	2	324	Broken	--	--	-----	---
	3	434	2.62	2.53	3.35	4.0×10^{-5}	[1]/
	4A	443	2.65	2.62	.88	3.0×10^{-5}	[1]/ 14286
	B[2]/	--	--	--	--	-----	17596
	5	409	[1]/	--	--	-----	---
	6	53	2.65	2.37	10.7	4.3×10^{-4}	5192
BH-11	7	68	2.66	2.53	4.82	[1]/	4385
	8	75	2.68	2.49	7.11	4.3×10^{-4}	9970
BH-10	9	19	2.71	2.00	26.4	2.1×10^{-3}	4999
	10	32	2.71	2.49	8.00	9.9×10^{-5}	7502
BH-7	11A	352	2.66	2.64	.83	2.0×10^{-5}	12549
	B[2]/	--	--	--	--	-----	9998
BH-9	12[3]/	145	2.68	2.37	11.8	5.9×10^{-4}	5440

[1]/ Specimen unable to be extracted from core.
[2]/ Duplicate tested tensile strength only.
[3]/ Oil saturation 3.25 percent.
[4]/ Refer to Reinemund, 1955 for sample locations.

The lower laboratory porosity values and lack of consistency between laboratory-measured and well logging values are not understood. Factors which could cause such differences include:

1. The nonrepresentativeness of the small laboratory test plug to the volume of rock being sampled by the logging tool.

2. Crystal structure changes in the rock core between the time the rock was cored and tested in the laboratory.

3. Incorrect calibration of the logging tools for grain density, and matrix velocity.

Whatever the explanation, laboratory determined gas porosities range from 0.83 to 12 percent in tables 1 and 4 below 152 m. The average is about 3.5 percent.

Transmissivity

Two zones in the Sears No. 1 well were isolated with inflatable packers for hydrologic tests and water sampling. A slug test, swabbing or bailer test, and a pressure-injection test were tried on the upper zone between 247 and 264 m.

In the slug test the drill stem above the packer was filled to the surface with water, the packer was then opened to the isolated formation, and the subsequent decay in head was observed with time. The test data and a plot of the ratio of residual head to initial head with time is shown on figure 35. The transmissivity of the 247 to 264 m zone is calculated to be $1.19 \times 10^{-3} m^2/d$ (Cooper and others, 1967).

This zone was then swabbed for water samples. At the same time the change in head over several swabbing intervals was used to conduct a "Skibitske" bailer test (see Ferris and others, 1962). The results of one such test was illustrated by figure 36. The transmissivity calculated

$$\text{from} \quad T = \frac{V}{12.57\, S' t}$$

where V = volume of water.
S' = change in head between swabbing intervals.
t = time between swabbings intervals.

gives a transmissivity of $4.4 \times 10^{-3} m^2/d$ of the same order of magnitude as that from the slug test.

A single packer was used to isolate a zone betwen 1,009 m and the bottom of the well at 1,143 m in the Sears No. 1 well. The second slug test was conducted in the same manner as the first. The test data are plotted in figure 38. The calculated transmissivity of $8.46 \times 10^{-5} m^2/d$ compare favorably to a transmissivity value of $8.6 \times 10^{-6} m^2/d$ estimated from a low permeability value for rocks of that zone.

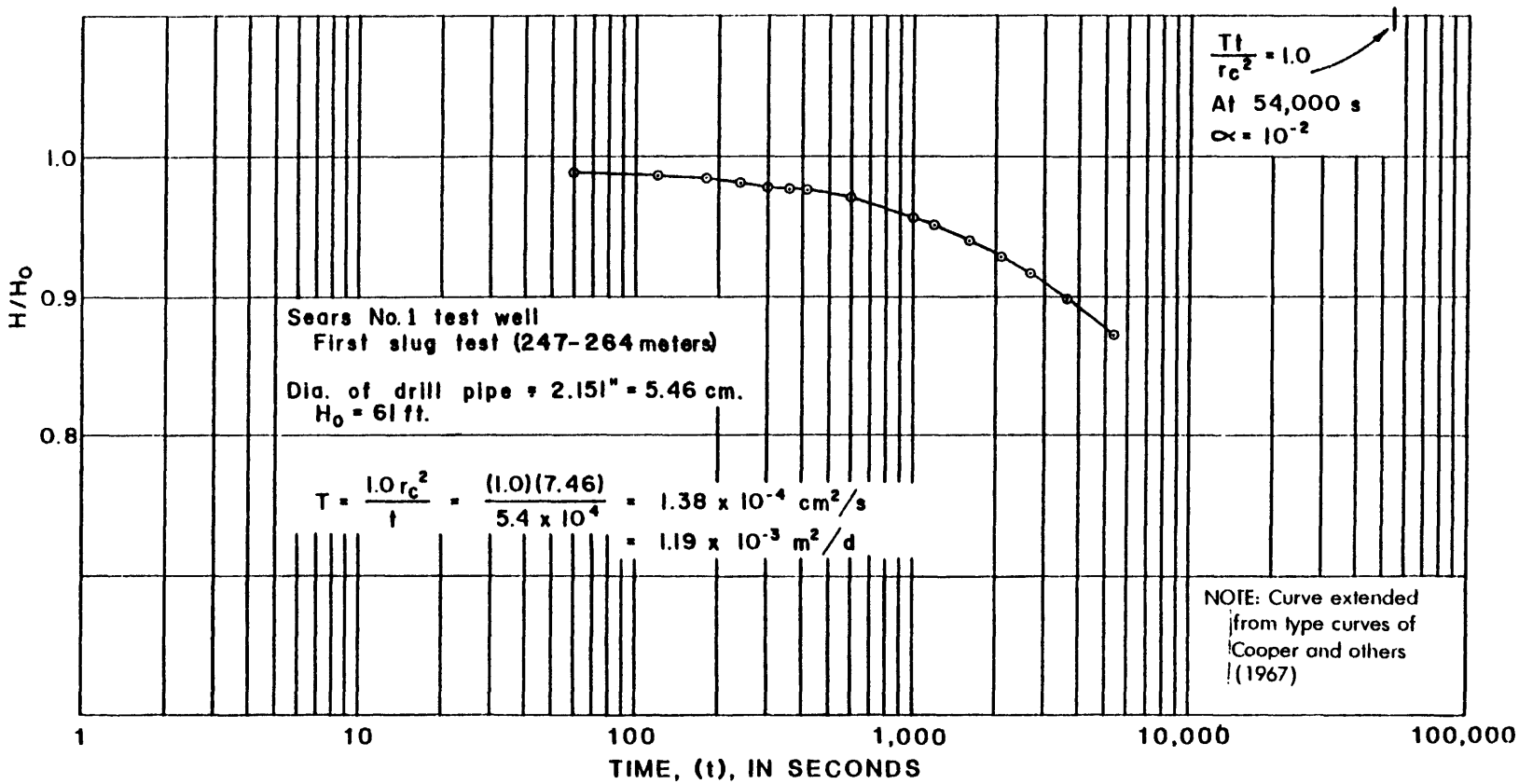

Figure 35. Decay of head with time of slug test of 247 to 264 meter zone.

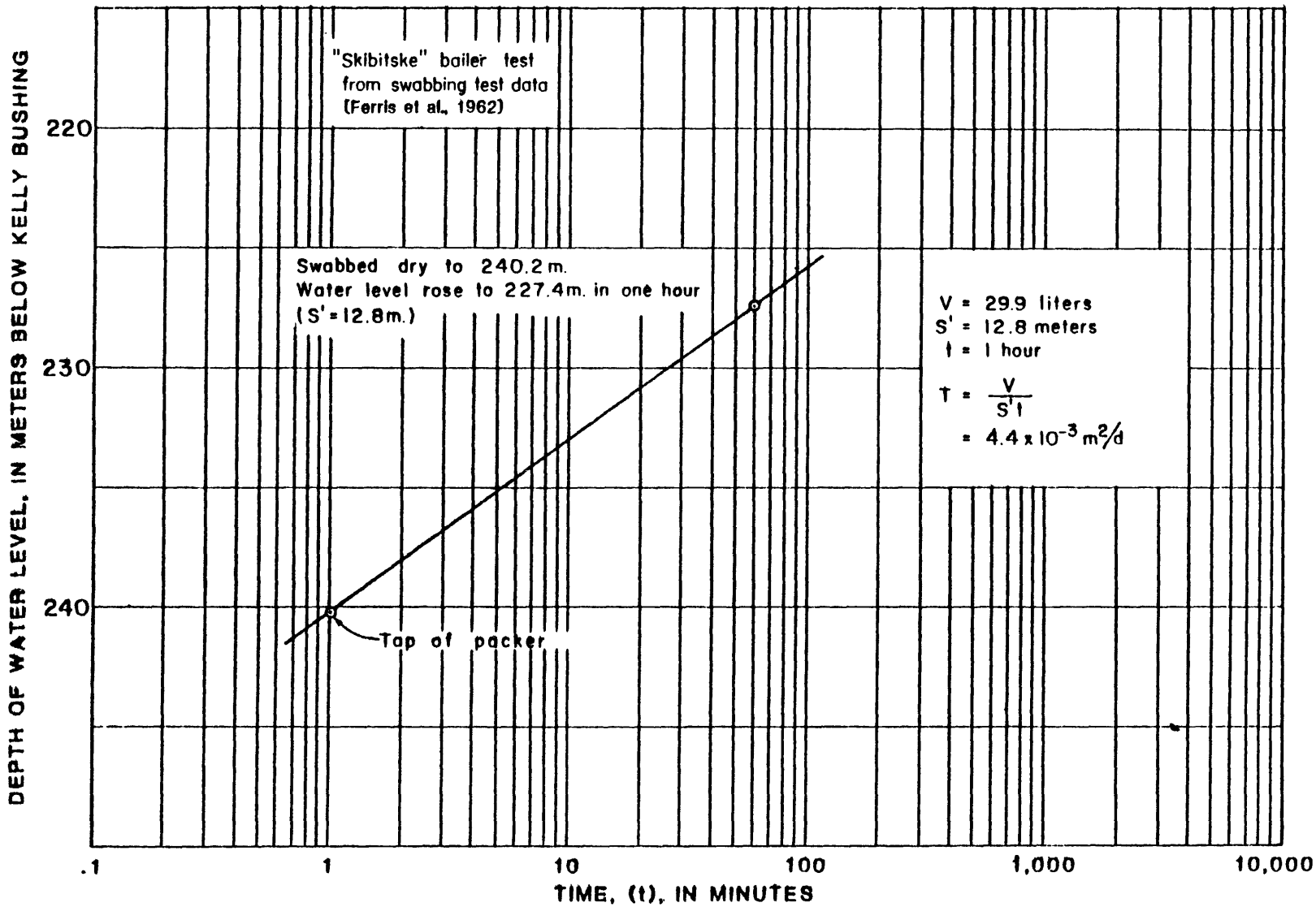

Figure 36. Increase of head with time from bailer test of the 247 to 264 meter zone.

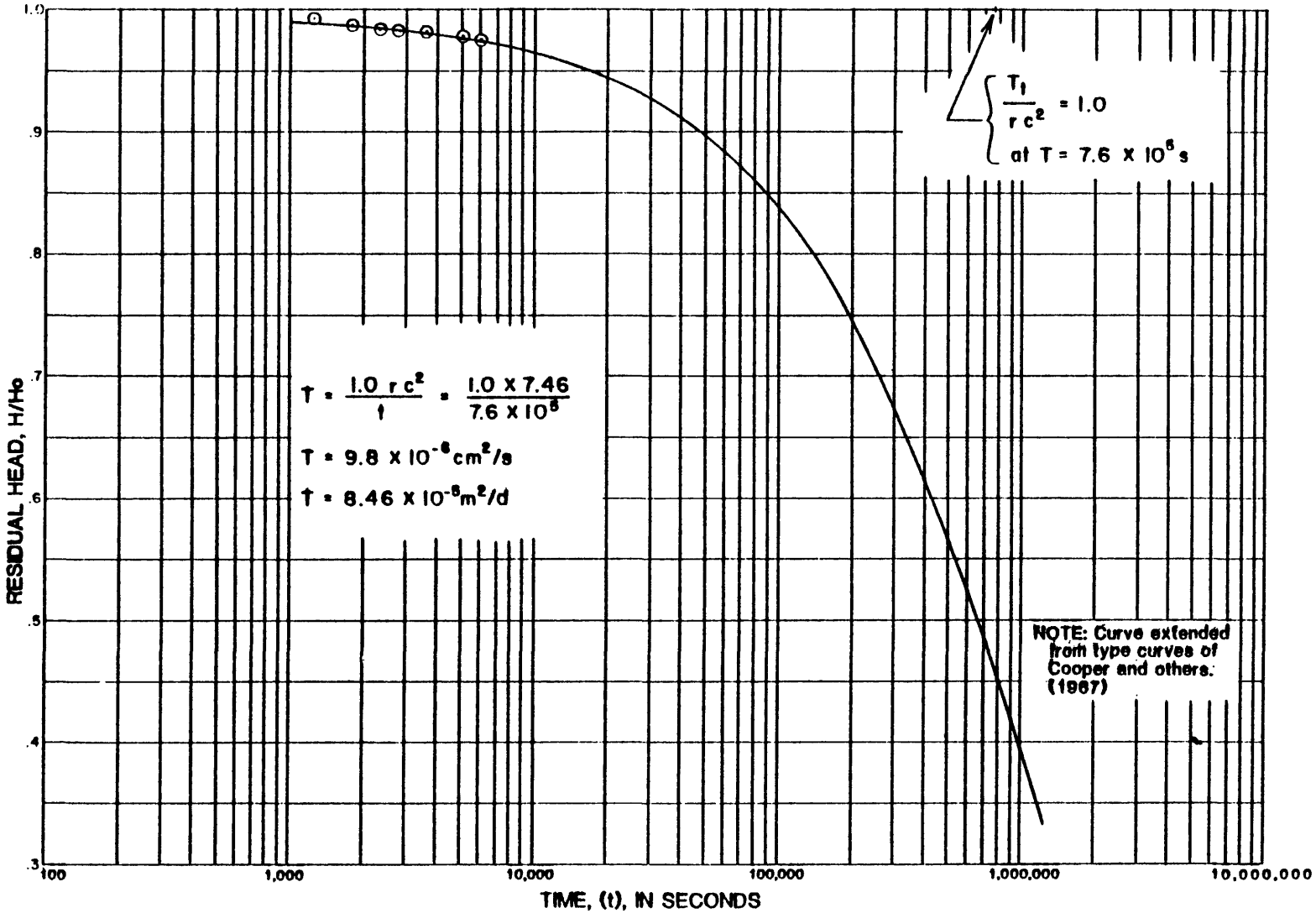

Figure 37. Decay of head with time from slug test of the 1009 to 1143 meter zone.

Permeability

Laboratory air permeability tests (tables 1 and 4) of Triassic core from the New Hill well and Deep River coal drill holes illustrate the low permeabilities characteristic of the Triassic rocks below the zone of weathering. Most values are in the microdarcy and nanodarcy range. Attempts to determine liquid permeability with water reconstructed from laboratory analyses of water pumped during packer tests of the Sears No. 1 well resulted in rupture of some samples having extremely low permeability. The apparent sensitivity to the water indicates swelling of clays (or other mineralogic changes) caused by use of water of probable different chemistry. Montmorillonite has been identified as the most abundant clay in samples from the Sears No. 1 well (Lee Avery, written communications, 1977). The logical explanations for water of different chemistry are:

1. The laboratory water used had the correct salinity but a different ionic make up.

2. The water samples pumped during testing of the Sears No. 1 well are not representative of the native formation water.

Average permeability of the sandstone between 247 and 264 m depth in the Sears No. 1 well can be calculated from the transmissivity of the zone which was derived from a slug test and is $1.19 \times 10^{-3} m^2/d$

$$K \simeq \frac{T}{H}$$

$$\simeq 7.1 \times 10^{-5} m/d$$

$$\simeq 1 \times 10^{-4} \mu m^2$$

$$\cong 100 \text{ microdarcies.}$$

where K = the hydraulic conductivity
T = the transmissivity
and H = the thickness of the aquifer.

Triassic rocks in well DRB 10 in the buried Dumbarton basin, South Carolina, is reported to have a hydraulic conductivity of approximately $6 \times 10^{-6} m/d$ or about 8 microdarcies.

Injection Tests

Pressure injection tests were run by raising the head on the water filled packer and drill-stem assembly with the mud pump, observing the decay of pump pressure with time, and calculating the volume of water injected from the pump displacement. The data plot for the 1,009 to 1,143 m test are given in figure 38.

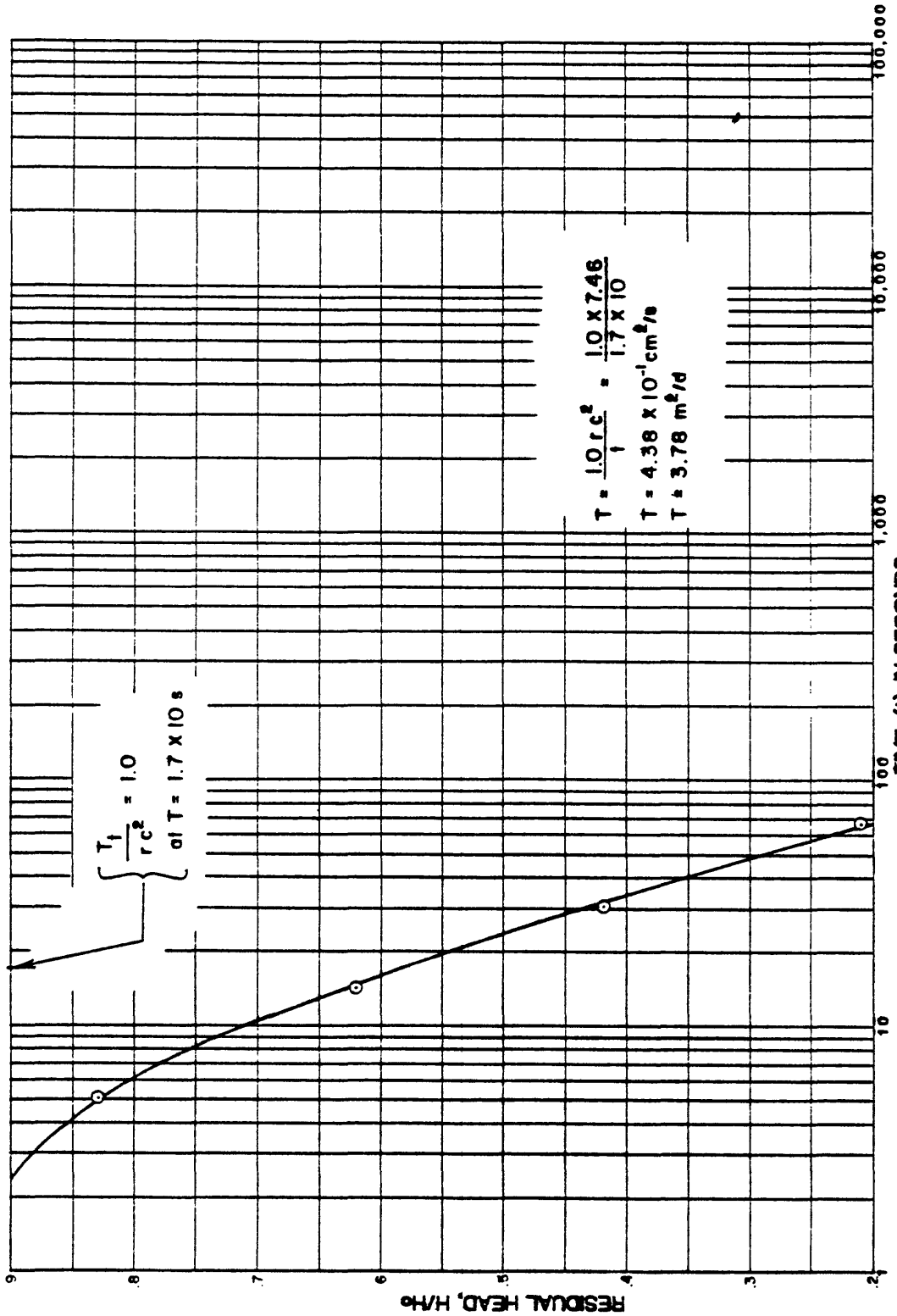

Figure 38. Decay of head with time for water injection tests of the 1009 to 1143 meter zone.

Treating both tests as slug tests gives transmissivities 6.44 x $10^{-2}m^2/d$ and 3.78 m^2/d for the 247 to 264 m and 1,009 to 1,143 m zones respectively. The test in the upper zone appeared to be a normal test. The lower zone appeared to fracture as the head increased above hydrostatic because pressure decay was much more rapid.

Ground-Water Circulation

Insufficient subsurface-head-distribution data are available to establish a predictable ground-water circulation pattern. The few near surface ground-water potentials indicate that the flow pattern is normal--that is, recharge occurring along the interstream areas and discharge occurring along and beneath the major streams. Ground water having dissolved-solids content greater than 2,400 mg/L--chiefly calcium-sodium chloride types--occurs along the eastern edge of the basin from Morrisville to Cary and southwest to Holly Springs (fig. 39). The location of these occurrences relative to the downfaulted blocks (fig. 3) along the east side of the basin indicates that the probable source of the high dissolved-solids content water is from flushing of saltwater upward along fracture zones that bound the blocks. No unusual head relationships were encountered in drilling the Sears No. 1 test well. The temperature log, however, indicated upward movement of water to the 550 m zone and downward movement to the 500 m zone. The resistivity and spontaneous potential (SP) logs from that well indicate that the native water of the formation is relatively fresh (<4,500 mg/L dissolved-solids content) to the bottom of the hole. The steep slope (lower gradient) of the Sears No. 1 temperature log tends to suggest deep meteroic circulation at New Hill. In contrast the temperature gradient of the Groce No. 1 well indicates poor ground-water circulation in the Sanford area.

The low permeabilities of the core samples and the low temperature gradient indicate the probability that circulation in the unweathered rock in the subsurface is through fractures.

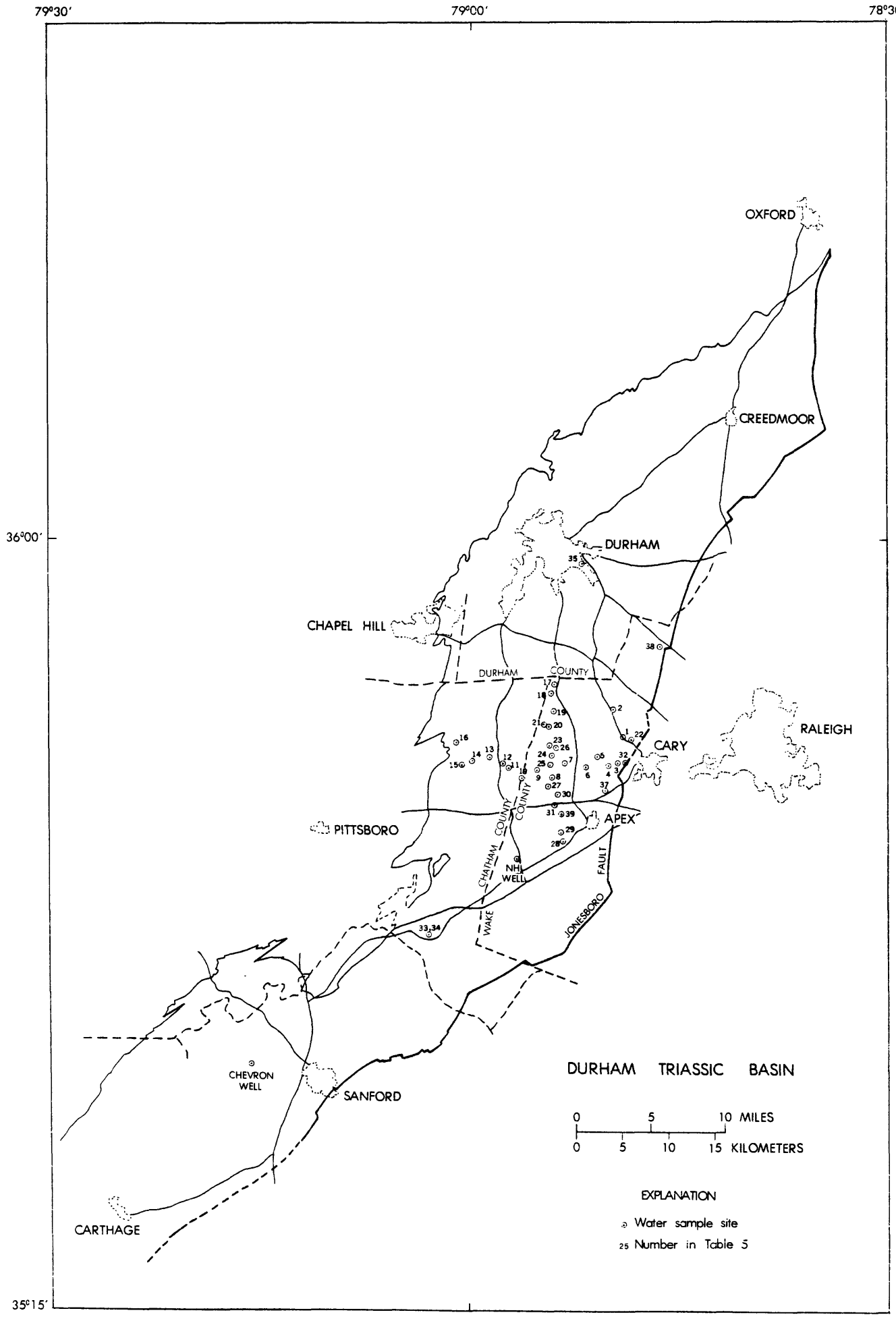
79°30′
79°00′
78°30′
36°00′
35°15′
OXFORD
CREEDMOOR
DURHAM
CHAPEL HILL
DURHAM COUNTY
RALEIGH
CARY
APEX
PITTSBORO
CHATHAM COUNTY
WAKE COUNTY
NHL WELL
JONESBORO FAULT
CHEVRON WELL
SANFORD
CARTHAGE
DURHAM TRIASSIC BASIN
0 5 10 MILES
0 5 10 15 KILOMETERS
EXPLANATION
Water sample site
25 Number in Table 5

INVESTIGATION OF WATER CHEMISTRY

The degree of compatibility of the waste to be injected to the fluid in the host rock can have a drastic affect on injection rates. Chemical reaction at the native-waste water interface can completely plug the available rock pores and change injection rates. Likewise, the chemistry of the rock may be important if swelling clays such as montmorillite are present.

Water Quality From Wells

Most shallow ground water (less than 90 m) (fig. 3) thus far tested is predominately a calcium bicarbonate type water (table 5). Dissolved-solids content is generally less than 250 mg/L. Softer water tends to be a $NaHCO_3$ type. However, in the area west and northwest of Cary, north of the Raleigh-Durham airport, and north of Carpenter, shallow ground water having high dissolved-solids content (greater than 2,400 mg/L) is present. From Cary near the eastern fault border and in a basinward direction there appears to be a progressive change from sodium and calcium sulfate types to calcium chloride and sodium chloride types. North of Carpenter near the common corners of Durham, Chatham, and Wake Counties water has a high dissolved-solids content.

All of the wells having high dissolved-solids content are on the northwestern side of major faults and penetrate red mudstone or conglomerate having a red mudstone matrix. Thus it is possible that all are in a similar hydrogeologic situation at the discharge end of the basin's subsurface flow pattern. The high dissolved-solids content of water found in shallow wells in the conglomerate and fanglomerate near Cary occur near the deeper downfaulted parts of the basin.

Water from the 115 m zone of the Sears No. 1 well (table 6) appears to be a sodium chloride type similar to that from wells 4 and 38. The sample from 247 to 264 m (if representative) is similar to wells 4 and 38 having only a slight increase in the concentration of calcium over sodium. The sample from the 1,009 to 1,143 m zone although higher in dissolved-solids content and calcium content than the water from either the 115 or 247 to 264 m zones or the drilling water, is known to be a mixture of the drilling (mud filtrate) water and the formation water. The small amount of water that did move into the test packer assembly from the 1,009 to 1,143 m zone is most probably from the invaded area and is a mixture of mud filtrate and formation water.

The similiarity of the ionic makeup (chiefly sodium-calcium chloride types) of water from the Dunbarton, South Carolina, Triassic basin to that of the Durham basin is striking. In contrast, ground water from the Culpepper, Virginia, basin to the northeast tend to be calcium sulfate types presumably caused by the widespread presence of gypsum. Water from well 32 (table 5) near Cary shows an ionic makeup characteristic of the gypsum bearing Permian Castile Formation near Jumping Springs, New Mexico, and the Triassic redbeds of the Newark basin, New Jersey.

Table 5 - Chemical analyses of ground water from the Durham basin, N.C.
[dissolved constituents are in mg/L unless otherwise indicated]

Map No. Fig. 38	Well Depth (m)	Yield (L/s)	Sample Date	Lat.	Long.	Seq. No.	Alkalinity	Bicarbonate	Calcium	Carbonate	Chloride	Conductance (μ mho)	Fluoride	Noncarbonate hardness	Total hardness	[1] Iron	Magnesium	[1] Manganese	Nitrate	pH (field)	Potassium	Residue (calculated sum)	Residue (dissolved)	Silica	Sodium	[1] Strontium (Sr)	Sulfate
1	61	0.01	05/09/73	362832	0784856	01	179	218	150	0.0	650	2420	0.3	470	650	40	66	70	--	6.8	3.4	1300	1580	48	220	2200	16
2	30	0.06	05/09/73	351708	0794802	01	153	186	56	0.0	110	660	0.3	120	270	10	31	0.0	1.8	7.5	2.1	340	384	31	19	400	0.8
3	67	0.32	05/09/73	354721	0794904	01	230	280	230	0.0	920	3300	0.4	870	1100	30	120	10	0.4	6.8	4.2	2020	2410	32	220	2800	8.0
4	53	0.32	05/09/73	354704	0794927	01	197	240	28	0.0	280	1300	0.4	0.0	87	--	4	--	0.0	7.8	3.5	680	715	12	240	400	8.8
5	30	1.1	---	354739	0795145	01	143	174	22	0.0	18	330	0.2	0.0	100	0.0	11	0.0	0.9	6.8	1.8	200	205	30	30	340	0.8
6	53	0.13	05/10/73	354549	0785408	01	115	140	11	0.0	4.0	240	0.2	0.0	45	--	4.3	--	0.0	7.6	1.6	150	160	27	35	23	0.8
7	78	0.13	05/10/73	350708	0785208	01	128	156	24	0.0	10	270	0.2	0.0	92	--	7.7	--	2.2	7.0	2.2	180	182	32	25	460	0.8
8	43	0.32	05/10/73	354610	0783357	01	164	200	31	0.0	10	330	0.1	0.0	110	--	8.2	--	0.0	8.0	1.7	210	215	24	32	640	0.8
9	23	0.76	05/10/73	355631	0795514	01	167	204	42	0.0	56	500	0.2	0.0	150	--	12	--	0.4	6.8	1.8	290	297	31	44	220	0.8
10	37	1.9	05/10/73	354624	0791606	01	11	13	3.5	0.0	5	67	0.1	2.0	13	20	0.9	10	9.3	5.9	1.7	69	70	34	6.9	80	0.8
11	--	--	05/10/73	364650	0791718	01	67	82	12	0.0	24	220	0.3	0.0	50	--	4.8	--	0.4	6.5	0.8	160	174	48	27	220	5.6
12	38	4.7	05/10/73	351650	0781729	01	125	152	35	0.0	42	370	0.2	0.0	120	--	7.4	--	0.4	6.4	0.9	240	241	44	29	740	0.8
13	59	0.32	05/10/73	350737	0790825	01	190	232	52	0.0	80	650	0.3	0.0	150	--	5.0	--	0.4	7.5	0.7	380	388	34	80	1400	10
14	37	0.63	05/11/73	350722	0790948	01	146	178	40	0.0	48	435	0.3	0.0	120	10	5.4	100	0.0	7.1	0.7	270	262	34	45	1100	4.0
15	34	--	05/11/73	360648	0792025	01	179	218	35	0.0	22	420	0.3	0.0	130	170	11	370	0.9	7.5	0.6	250	268	30	39	600	8.4
16	30	0.44	05/11/73	350831	0792057	01	161	196	78	0.0	130	740	0.2	89	250	130	13	810	0.0	7.4	0.7	410	490	32	47	1800	8.8
17	41	0.32	---	351144	0782349	01	331	404	140	0.0	250	1410	0.3	240	570	30	52	40	6.2	7.4	2.5	810	864	21	68	2200	68
18	--	--	05/11/73	350108	0785403	01	105	168	42	0.0	10	300	0.3	15	120	40	3.7	280	0.0	7.7	0.9	200	208	37	19	860	1.6
19	30	0.25	05/11/73	351012	0781357	01	312	380	80	0.0	100	850	0.2	0.0	220	60	4.0	90	3.1	7.5	0.7	510	500	22	100	2400	6.4
20	12	--	05/11/73	350920	0791412	01	20	24	40	0.0	110	570	0.1	150	170	180	17	10	44	6.2	1.2	340	380	52	34	360	34

1/Dissolved constituent in micrograms/liter (ug/L)

Table 5 - Chemical analyses of ground water from the Durham basin, N.C.
[dissolved constituents are in mg/L unless otherwise indicated]
Continued

Map No. Fig. 38	Well Depth (m)	Yield (L/s)	Sample Date	Lat.	Long.	Seq. No.	Alkalinity	Bicarbonate	Calcium	Carbonate	Chloride	Conductance (μ mho)	Fluoride	Noncarbonate hardness	Total hardness	[1] Iron	Magnesium	[1] Manganese	Nitrate	pH (field)	Potassium	Residue (calculated sum)	Residue (dissolved)	Silica	Sodium	[1] Strontium (Sr)	Sulfate
21	24	0.32	05/11/73	350922	0790425	01	218	266	60	0.0	82	710	0.3	32	250	--	25	--	1.3	6.8	1.4	410	455	44	48	400	14
22	145	0.19	05/12/73	361822	0784822	01	92	112	74	0.0	210	2400	0.4	130	220	40	7.5	290	0.3	8.0	3.4	417	1500	12	430	--	700
23	32	0.32	05/14/73	352810	0791408	01	125	152	19	0.0	6	253	0.3	0.0	67	20	4.7	30	0.0	7.0	1.4	170	167	34	31	360	2
24	53	0.38	05/14/73	354705	0791400	01	200	244	35	0.0	28	470	0.2	0.0	120	50	8.8	30	0.3	7.8	2.2	280	287	27	56	640	4.4
25	30	1.4	05/14/73	350651	0791415	01	30	36	3.7	0.0	4	80	0.1	0.0	15	700	1.3	30	1.3	6.3	0.8	79	63	39	11	70	0.4
26	34	0.16	05/14/73	352735	0781400	01	154	188	21	0.0	16	339	0.2	0.0	75	30	5.4	10	0.4	7.5	1.4	210	197	27	45	370	0.4
27	76	0.13	05/14/73	352556	0785109	01	154	188	11	0.0	14	335	0.6	0.0	35	0.0	1.8	0.0	0.3	8.5	1.2	210	204	20	65	210	0.4
28	46	0.32	05/14/73	360244	0791312	01	62	76	8.8	0.0	5	140	0.3	0.0	37	2200	3.7	80	0.0	6.3	1.4	120	113	44	15	120	0.4
29	99	0.09	05/14/73	350305	0791329	01	108	132	18	0.0	11	250	0.6	0.0	75	40	7.2	40	0.0	7.3	2.9	160	157	33	24	320	2
30	24	1.1	05/15/73	352517	0792340	01	116	142	18	0.0	4	230	0.3	0.0	78	820	8.0	80	0.0	7.2	2.2	160	150	37	20	300	0.4
31	33	0.63	05/15/73	350442	0791348	01	116	142	21	0.0	3.5	230	0.3	0.0	77	70	5.9	30	0.0	7.7	3.4	150	149	29	20	360	0.4
32	122	0.95	05/15/73	351002	0790940	01	87	106	100	0.0	4	620	0.3	210	300	3200	13	1900	0.0	7.0	0.6	430	461	29	10	120	220
33	183	0.63	--	355615	0792254	01	154	188	5.2	0.0	36	415	0.7	0.0	16	10	0.7	20	0.0	8.7	0.8	250	254	19	90	50	5.2
34	107	0.95	05/18/73	355615	0792254	02	80	98	11	0.0	7	190	0.2	0.0	37	30	2.2	10	1.8	7.7	1.0	130	130	33	26	140	1.2
35	91	0.76	05/21/73	355440	0792150	01	75	92	11	0.0	3	160	0.2	0.0	40	80	3.0	190	0.3	7.6	1.4	120	119	34	19	100	2.8
37	232	0.38	05/23/73	351556	0795000	01	105	128	15	0.0	18	285	0.2	0.0	65	370	6.7	20	8.4	7.5	1.8	190	177	37	34	130	2
38	152	0.19	05/23/73	355407	0791604	01	190	232	36	0.0	300	1350	0.5	0.0	150	30	15	10	0.9	8.7	2.6	740	724	38	220	520	10
39	88	0.09	06/04/73	360548	0792025	01	149	182	16	0.0	3.4	300	0.3	0.0	52	10	2.8	10	0.0	--	1.8	180	196	18	51	280	0.8

1/Dissolved constituent in micrograms/liter (ug/L)

Table 6 - Chemical analysis of water from Sear No. 1, N.C. Test Well
(Dissolved constituents are in mg/L unless otherwise indicated)

No.	Depth (m) source	Date	Lat.	Long.	Seq. No.	Alkalinity, Total $CaCO_3$	Bicarbonate HCO_3	Cadmium Cd 1/	Calcium Ca	Carbonate CO_3	Chloride Cl	Cobalt Co 1/	Copper Cu	Fluoride F	Noncarb. Hardness	Total Hardness
1.	115	12/21/75	354133	0785635	11					17						52
2.	Mud Line	04/04/76	354133	0785635	12					15						39
3.	259	04/16/76	354133	0785635	01	85	104	0	18	0	93	0	1	0.5	0	47
4.	259	04/16/76	354133	0785635	04	0	0	3	62	0	83	32	300	0.8	170	170
5.	1018	04/17/76	354133	0785635	08	0	0	4	30	0	41	14	130	0.5	84	84
6.	1018	04/17/76	354133	0785635	09	0	0	1	96	0	200	31	420	0.9	250	250
7.	1018	04/18/76	354133	0785635	10	0	0			0	75			1.4		

1/ Dissolved constituent in µg/L

Table 6 - Chemical analyses of water from Sears No. 1 N.C. Test Well
[Dissolved constituents are in mg/L unless otherwise indicated.]
Continued

Iron Fe 1/	Lead Pb 1/	Magnesium Mg	Manganese Mn 1/	pH (Field)	Potassium K	Residue (Calculated Sum)	SAR	Silica SiO_2	Sodium Na	Sulfate So_4	Zinc Zn 1/
		2.3		8.9	3.2		7.9		130		
		0.3		8.0	4.5		5.9		84		
10	0	0.4	380	8.5	4.8	283	5.6	3.9	88	23	30
26000	2000	2.6	3400	8.9	10	342	3.2	28	96	16	12000
12000	2000	2.1	1600	9.0	5.7	179	1.9	19	40	14	11000
31000	4200	3.4	4300	9.0	11	535	3.6	34	130	9.7	10000
				8.9				82		1.4	

Formation Factor and SSP

The borehole geophysical logs were used to crosscheck the accuracy and representativeness of samples taken from the 247 to 264 m and 1009 to 1143 m zones and to give additional insight into the native-water chemistry of the remainder of the hole.

The salinity of formation waters is commonly estimated from the borehole logs by using one or both of the following relationships:

1. $SSP = -K \log \frac{Rmf}{Rw}$

where SSP = the static spontaneous potential in millivolts.
K = a constant related to absolute temperature.
Rmf = the resistivity of the drilling mud filtrate in ohm-meters at a specified temperature.
Rw = the resistivity of the interstitial water in ohm-meters at a specified temperature.

2. The relationship of the formation factor (f) to porosity (ϕ), water resistance (Rw), and resistivity of the water saturated formation (Rt).

$$F = \frac{Rt}{Rw} = \frac{1}{\phi^2}$$

Water resistivities at six depths in the Sears No. 1 well derived from the relation $(Rw = \frac{Rt}{F})$ are given in table 7 and plotted on figure 40. F values are from laboratory analyses, Rt values are taken from the deep induction curve (ILD) of plate 1.

Figure 40 shows that Rw calculated from laboratory-measured formation factors ranged from about 1.0 ohm-meters to about 14 ohm-meters. This indicates that formational waters at the Sears No. 1 test site could have a dissolved-solids equivalent ranging anywhere from about 350 to 5,500 mg/L sodium chloride.

The water analyses from the 247 to 264 m zone indicate a dissolved-solids of approximately 560 mg/L when corrected to equivalent sodium chloride. Alger (1966), Schlumberger (1972), or Brown (1971) indicate that, at 25°C, water containing 560 mg/L dissolved-solids should have a resistivity of about 10 ohm-meters. No laboratory formation-factor (Ff) data are available for the 247 to 264 m zone; however, water resistivities calculated from Ff values above and below the sampled zone are approximately 10 ohm-meters.

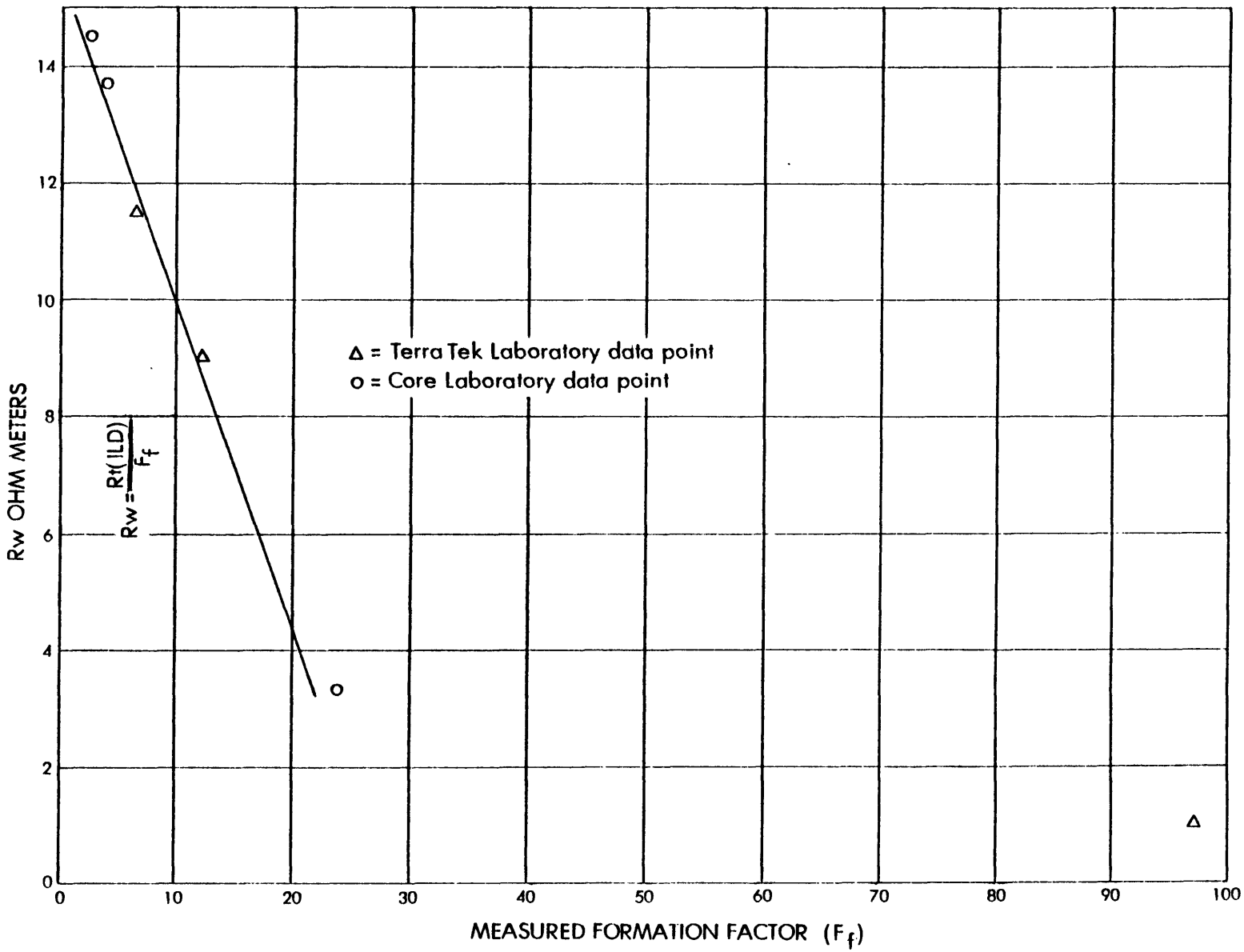

Figure 40. Resistivity of water versus calculated formation factors of core samples.

Table 7 - Formation Factors at Selected Depths - Sears No. 1 Well

Depth (Meters)	Formation Factor - F_f (meas.)	Rt (LLD 10g - Ohm meters)	$R_w = \frac{Rt}{Ff}$ meas.	Porosity (meas. - percent)	Formation Factor - $F_f = \frac{1}{\phi 2}$ (Calculated)	$R_w = \frac{Rt}{Ff}$ (calcu.)
154	2.74	40	14.6	5	400	0.10
157	25.0	80	3.2	8.9	127	0.63
330	3.64	50	13.7	4.7	452	0.11
744	6.5	75	11.5	0.9	12346	0.006
745	12	40-110	9.2	6.2	69.4	0.58-1.58
961	96	100-200	1.04-2.08	2.8	1275	0.078-0.157
1138	67	>100		2.5	1600	
1142	18	>100		0.9	12346	

Similarly, Ff values from laboratory measurements and Rt from the ILD log indicate interstitial water below 960 m is not highly saline. This formation water at 1 to 2 ohms at 25°C is equivalent to a sodium chloride concentration of 2,200 to 4,500 mg/L. The analysis of the water sampled from the 1,018 to 1,143 m zone is much less saline than this indicating a mixed (diluted) sample was collected.

Water resistivities calculated (table 7) using Ff values derived from log porosities (ϕ) using the relation:

$$Ff = \frac{Rt}{Rw} = \frac{1}{\phi m}$$

where Ff, Rt, Rw, and ϕ have the values stated above and m = the "appropriate" cementation factor (Schlumberger, 1972), are one to two orders of magnitude lower than those from laboratory calculated Ff values.

Figure 41 is a plot of porosity from the density and sonic logs versus resistivity from the induction log (ILD).

Apparent water resistivities from these curves at Ff = 25 and ϕ = 20 (Ff value from the standard curve for $F = \frac{1}{\phi 2}$) are 0.9 ohm-meter from the sonic-porosity plot and 0.7 ohm-meter from the density-porosity plot. By comparison, Rw calculated for a measured Ff of 24 for the 157.2 m sample is 3.3 ohm-meters.

Apparent Rw's calculated by Schlumberger (written communication, 1977) from the same log data and the same relationship of

$$F = \frac{1}{\phi^2} = \frac{Rt}{Rw}$$

range from 0.41 ohm-meter at 152 m to 0.35 ohm-meter at the bottom, indicating sodium chloride concentrations of about 11,000 mg/L.

The explanation for the disparity is apparently related to the assumption that $Ff = \frac{1}{\phi 2}$ at low dissolved-solids concentrations and low porosities. Alger (1966) states, ". . .the customary relationships between F and porosity used in oil field interpretations usually do not apply to fresh water sands. . . . F varies in fresh water sands not only with porosity, but also with Rw and grain size."

Figure 42 shows the relation of measured formation factor versus the measured porosity of core samples. Formation factors appear to be controlled by an entirely different set of physical laws below a porosity of 0.04. Figure 43 illustrates the relation of formation factor to depth.

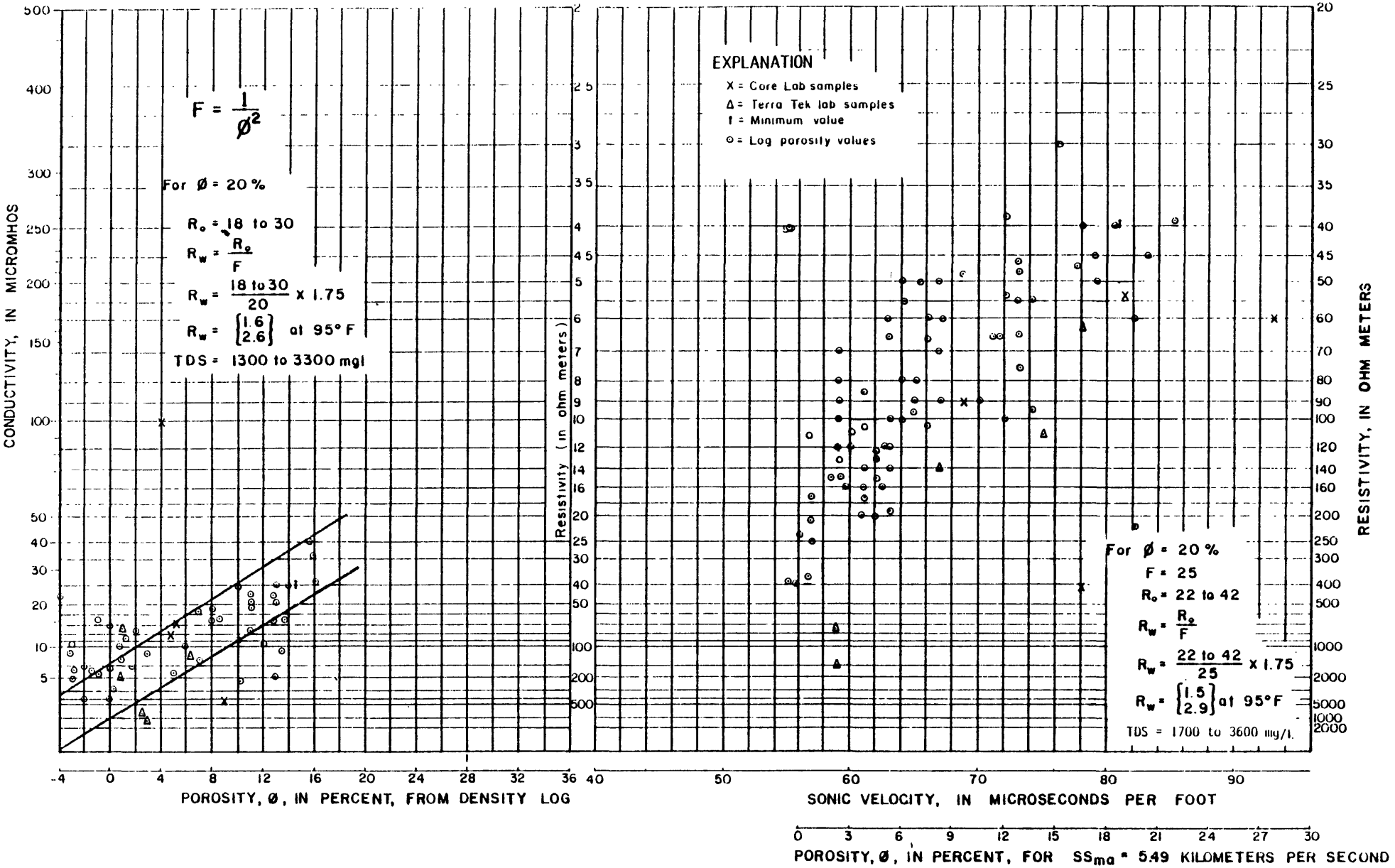

Figure 41. Density porosity and sonic porosity versus resistivity and conductivity of Triassic rock in Sears No. 1 Well.

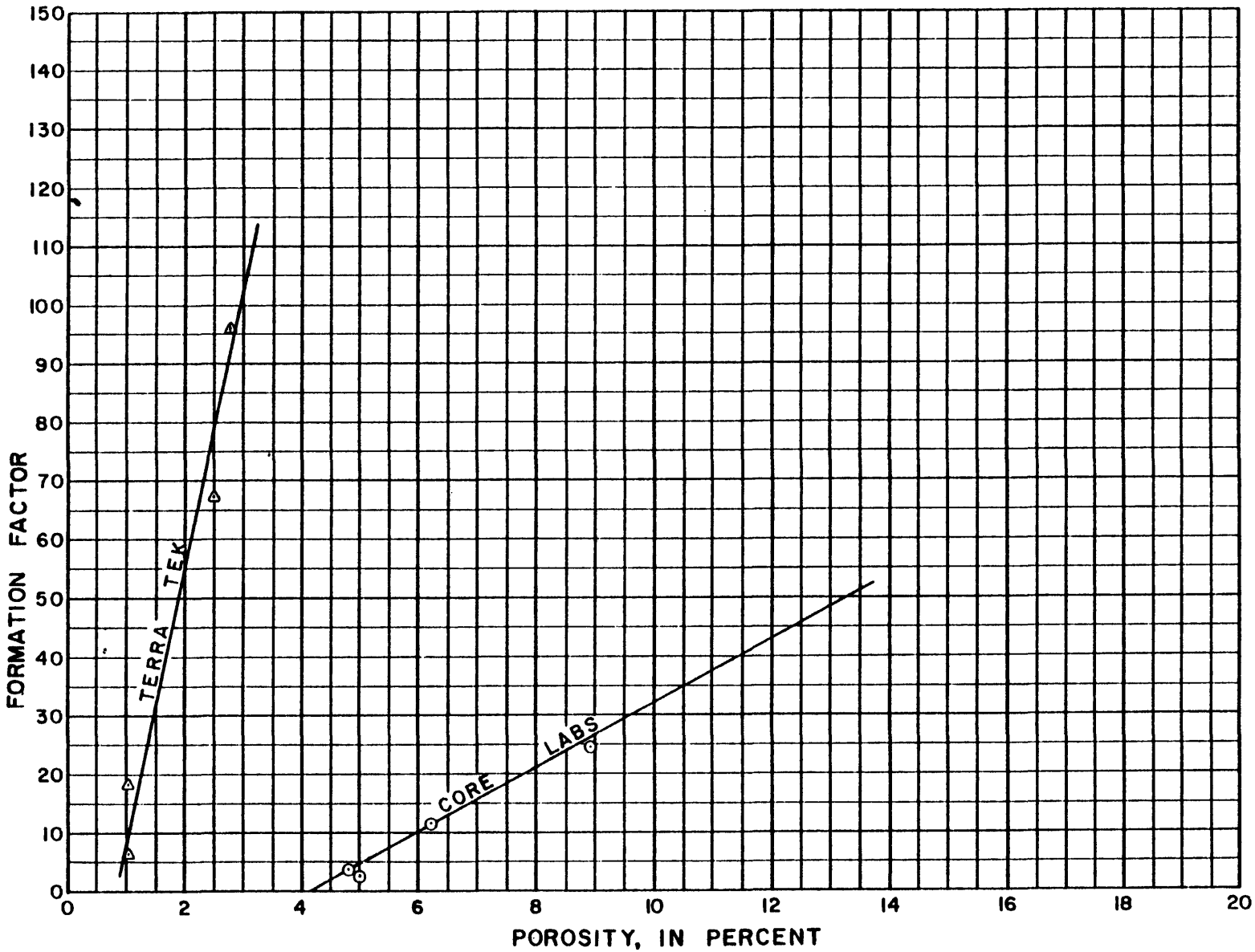

Figure 42. Formation factor versus measured porosity of core samples.

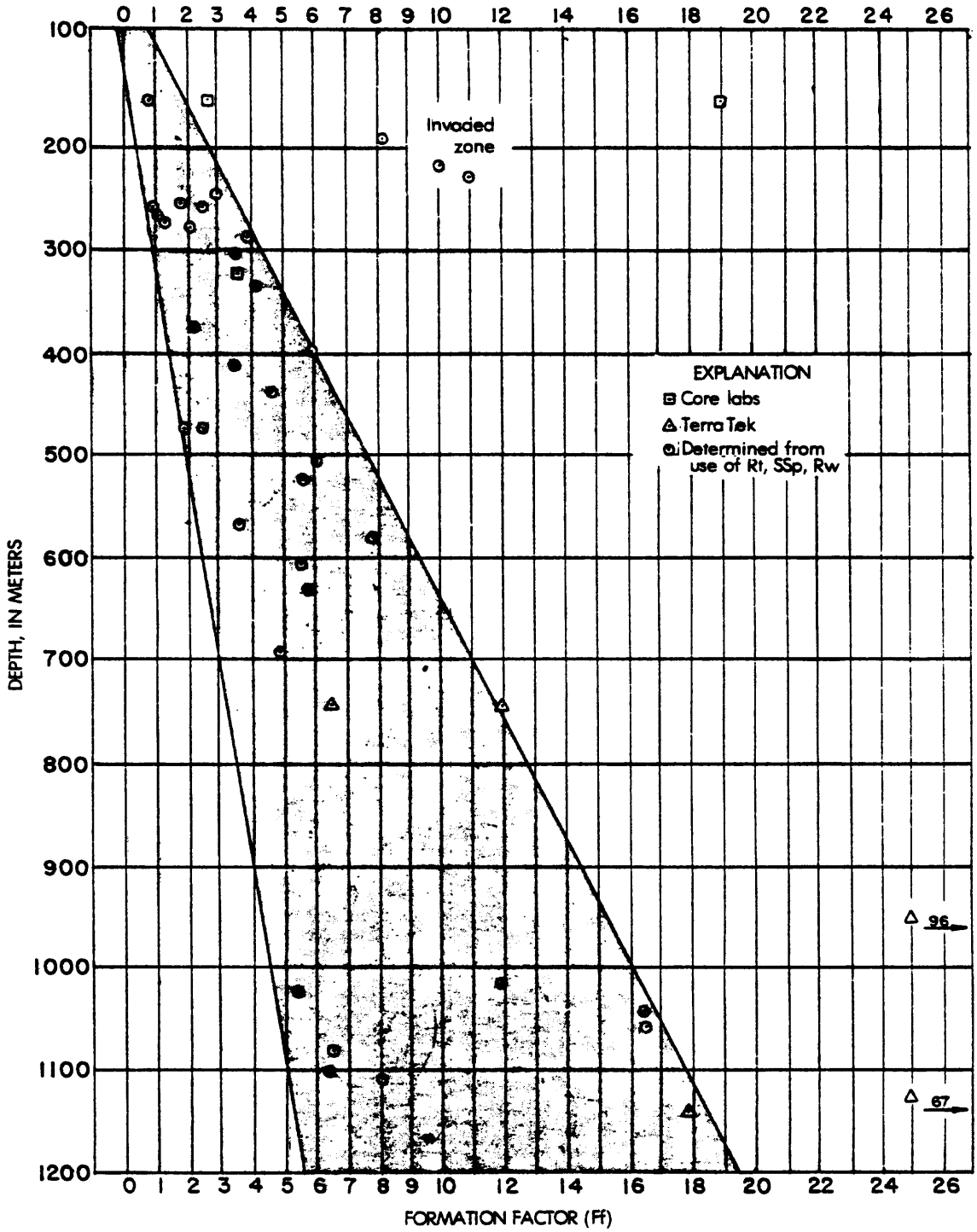

Figure 43. Formation factor versus depth.

Data from computation of interstitial water resistivity based on the relation

$$SP = -K \log Rmf/_{Rw}$$

are presented in table 8. The SSP values given in table 8 are those assumed from a log deflection of 5 millivolts per division. Formation factors calculated from the SP log-derived Rw and Rt from the ILD curve are given in table 9. Calculated Rw for the 247 to 264 m zone range from 5.3 to 12.4 ohm-meters at 25°C. This is equivalent to a range of concentrations of 400 to 920 m zone. However, the Rw values in table 8 increase with depth contrary to most natural occurrences. This may be caused in part by the increased shale content with depth. In fact, use of the SSP deflection to obtain reliable Rw values opposite very low permeability formations such as are represented by the deeper parts of the New Hill well may be invalid (Schlumberger, 1972).

Table 8 - Resistivity of Formation Water using SP Log - Sears No. 1 Well

Depth Top SSP (m)	SSP, (mv)	Temp. @ SSP °F	Temp. @ SSP °C	Rmf @ Form. Temp. (Ω m)	R_{mf}/R_{we} (K = 70) (Ω m)	Rwe @ Form. Temp. (Ω m) $R_{we} = \frac{R_{mf}}{R_{mf}/R_{we}}$	Rwe @ 77°F (NaCl) (Ω m)	Rw @ 77°F ($NaHCO_3$) (Ω m)
154	+10	71.5	22	21.6	.72	30	28	49
191	-11	72	22	21.6	1.48	14.6	13.6	25
220	-17	73	23	21.4	1.70	12.6	12.2	21
229	-36	73	23	21.4	3.25	6.58	6.2	11
248	-39	74	23	21.2	3.70	5.73	5.3	9
257	-16	74	23	21.2	1.70	12.5	12.1	21
259	-21	74	23	21.2	2.03	10.4	10	18
262	-15	74	23	21.2	1.65	12.8	12.4	22
270	-18	74.5	23	21.1	1.77	11.9	11.4	20
278	-18	75	24	21.1	1.77	11.9	11.4	20
282	-15	75	24	21.1	1.65	12.8	12.4	22
289	-23	75	24	21.1	2.30	9.17	9.0	16
306	-17	76	24	20.9	1.70	12.3	12.0	21
338	-17	76.5	24	20.9	1.80	11.6	11.6	20
377	-20	78	26	20.4	1.96	10.4	10.5	18
398	-34	78	26	20.4	3.20	6.38	6.27	11
413	-20	78.5	26	20.3	1.96	10.36	10.7	19

Table 8 - Resistivity of Formation Water using SP Log - Sears No. 1 Well
Continued

Depth Top SSP (m)	SSP, (mv)	Temp. @ SSP °F	Temp. @ SSP °C	Rmf @ Form. Temp. (Ω m)	Rmf/Rwe (K = 70) (Ω m)	Rwe @ Form. Temp. (Ω m) $Rwe = \frac{Rmf}{Rmf/Rwe}$	Rwe @ 77°F (NaCl) (Ω m)	Rw @ 77°F ($NaHCO_3$) (Ω m)
440	-25	79	26	20.1	2.33	8.62	8.9	16
477	-15	80.5	27	19.8	1.65	13.2	14.5	25
478	-14	80.5	27	19.8	1.60	12.4	13.0	23
508	-4(?)	81	27	19.7	1.11	17.7	19.0	33
526	-16	82	28	19.5	1.70	11.5	12.3	22
570	-7	83	28	19.3	1.20	16.1	17.0	30
582	-20(?)	83	28	19.3	1.96	9.85	11.0	19
609	-4	84	29	19.1	1.11	17.2	19.0	33
633	-15	84.5	29	19.0	1.65	11.5	13.6	24
999	-5	93.5	34	17.0	1.17	14.5	17.5	31
1019	-26	94	34	16.9	2.35	7.19	8.7	15
1025	-14	94	34	16.9	1.60	10.6	13.0	23
1043	-13	95	35	16.7	1.52	13.9	17.0	30
1057	-8	95	35	16.7	1.28	13.0	16.0	28
1082	-5	95.5	35	16.6	1.17	14.2	17.2	30
1102	-6	96.5	36	16.4	1.20	13.7	16.8	29
1108	-5	97	36	16.3	1.17	13.9	17.5	31

Table 9 - Formation Factors from SP and Induction Logs - Sears No. 1 Well

Top Depth (m)	Rt (Form. Temp.) (Ω m)	Rw (from SP NcHCO3 equiv. at 77°F) (Ω m)	$F_f = \frac{Rt}{Rw}$	Rt (25°C) (Ω m)	Porosity (percent)
338	84	20	42	84	2-12
273	22	20	1.0	21	15.5
262	57	22	2.5	54	11
259	39	18	.94	17	13
257	39	21	1.8	37	11
247	27	9	2.9	26	13-16
229	120	11	0.4-3.2	4-35	13.4
219	220	21	0.4-3.0	8-63	13
191	<220	25	0.2-2.6	5-65	10.2
1025	100	23	5.4	125	1.5
1101	150	29	6.4	185	-2
1057	380	28	16.6	465	0
1042	400	30	16.5	495	-2
154	<40	49	<.76	<37	14
278	39	20	1.9	38	16
282	47	22	2.1	46	11
289	64	16	3.9	62	13
306	75	21	3.5	73	11
377	38	18	2.2	39	10.1
398	64	11	5.9	65	13.6
413	65	19	3.5	66	8.3
440	90	16	5.7	91	10
468	47	25	1.9	48	13
478	55	23	2.5	57	7
508	190	33	6.1	200	5
526	120	22	5.7	126	3

Table 9 - Formation Factors from SP and Induction Logs - Sears No. 1 Well
Continued

Top Depth (m)	Rt (Form. Temp.) (Ω m)	Rw (from SP NcHCO3 equiv. at 77°F) (Ω m)	$F_f = \frac{Rt}{Rw}$	Rt (25°C) (Ω m)	Porosity (percent)
570	100	30	3.6	109	6
582	140	19	7.9	150	7
609	170	33	5.6	184	-1
633	130	24	5.8	140	0.8
998	100	31	3.9	120	0.6
1019	130	15	12	180	0
1082	160	30	6.5	196	-1.5
1108	200	31	8.1	250	-3

EVALUATION OF TECHNIQUES

The success of a technique used for subsurface waste-storage evaluation must be the degree to which that method meets the data needs of the study quickly and economically and (or) the degree to which that method in combination with other methods reduces the number of possible models of the subsurface environment. The "data needs" of this study are primarily geological and hydrological ones concerning the ability of the host rock to accept liquid waste, the competency of the host and overlying rock to contain the waste isolated from man's environment while degradation occurs, and the identification and evaluation of those natural resources that must be protected from contamination.

The "techniques" used were selected for their possible definition of several parameters which determine waste-disposal "suitability" in a rock suite where subsurface data are almost nonexistant. These parameters included: (1) the external geometry of the Durham Triassic basin for clues to sedimentary thickness and tectonic evolution; (2) the internal geometry of the basin lithofacies for their obvious control on spatial distribution of porosity and permeability; (3) the occurrence and chemistry of ground water for compatibility with and control of movement of waste fluids; and (4) the physical character of rock samples representative of potential rock reservoirs and seals.

Geologic Mapping

Reconnaissance geologic mapping helped define lithofacies (or depositional environments) and the overall architecture of the Durham Triassic basin. None of the existing maps were 100 percent usable "as is" because of past emphasis on chronostratigraphic units which had no specific relation to spatial distribution of porosity and permeability. The rapid vertical and lateral facies changes characteristic of the bulk of the Triassic deposits, the extensive postdepositional faulting, the weathered nature and low density of outcrops make mapping extemely difficult except on a gross scale. Chert and coal beds proved to be the only reliable marker horizons. Many of the critical geological associations made in figure 3 were made after the intrabasin structural relations had been defined by other means. By itself, geologic mapping for definition of permeability-porosity distribution is a very poor approach in the continental sedimentary rock suite.

Paleocurrent Mapping

A map of paleocurrent direction in the fluvial sandstones proved to be a valuable tool to define the depositional processes and geometry of depositional environments in the Durham Triassic basin. The deposition of coarse fan debris normal to the basin margins and the position of the lacustrine and paludal deposits relative to them further support the tectonic control on Triassic deposition. The existence and flow direction of longitudinal streams and the associated reworked fluvial deposits were established with this technique. The paleocurrent data in combination with the structural and surface geologic data create a predictive model of subsurface facies distribution.

Palynology and Paleontology

The temporal and lateral equivalency of Triassic and Jurassic spore and pollen established by Cornet (1975, 1977) for the East Coast Triassic and Jurassic basins was helpful in unravelling some of the structural complexities of the Durham Triassic basin. Specifically, the knowledge of the evanescence or non-evanescence of laterally discontinuous black shales and coal zones solved the relative vertical displacement of some juxtaposed intrabasin blocks. Expertise in this field and experience in the Triassic are rare, thus its use will no doubt be limited to specific problems not resolveable by other methods. The microfossils characteristic of the Triassic have life spans too great to be useful for other than establishing the nature of particular facies environment.

Side-looking airborne radar (SLAR)

Side-looking airborne radar mapping was used for the same purposes as the Landsat imagery. It proved to be superior to Landsat imagery for defining basin lineaments by giving much better detail. Basin outlines were visible on most images as a difference in apparent relief and as a tonal change. In addition diabase dikes had unique raised outlines and could be mapped directly from the rectified image. Some tonal changes could be identified with gross lithologic changes within the basin, but SLAR mapping could not be used for direct mapping of geologic features.

The Geological Survey-owned, SLAR equipment used was of the AN/APS-94D type developed for military surveillance and operates at a lower frequency than most commercial types. Comparison with commercial imagery for the same areas of the basins shows the Geological Survey equipment to be far superior to the commercial for geologic illumination but to have poorer geographic rectification and yawl control.

Commercial SLAR imagery is expensive, but large areas can be covered quickly in any kind of weather. Linear geologic features parallel to the SLAR look direction will not be illuminated necessitating flight lines normal to one another for comprehensive coverage. The geologic information derived from the SLAR images proved invaluable in extending and defining the structural-stratigraphic model produced from sparse outcrop data and geologic mapping.

Aeromagnetic Mapping

The shape and distribution of the magnetic anomalies on the aeromagnetic maps of the Durham Triassic basin convey an immediate qualitative feel for the lateral distribution of intrabasin features. Some anomalies can be used for depth estimates of basin fill. The accuracy of these estimates depends on the depth method used and input parameters. The accuracy of one procedure depends on the degree to which the applicable magnetic susceptibles are known. The shape and distribution of the magnetic anomalies compare favorably with the distribution of SLAR lineaments. The aeromagnetic map is superior to most other techniques for mapping diabase dikes. Flight-line spacing must have smaller spacing than the maximum dimension of the unit to be sensed, and the direction should be normal to the regional trend for best results. Some detail is lost with "state-of-the-art" computer contouring. Computer printing of flight-line magnetic data, however, is worthwhile. The quality of aeromagnetic maps from surveys flown at one-mile spacing in the Durham Triassic basin do not compare favorably with those flown at one-half mile spacing. Aeromagnetic mapping was very cost effective for this project and complements the SLAR lineament map and the other geophysical interpretations.

Gravity

The gravity maps and profiles prepared for this project have probably contributed most toward an understanding of the topography of the basement surface and the consequent thickness of the Triassic rocks. Accurate depth estimates to basement depend on accurate knowledge of the density contrast between the Triassic rocks and basement. The average density of the rocks in the Durham Triassic basin is now known from the subsurface samples and acoustic velocity characteristics, but velocity variations in the underlying basement rock is not known with certainty.

Gravity work is time consuming but relatively inexpensive. Station density must be great enough that the smallest desired gravity feature is measured. Adequate bench mark or other spot vertical control is absolutely essential for accurate work. Surveying in vertical control is even more time consuming and expensive.

The profiles constructed from residual gravity profiles prepared for this project compare favorably with the aeromagnetic and resistivity models indicating that it is a highly useful for describing basin geometry.

Resistivity Profiling

Electrical resistivity sounding data put together in profile form is the only technique used in the Durham Triassic basin which offers any potential to describe the spatial distribution of discrete facies. The technique actually measures electrical conductivity of the Earth's surface leading to an infinite number of bed thickness-resistivity combinations that will satisfy the observed reading. Local empirical and field data must be used to reduce the number of possible models to a practicable level. A characteristic basement resistivity must be estabished by making local soundings in representative crystalline rocks. The technique can be further calibrated for depth, layer sequence and frequency, and characteristic resistivities by making soundings at well sites where good geophysical and geologic log data are available. The method also requires several miles of reasonably straight road remote from electrical interference such as pipe lines, powerlines, or fences.

The profiles constructed from the soundings made in the Durham Triassic basin show good correlation with the gravity and aeromagnetic profiles indicating that this technique can also be used to describe basin geometry. In addition, with proper calibration the method gives a good to excellent picture of lateral thickness and continuity of electrical units which, in most cases, can be related to lithofacies distribution and faulting.

Seismic Profiling

Modern seismic reflection work using multiple stacking, digital recording, and computer processing of the record is undoubtedly the best technique possible to determine lateral continuity of facies, degree of faulting, and basement topography in the Triassic basins. Use of less sophisticated equipment and 6-fold stacking in the Durham Triassic basin enabled construction of a basement profile that agrees reasonably well with the local sounding and gravity data. However, resolution of individual facies and layering was defeated by the obviously close-spaced faulting and high background noise. The layering and basement configuration along a line shot by a commercial company in the Sanford area compared favorably with the resistivity profile along the same line.

The method requires reasonably straight roads, local governmental permission to blast or run vibrating equipment, but more importantly, the method is prohibitively expensive except in those instances where the need for the data is known to justify the cost.

Test Drilling

Test drilling during a subsurface investigation or the data derived from prior test drilling for other purposes is absolutely essential to the evaluation of potential waste storage in the Triassic or any other rock suite. Without test drilling there is no quantitative data on depth, rock porosity and permeability, acoustic velocity, magnetic susceptibility, and resistivity, layering sequence and thickness and water quality with which to calibrate the other techniques used to extrapolate and mould the point-potential data into a three-dimensional model. Project test drilling is sometimes the only opportunity to do hydrologic testing.

Test drilling data is so important to the quality of the project results and so expensive that its existing density and quality should determine the inception and funding of subsurface investigations.

Borehole Geophysics

The stratigraphic test well offers a unique opportunity to obtain continuous borehole geophysical data. The geophysical logs from the Sears No. 1 and Groce No. 1 wells extended the usefulness of the well samples and surface geophysical data measurably. This borehole technique is unsurpassed for obtaining a more precise record of the vertical change in porosity, density, resistivity, sonic velocity, and radioactivity. It gives much more precise vertical limits to the individual drill samples. The logs were especially helpful to cross-check and calibrate the resistivity and seismic surveys and to establish a reliable average density for the gravity work. The resistivity and SP logs complemented the water sampling as a means of determining subsurface water quality.

Water Sampling

At least a gross concept of regional ground-water circulation patterns in the Durham Triassic basin is possible from areal sampling of water wells. Insufficient sampling was done in the Durham area to establish other than that dissolved-solids increase toward the southeastern, deeper part of the basin. There is some suggestion from the data that the increases are related to the smaller substructures illustrated in figure 21.

Sampling with a packer such as was done in the Sears No. 1 well for vertical change in water quality is difficult and time consuming if a reliable sample of formation water rather than mud filtration is to be obtained. Water samples are absolutely necessary for calibration if subsurface water quality is to be determined from well logs. The well must be allowed to flow or be pumped until water chemistry stabilizes. Where it is not possible to obtain a representative sample of formation water and sufficient control does exist (including calibrated resistivity, temperature, and SP logs, resistance of the mud fluid, and some concept of the ionic species probably present) the well-logging method is the next best method of determining water chemistry.

Hydrologic Testing

The data value and effectiveness of the hydrologic testing techniques used on the Sears No. 1 well are adequately documented elsewhere. Stressing the aquifer or potential storage reservoir by addition or removal of fluid gives data about in situ conditions that cannot be simulated in the laboratory with rock samples.

No attempt was made to determine the rate and direction of ground-water flow, except that head measurements were made in the Sears No. 1 test well at every opportunity. It is recognized, however, that the data about the areal and vertical distribution of head is essential to an understanding of ground-water circulation and a proper evaluation of the basin's waste-storage potential.

Analysis of Physical Properties of Rock

Laboratory analyses of rock samples taken at six intervals in the Sears No. 1 well were successfully used to calibrate or to cross-check other data and techniques. Extreme care must be exercised in the extrapolation of such data to actual subsurface conditions. Samples must be unweathered and protected from drying insofar as possible. The freshness of the "unweathered" road-cut sample is questionable. Fractured rock can rarely be correctly sampled in a cored hole. The accuracy and reliability of the laboratory data depends directly on the laboratory's ability to simulate field conditions, that is, use of a laboratory prepared water of the correct salinity but of different ionic constituents can cause clay swelling and erroneous results when such water is flushed through the laboratory sample.

SUMMARY

The geophysical and geologic data presented in this report describe a fault graben more complex than has been previously described for the Durham Triassic basin. The Durham Triassic basin was apparently produced by a deep crustal master fault expressed at the surface as a series of en echelon positive fault blocks which supplied sediment and negative blocks to receive it. The resulting irregular linear basin contains a spatial facies distribution that reflects a combination of changing tectonic-climatic elements. For example, the Colon cross-structure was depressed during earliest sedimentation and elevated later. Different facies representing different environments were deposited in separate parts of the larger graben at the same time. The Cumnock, Pekin, and Sanford Formations as mapped by Reinemund (1965) are in part facies of one another.

The present Durham Triassic basin is not a simple half graben bounded on one side by a single master fault nor do the Triassic rocks dip eastward monoclinally toward the Jonesboro fault. Instead, the eastern border is step faulted and the Durham Triassic basin is cut into a series of southeasterly rotated, post-depositional slices that trend approximately N. 45° E. subparallel to the eastern border of the Sanford and Wadesboro subbasins. The slices are terminated to the northeast and sometimes to the southwest by faults that trend nearly due north causing the basin to be subdivided into relatively unfractured diamond- and triangular-shaped blocks by faults or wide fracture zones. The presence of a step-faulted eastern border implies that some of the conglomerate-fanglomerate along the eastern border formerly thought to be a late depositional product is actually an earlier one.

The alluvial fans, the angularity of the sand, the poor sorting of the fines, the size of the boulders in the fanglomerates, and the freshness of the feldspar in the Durham basin all point to short transport distance from an elevated source area to a nearby valley floor or graben of low relief. The depositional environment is not unlike modern deposition in intermontane basins of the Basin and Range Province or of the Salton Trough of Southern California. The tentative paleocurrent data indicate a major extrabasin source to the northeast for much of the Durham subbasin. Sediment from the basin-margin fans was distributed southwestward by longitudinal streams.

The low porosity and permeability measured or calculated for the Durham Triassic rocks is in part a consequence of the poor sorting characteristic of this environment, extensive lithification and cementation, and possibly in part caused by swelling of montmorillite during laboratory tests. The more porous rock--principally horizons in the coarse arkosic sandstone unit--has porosities in the microdarcy range and transmissivities ranging from 1×10^{-3} to $1 \times 10^{-7} m^2/d$ (assuming test results were not invalidated by swelling of montmorillite clay).

The low temperature gradient and apparent relatively freshwater to the bottom of the Sears No. 1 test well indicates deep circulation through fractures.

Several geophysical and remote sensing techniques were tried in the Durham Triassic basin to overcome the almost total lack of subsurface data. A combination of SLAR lineaments with aeromagnetic and simple Bouguer gravity maps delineate the probable basin architecture. Residual gravity, aeromagnetic, seismic, and resistivity profiles all give more specific information about the geometry of the basin fill or basement topography. All need to be calibrated to a certain degree with local data. Modern seismic profiling gives the best data about basin structure and distribution of lithofacies but is prohibitively expensive for most projects. Resistivity profiling requires the most exhaustive calibration but is the only method other than seismic that is suited for detailing spatial facies relationships with minimum cost. Use of aeromagnetic, gravity, and resistivity data synergistically to model Triassic basin internal and external geometry, supplemented with reliable test-well data, offers the most economical approach to defining a framework for more specific waste-disposal studies.

The samples and borehole geophysical logs from the Groce No. 1 well and the Sears No. 1 well confirm the simultaneous deposition of the different facies in separate parts of the basin, the cyclicity of the original sediments, and the general imperviousness of the rocks. The samples and logs from the New Hill well indicate that slightly permeable sandstones and siltstone of the tan arkosic unit interfinger with dense, essentially nonpervious, red mudstones and argillites creating--in the vertical sense--low permeability reservoirs sandwiched between impervious facies. The lateral extent of reservoir rock is limited by the nearest facies (permeability) change and the boundaries of the individual structural blocks.

There is an apparent slightly higher porosity indicated from the density logs than from the laboratory analysis of core. The mean density-log porosity was 6.4 percent. That from tested core was 5.4 percent. However, those porosities derived from the neutron and sonic logs are substantially higher than either. Undoubtedly, part of the discrepancy is assignable to poor log compensation for a badly washed out and irregular hole and part perhaps to post-drilling mineralogical changes within the tested core. However, the higher porosities exhibited by the New Hill well are consistent with those observed from the Groce No. 1 well.

Transmissivities from various tests at two different depths range about 1×10^{-6} to $1 \times 10^{-1} m^2/d$. Permeabilities are in the micro- and nanodarcy range. An estimate of permeability derived from the transmissivity of $1.2 \times 10^{-3} m^2/d$ of the 247 to 264 m zone is about 100 microdarcies compared to about 8 microdarcies for well DRB 10 of the Dumbarton, South Carolina, basin.

Attempts to determine liquid permeabilities of core in the laboratory resulted in rupture of some samples. The obvious sensitivity to water suggests that interstitial clay swelling was caused by flushing with water having ionic makeup different from the formation water. Indeed, montmorillonite was later found to be the most abundant clay present in the Sears No. 1 well drill cuttings. The presence of montmorillonite probably affects much of the inhole and laboratory analyses.

Insufficient data were available to establish the rate and direction of movement of ground water in the basin. The low temperature gradient of the Sears No. 1 well compared to the Groce No. 1 well indicates deeper circulation of meteoric water at the Sears No. 1 site than at the Groce No. 1 site. No unusual head relations were observed in the Sears No. 1 well, and the sonic log does not indicate any of the shales are over-pressured. The shape of the temperature anomalies on the Sears No. 1 log suggests that there is low-volume water movement down the hole to the 550 m level and up the hole below that point. If correct, water must be leaving the borehole through fractures or relatively permeable sandstone at about the 550 m level. If deep circulation does occur at the New Hill site and if the measured transmissivities are approximately correct, then circulation must take place through an extensive fracture system.

Acoustic televiewer images of selected parts of the New Hill well bore show many irregular openings. They appear to be parallel to bedding and are probably caused by solution of circulating drilling fluid. A few openings may be related to either fractures or crossbedding. Two short vertical fractures are identifiable on the images. Both could possibly have been induced by the drilling and testing procedures. Injection pressure tests of the 1009 to 1143 m zone indicate that the rock fractures at 9,500 kilopascal (kPa) above hydrostatic or that the packers failed during the testing. No change in head was noted at the surface.

The spontaneous potential and resistivity log responses, though not conclusive, indicate that the water in the formations at the New Hill site ranges not greater than 350 to 5,500 mg/L equivalent sodium chloride from top to bottom, respectively. This also suggests some circulation at depth.

The basin contains resources--chiefly ground water, oil shale, and coal. The coal and oil shale occur together, and the potential economic occurrences are approximately confined to the Sanford area. No potable ground water was found below 100 m in the Chevron well. Ground-water yields of the Triassic rocks of the Durham Triassic basin are characteristically low and domestic supplies are confined to the uppermost rock units.

Target areas in the basin considered to merit further consideration for waste storage are outlined in figure 44. The criteria used to prepare this map include: remoteness from known or potential natural resources; thickness of sedimentary section (depth to basement); and projection of the locations where the slightly permeable facies are sandwiched between or overlain by the dense, argillaceous rock types in the subsurface.

The low porosity and permeability, the general faulted and fractured nature, the presence of swelling clays, the limited spatial extent of the zones of slightly higher permeability indicate that large volumes of wastes cannot be safely injected and stored in the Durham Triassic basin. It is possible that a small volume of liquid waste could be injected and contained within the more permeable layers until acceptable degradation occurs. Data concerning the in situ pressures and the orientation with which fracturing occurs in these rocks are not available to further evaluate that possibility. It is also possible that the thick, dense, argillaceous, essentially nonpervious rocks in the basin are suitable sites for subsurface storage of liquid wastes in containers in man-made caverns.

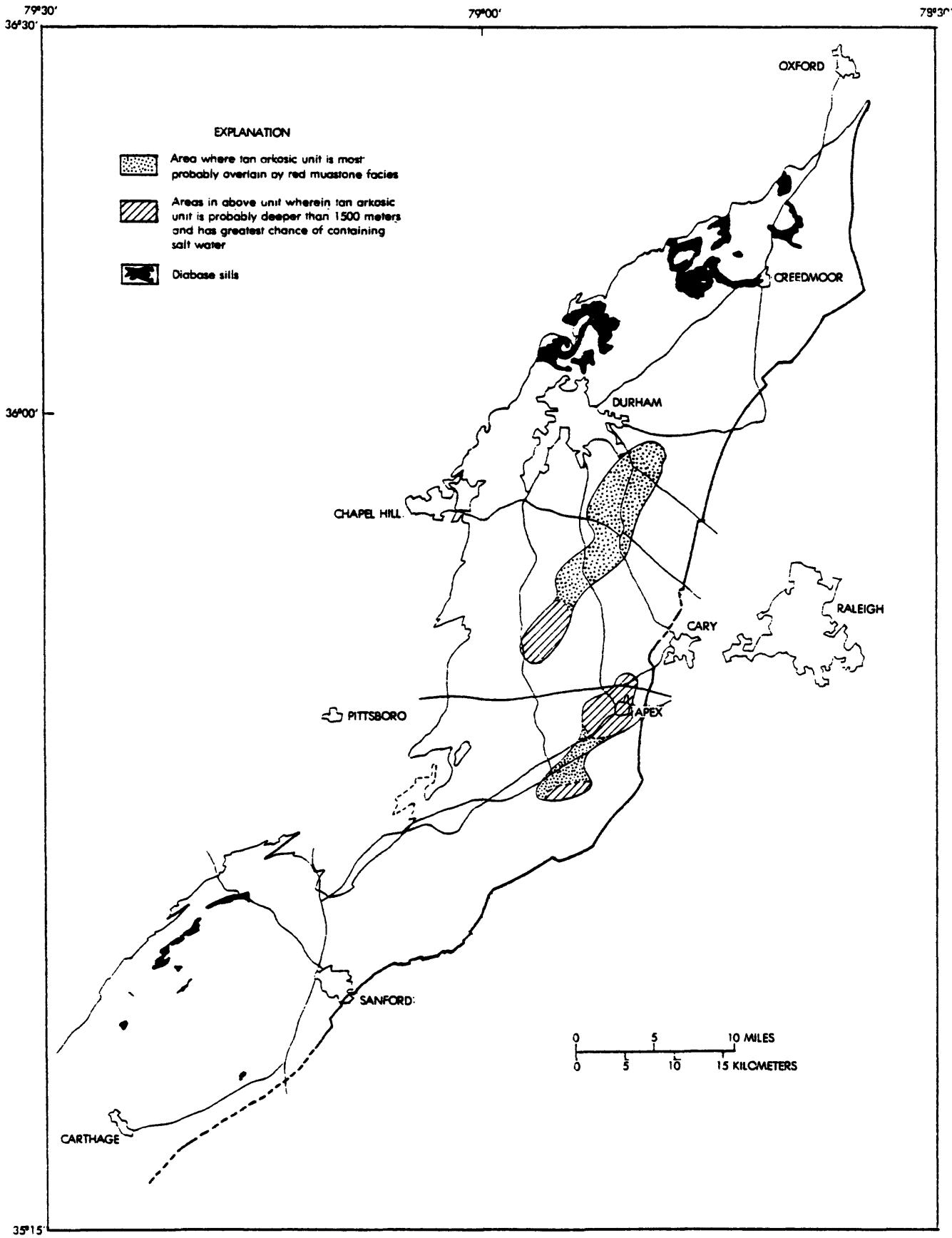

Figure 44. Areas meriting further study in the Durham Triassic basin.

SELECTED REFERENCES

Abdel-Monen, A. A., and Kulp, J. L., 1968, Paleogeography and the source of sediments of the Triassic basin, New Jersey, by K-Ar dating: Geological Society of American Bulletin, v. 79, p. 1231-1241.

Ackerman, H. D., Bain, G. L., and Zohdy, A. A. R., 1976, Deep exploration of an East-Coast Triassic basin using electrical resistivity: Geology, v. 4, no. 4, p. 137-140.

Alger, R. P., 1966, Interpretation of electric logs in fresh water wells in unconsolidted formations: Tulsa, Oklahoma, Society of Professional Well Log Analysts, 7th Annual Logging Symposium, May 8-11, p. CC1-CC5.

Anderson, E. M., 1951, The dynamics of faulting and dyke formation, with applications to Britain, 2nd ed.: Oliver and Boyd, 206 p.

Avary, Lee, 1977, Clay mineralogy of the Durham basin: North Carolina University at Chapel Hill, N.C., 14 p.

Bain, G. L., 1973, Feasibility study of East Coast Triassic basins for waste storage-data availability: U.S. Geological Survey Open-File Report, 113 p.

_____, 1977, Wrench-fault tectonic origin of East Coast Triassic basins (abs.): Geological Society of America Abs. with programs, Southeastern section, v. 9, No. 2.

Bain, G. L., and Bizdorf, R. J., 1977, Structural reinterpretation of the Durham-Wadesboro basin, North Carolina (abs.): Geological Society of America Abs. with Programs, Southeastern section, v. 9, no. 2.

Bain, G. L., and Harvey, B. W., 1977, Field guide to the geology of the Durham Triassic basin: Carolina Geological Society fieldtrip guidebook, North Carolina Division of Mineral Resources, 83 p.

Bain, G. L., and Thomas, J. D., 1966, Geology and ground-water in the Durham area, North Carolina: N.C. Dept. Water Resources, Ground-Water Bull. 7, 147 p.

Bell, Henry III, Butter, J. R., Howell, D. E., Whallen, W. H., 1974, Geology of the Piedmont and Coastal Plain near Pageland, South Carolina and Wadesboro, North Carolina: S. S. State Devel. Board, Div. of Geol., (Carolina Geol. Soc. Field-Trip Guidebook), 23 p.

Birch, F., 1942, Handbook of physical constants: Geological Society of America Special Paper 36.

Brown, D. L., 1971, Techniques for quality of water interpretations from calibrated geological logs, Atlantic Coastal area: Ground Water, July-Aug., v. 9, no. 4, 13 p.

Campbell, M. R., and Kinball, K. W., 1923, the Deep River coal field of North Carolina: North Carolina Geological and Economic Survey Bull. 33, p. 25-28, 64-79.

Chinnery, M. A., 1966, Secondary Faulting: Canadian Journal of Earth Science, v. 3, p. 163-190.

Conley, J. F., 1962, Geology and mineral resources of Moore County, North Carolina: North Carolina Divison Mineral Resources Bull. 76, 40 p.

Cooper, H. H., Jr., Bredehoeft, J. D., and Papadopulos, I. S., 1967, Response of a finite-diameter well to an instantaneous charge of water, American Geophysical Union, Water Resources Research, v. 3, no. 1, p. 263-269.

Cornet, Bruce, 1975, Geological history of the Newark super group in capsule form: Unpub. paper, Pennsylvania State Univ., 3 p.

_____1977, The palynostratigraphy and age of the Newark super group: Pennsylvania State Univ., PhD dissertation, 508 p.

Cornet, W. B., and Traverse, A. A., 1975, Palynological contributions to the chronology and stratigraphy of the Hartford basin in Connecticut and Massachusetts: GeoScience and Man, v. 11, p. 1-33.

Custer, R. L. P., 1966, Paleocurrents of the Triassic Durham basin North Carolina: A thesis submitted to the Graduate Faculty of North Carolina Univ. at Raleigh, 34 p.

_____1967, Occurrence of limestones in the Durham Triassic basin (abs.): Elisha Mitchell Scientific Society Journal, v. 84, no. 3, p. 176.

deBoer, Jelle, 1960, Paleomagnetic-tectonic study of Mesozoic dike swarms in the Appalachians: Journal Geophysical Research, v. 72, p. 2237-2250.

Delevoryas, T., and Hope R. C., 1971, A new Triassic Cycad and its phyletic implications: Postilla, no. 150, 21 p.

Dennison, J. M., and Wheeler, W. H., 1975, Stratigraphy of Precambrian through Cretaceous strata of probable fluvial origin in Southeastern United States and their potential as uranium host rocks: Southeastern Geology, Spec. Pub., no. 5, 210 p.

Dittmar, E. I., 1979, Environmental interpretation of paleocurrents in the Triassic Durham basin: Unpub. Master's thesis, Univ. of North Carolina at Chapel Hill, N.C., 91 p.

Ebasco Services, 1975, Fault investigation-Shearon Harris nuclear power plant for Carolina Power and Light Co.: Ebasco Services, Inc., New York, N.Y., v. 1 and 2, 620 p.

Emmons, Ebenezer, 1852, Report of Professor Emmons on his geological survey of North Carolina: Ex. Doc. no. 13, Seaton Gales, Raleigh, N.C., 181 p.

_____1856, Geological report of the midland counties of North Carolina: George P. Putman and Co., New York, N.Y., 347 p.

Ferris, J. G., Knowles, D. B., Brown, R. H., and Stallman, R. W., 1962, Theory of aquifer tests: U.S. Geological Survey Water-Supply Paper 1536-E, 174 p.

Fontaine, W. M., 1883, The older Mesozoic flora of North Carolina, pt. 3, p. 97-128, in Contributions to the knowledge of the older Mesozoic flora of Virginia: U.S. Geological Survey Monograph 6, 144 p.

Glaeser, J. D., 1966, Provenance, dispersal and deposition environments of Triassic sediments in the Newark-Gettysburg basin: Pennsylvania Geological Survey Report G-43, 168 p.

Guyod, Hubert, 1944, Guyod's electrical well logging: Welex Bull. A132, 103 p.

Hafner, W., 1951, Stress distributions and faulting: Geological Society of America Bull., v. 62, p. 373-398.

Harrington, J. W., 1951, Structural analysis of the west border of the Triassic basin: Geological Society of America Bull., v. 62, no. 2, p. 149-158.

Hodgson, R. A., Gay, S. P., Jr., and Benjamins, J. Y., editors, 1974, Proceedings of the first international conference on the new basement tectonics: Utah Geological Association Pub. No. 5, 636 p.

Hooks, W. G., and Ingram, R. L., 1955, The clay minerals and the iron oxide minerals of the Triassic red beds of the Durham basin, N. C., Am. Jour. Sci., v. 253, p. 19-25.

Hope, R. C., and Patterson, O. F., 1969, Triassic flora from the Deep River basin, North Carolina: North Carolina Divison Mineral Resources Spec. Pub. 2, 12 p.

Hubbert, M. K., 1951, Mechanical basis for certain familiar geologic structures: Geological Society America Bull., v. 62, p. 355-372.

Jones, T. R., 1862, Monograph of the fossil Estheridae: Palaeontogr. Soc. London, p. 1-134, pls. 1-5.

Keys, W. S., Eggers, D. E., and Taylor, T. A., 1979, Borehole geophysics as applied to the management of radioactive waste--site selection and monitoring, in Carter, M. W., and others, eds., Management of Low-Level Radioactive Waste: Elmsford, New York Pergamon Press, Inc., W. 2, p. 955-982.

Keys, W. S., and MacCary, L. M., 1971, Application of borehole geophysics to water-resources investigation: Techniques of Water-Resources Investigations of the U.S. Geological Survey, Book 2, Ch. E1. 126 p.

Klein, G. deV., 1969, Deposition of Triassic sedimentary rocks in separate basins, eastern North America: Geological Society America Bull., v. 80, p. 1825-1832. Krynine, P. D., 1950, Petrology, stratigraphy and origin of the Triassic sedimentary rocks of Connecticut: Connecticut Geological and Natural History Survey Bull., v. 73, 247 p.

Mann, V. I., and Zablocki, F. S., 1961, Gravity features of the Deep River Wadesboro Triassic basin of North Carolina: Southeastern Geology, v. 2, no. 4, p. 191-215.

Marine, I. W., and Siple, G. E., 1974, Buried Triassic basin in the central Savannah River area, South Carolina and Georgia: Geological Society America Bulletin, v. 85, p. 311-320.

McKee, E. D., 1959, Paleotectonic map of the Triassic system: U.S. Geological Survey Miscellaneous Geological Investigations Map 1-300, 33 p., 9 pls.

McKinstry, H. E., 1953, Shears of the second order: American Journal Science, v. 251, p. 401-414.

Moody, J. D. and Hill, M. J., 1956, Wrench-fault tectonics: Geological Society America Bulletin, v. 67, no. 9, p. 1207-1246.

Murrary, G. E., Jr., 1938, New fossil localities in the Durham Triassic basin: Science, v. 87, p. 2261.

Olmstead, D., 1825, Report on the Geology of North Carolina conducted under the Board of Agriculture: Board of Agriculture Report, Part II, 44 p.

Parker, J. M., III, 1978, The geology and mineral resources of Wake County, North Carolina: North Carolina Divison Mineral Resources Bulletin 86, 122 p.

Patterson, O. F., III, 1969, The depositional environment and paleoecology of Pekin Formation (Upper Triassic) of the Sanford Triassic basin, North Carolina: Unpub. Master's Thesis, North Carolina State University at Raleigh, North Carolina, 104 p.

Peterson, M. N., A., and von der Broch, C. C., 1965, Chert: modern inorganic deposition in a carbonate precipitating locality: Science, v. 149, p. 1501-1503.

Prouty, W. F., 1931, Triassic deposits of the Durham basin and their relation to other Triassic basins of Eastern United States: American Journal Science, 5th ser., v. 21, p. 473-490.

Randazzo, A. F., and Copeland, R. E., 1975, The geology of the northern portion of the Wadesboro Triassic basin, North Carolina: Southeastern Geology, v. 17, no. 3, p. 115-138.

Randazzo, A. F., Swe, W., and Wheeler, W. H, 1970, A study of the tectonic influence in Triassic sedimentation -- the Wadesboro basin, Central Piedmont: Journal Sedimentary Petrology, v. 40, no. 3, p. 998-1006.

Redfield, W. C., 1856, On the relations of the fossil fishes of the sandstone of Connecticut and other Atlantic States to the Liassic and other Oolitic periods: American Journal Science, 2nd ser., v. 22, no. 66, p. 357-363.

Reinemund, J. A., 1955, Geology of the Deep River coal field, North Carolina: U.S. Geological Survey Professional Paper 246, 159 p.

Russell, I. C., 1892, The Newark system: U.S. Geological Survey Bulletin 85, 344 p., 13 pls., 4 figs.

Sanders, J. E., 1963, Late Triassic tectonic history of northeastern United States: American Journal Science, v. 261, p. 501-524.

Schlumberger, 1972a, Log interpretation charts: Schlumberger Limited, 92 p.

_____1972b, Log interpretation, volume 1 - principles: Schlumberger Limited, New York, N.Y., 113 p.

Shearer, R. D., 1927, A cross section through the Triassic basin: Unpub. Master's Thesis, Univ. North Carolina at Chapel Hill, N.C., 23 p.

Smith, N. D., 1970, The braided stream depositional environment: comparison of the Platte River with some Silurian clastic rocks, north-central Appalachians: Geological Society of America Bulletin, v. 81, no. 10, p. 2993-3013.

Sumner, J. R., 1977, Geophysical investigation of the structural framework of the Newark-Gettysburg Triassic basin, Pennsylvania: Geological Society of America Bulletin, v. 88, p. 935-942.

Swain, F. M., and Brown, P. M., 1972, Lower Cretaceous Jurassic (?) and Triassic Ostracoda from the Atlantic Coastal region: U.S. Geological Survey Professional Paper 795, 55 p., 9 pls.

Van Houten, F. B., 1977, Triassic-Liassic deposits of Morocco and eastern North America - comparison: American Association Petroleum Geologist Bulletin, v. 61, no. 1, p. 79-99.

Vilbrant, F. C., 1927, Oil-bearing shales of the Deep River valley: North Carolina Division Mineral Resources Bulletin, Economic Paper 59, 23 p.

Ward, L. F., 1899, Status of the Mesozoic floras of the United States: U.S. Geological Survey 20th Annual Report, pt. 2, p. 211-748.

Whitehead, J. W., 1962, The petrology of the Sanford basin Triassic sediments, North Carolina: A thesis presented to the Faculty of the Graduate School, Missouri University, 174 p.

Wilcox, R. E., Harding, T. P., and Seely, D. R., 1973, Basic wrench tectonics: American Association Petroleum Geologists Bulletin, v. 57, p. 74-96.

Woodworth, J. B., 1902, The Atlantic coast Triassic coal fields: U.S. Geological Survey 22nd Annual Report, pt. 3, p. 25-53.

Wyllie, M. R, J., Gregory, A. R., and Gardner, G. H. F., 1956, Elastic Wave Velocities in Heterogeneous and Porous Media: Geophysics, v. 21, no. 1.

_____1958, An experimental investigation of factors affecting elastic wave velocities in porous media: Geophysics, v. 23, no. 3.

Zablocki, F. S., 1959, A gravity study of the Deep River Wadesboro Triassic basin of North Carolina: Unpub. Master's Thesis, North Carolina University at Chapel Hill, N.C., 44 p.

Zohdy, A. A. R., 1974, The use of Dar Zarrouk curves in the interpretation of VES data: U.S. Geological Survey Bulletin 1313-D, 41 p.

Zohdy, A. A. R., and Bisdorf, R. J., 1975, Computer programs for the forward calculation and automatic inversion of Wenner sounding curves: National Technical Information Service, PB-247265/AS, Springfield, Virginia.

☆ U.S. GOVERNMENT PRINTING OFFICE: 1982 – 361-614/59